92PC92104-TPR-12

ADVANCED THERMALLY STABLE JET FUELS

Technical Progress Report
April 1995 - June 1995

H.H. Schobert, S. Eser, A. Boehman, C. Song, P.G. Hatcher, , M.M. Coleman

Contributions from:

R. Arumugam, J. Bortiatynski, R. Byrne, K. Gergova, M. Kondam, E. Korobetskaya, W.-C. Lai, S. Martin, D. McKinney, P. Saghani, E. Yoon and J. Yu

August 1995

Prepared for U.S. Department of Energy
under
Contract No. DE-FG22-92PC92104

OBJECTIVES i

SUMMARY ii

TECHNICAL PROGRESS 1

Task 1. Investigation of the Quantitative Degradation Chemistry of Fuels 1

1. Characterization and Degadation Studies of Coal- and Petroleum-Derived Aviation Jet Fuels and Middle Distillates. (Contributed by Wei-chaun Lai and Chunshan Song) 1
2. Thermal Decomposition of n-Alkanes in Near-critical and Supercritical Regions: Product Distributions and Reaction Mechanisms (Contributed by Jian Yu and Semih Eser) 9
3. The Use of Site-Specific ^{13}C-labeling to Examine the Thermal Degradation of Jet Fuel Components (Contributed by Daniel, E. McKinney, Jacqueliine M. Bortiatynski, and Parick G. Hatcher) 18

Task 2. Investigation of Incipient Deposition 21

1. Deposit Growth During Heating of Coal Derived Aviation Gas Turbine Fuels (Contributed by Prashant C. Sanghani and André Boehman) 21

Task 3. Characterization of Solid Gums, Sediments, and Carbonaceous Deposits 23

1. Effects of High Surface Area Activated Carbons on Thermal Stressing of Model Compounds(Contributed by Katia Gergova, Rathnamala Arumugam, and Semih Eser 23

Task 4. Coal-Based Fuel Stabilization Studies 27

1. Further Studies on Potential Jet fuel Stabilizers. (Contributed Emily M. Yoon and Michael M. Coleman) 27

Task 5. Exploratory Studies on the Direct Conversion of Coal to High Quality Jet Fuels 30

1. Novel Approaches to Low-Severity Coal Liquefaction and Coal/Resid Co-processing using Water and Dispersed Catalysts. (Contributed by Russell Byrne and Chunshan Song) 30
2. Exploratory Studies on the Possibility of Non-Radical Hydrogen Transfer under Low Temperature Liquefaction Conditions. (Contributed by Shona Martin) 35
3. Low-temperature routes to hydrogenation of Pittsburgh No. 8 coal. (Contribured by Elena Korbetskaya) 40

(Con't)

4. Exploratory Studies on Coal Liquids Upgrading using Mesoporous Molecular Sieve Catalysts (Contributed by Madhusudan Reddy Kondam and Chunshan Song 42

Appendix I. Tables 47

Appendix II. Figures 58

OBJECTIVES

The Penn State program in advanced thermally stable jet fuels has five objectives: 1) development of mechanisms of degradation and solids formation; 2) quantitative measurement of growth of sub-micrometer and micrometer-sized particles suspended in fuels during thermal stressing; 3) characterization of carbonaceous deposits by various instrumental and microscopic methods; 4) elucidation of the role of additives in retarding the formation of carbonaceous solids; and 5) assessment of the potential of production of high yields of cycloalkanes and hydroaromatics by direct liquefaction of coal.

SUMMARY

The oxidative and thermal stabilities of ten fuels have been studied by differential scanning calorimetry and in microautoclave reactors. The compositions of the stressed fuels (as well as the unreacted fuels) were characterized by gas chromatography and gas chromatography/mass spectrometry. In addition, simulated distillation curves were determined by thermogravimetric analysis. The order of oxidative stability is Jet A > JP-8P > Jet A-1 > JP-7 ≈ JPTS > FT-MD > JP-8C. There is an inverse relationship between oxidative stability and thermal stability. The fuels with higher contents of 1- to 3-ring cycloalkanes and/or hydroaromatics are more stable than those with higher contents of long-chain alkanes, in terms of less gas formation. Among the paraffinic fuels, higher stability, in terms of less gas formation, was observed for those fuels having narrower distribution of alkanes with relatively shorter chains (e.g., Jet A-1). Those fuels with lower aromatics contents and more hydrogen-donor compounds exhibit less solid formation. Overall, coal-derived JP-8C and HRI-MD have the best thermal stability among the ten fuels studies, in terms of less gas or solids formation.

The product distributions and reaction mechanisms for the thermal decomposition of *n*-alkanes in near-critical and supercritical regions were studied. The emphasis of the work in this reporting period has been placed on reaction mechanisms and product distributions.

Work is continuing on obtaining additional ^{13}C-labeled jet fuel components for future thermal stressing studies. Compounds of current interest include 6-^{13}C-dodecane and 1-cyclohexyl-1-^{13}C-hexane.

Further analysis of the formation of solids from the thermal stressing of decane and decalin has been performed.

High-surface-area activated carbons suppress carbon deposition and help retard the degradation of dodecane. Surface area higher than 2000 m2/g does not increase the catalytic effect

and the ability of the carbon to suppress deposition during thermal stressing. Toluene extraction of activated carbons before thermal stressing resulted in an increase in the effectiveness of the activated carbon added. The concentration of naphthalene in the stressed liquids depends on both H-transfer reactions and degradation processes that took place during thermal stressing. Unusual tubular deposits were formed on the carbonaceous overlayer of Maxsorb carbons, and PX-21 carbon, after they were stressed with dodecane and decalin at 425°C.

Tetrahydroquinoline appears to be a superior additive for inhibiting the thermal degradation of dodecane because it has four transferable hydrogens, it is relatively stable at 425°C, the N–H bond is weaker than the C–H bond, and the radicals formed are stabilized by delocalization through the aromatic ring.

There are strong synergistic effects between water and dispersed molybdenum sulfide catalyst for promoting liquefaction of Wyodak subbituminous coal and Pittsburgh #8 bituminous coal at temperatures ≤375°C. The promoting effects of water are more pronounced for the lower rank subbituminous coal. At temperatures ≥400°C, water has a negative impact on the catalytic liquefaction of both coals. This effect is more dramatic for Wyodak than for Pittsburgh #8 coal.

Preliminary studies of Wyodak have been conducted to determine if non-radical pathways are responsible for hydrogen incorporation at mild conditions (350°C, 1000 psi H_2, and 30 minutes reaction). Conversions of Wyodak at 350°C are found not to be catalyzed by mineral matter present in the coal.

In further efforts to examine low-temperature, low-pressure pathways to hydrogenation of coal, Pittsburgh #8 was reacted in hydrogen without solvent or catalyst at 300°C. No evidence of hydrogenation was observed.

In the preparation of mesoporous molecular sieve catalysts for upgrading coal liquids, it was found that sodium aluminate is a good source of aluminum for synthesis of the mesoporous aluminosilicates. Differential scanning calorimetry can be used to determine the relative acidities of the molecular sieves. Platinum loading on samples of a mesoporous molecular sieve Al-MCM-41 by wet impregnation yielded large crystallites with good uniformity. These mesoporous molecular sieves are capable of converting large molecules like 1,3,5-triisopropylbenzene.

Task 1. Investigation of the Quantitative Degradation Chemistry of Fuels

1. Characterization and Degradation Studies of Coal- and Petroleum-Derived Aviation Jet Fuels and Middle Distillates. (Contributed by Wei-Chuan Lai and Chunshan Song)

Introduction

The thermal stability of jet fuels plays an important role in the design and development of future high Mach aircraft. It was reported that the fuel in future hypersonic aircraft may experience temperatures in the range of 400-500 °C. The temperatures are much higher than the current maximum operating temperature (below 300 °C) for the conventional aviation jet fuels. When the fuels are exposed to such high temperatures, serious pyrolytic degradation of the fuels will occur and will result in the formation of solid deposits on critical aircraft systems such as fuel pipeline, filter, and engine parts [1]. This means that advanced jet fuels are required for hypersonic aircraft. The development of such fuels warrants detailed study of pyrolytic degradation of hydrocarbon fuels.

The future fuels might derive not only from petroleum, but also from hydrocarbon resources such as coal, tar sands, and oil shale. The scope of this report concentrates on the characterization and degradation study of ten fuels including four coal-derived fuels and six petroleum-derived military and commercial jet fuels. The chemical composition of the fuels are characterized using gas chromatography (GC) and gas chromatography - mass spectrometry (GC-MS) with the help of temperature-programmed retention indices [2]. In addition, one of the objectives of this work is to enhance the intrinsic stability of jet fuels by optimizing fuel composition. Many of the physical and chemical properties of fuels, e.g., volatility and critical properties, are determined by distillation curve. Thus, the distillation curves were determined to serve as the guidelines for the formulation of future candidate surrogate distillate fuels, which have the advantage of exploring the effects of fuel chemical composition on the stability at a manageable level because they are composed of a relatively much smaller number of hydrocarbons [3]. Distillation curves generally were obtained from simulated distillation data by GC (ASTM D 2887 and ASTM D 86) [4, 5]. The simulated distillation results by GC are susceptible to several error sources; for example, the GC column is not separating the sample in accordance with the boiling point order, and the compounds have quite different response factors to the GC detector, and inaccurate areas under the chromatogram are obtained due to a few factors such as poor baselines. In this work, the simulated distillation curves were determined by thermogravimetric analysis (TGA), which is a reliable and rapid tool for this purpose.

In short, the present work reports on ranking the stability of current fuels, identifying thermally stable compounds in fuels, and elucidating the relative stabilities of the fuels by their chemical composition. The thermal stability study was carried out in tubing bomb reactors at 450

°C under N_2. The thermo-oxidation stability of fuels was examined by high-pressure differential scanning calorimetry (DSC). In other words, the temperature for onset of oxidative degradation, i.e., the onset temperature for the oxidation exotherm, of the fuels was used as the oxidation stability criterion and was measured by DSC under dynamic mode (temperature linearly increasing).

Experimental

Samples. Ten jet fuels and middle distillates were studied. Four coal-derived fuels include JP-8C from hydrotreating of liquids produced from the Great Plains Gasification plant [6], and middle distillates derived either from direct coal liquefaction (WI-MD from Wilsonville plant and HRI-MD from HRI) or from indirect coal liquefaction (FT-MD from Fischer-Tropsch synthesis). Six petroleum-derived military and commercial jet fuels include JPTS (thermally stable jet fuel), JP-7, JP-8P, JP-8P2, Jet A, and Jet A-1. The fuel densities range from 0.76 g/cm^3 (FT-MD) to 0.96 g/cm^3 (WI-MD) with most falling in a smaller range of 0.79 to 0.81 g/cm^3 (JPTS, JP-7, JP-8P, Jet A, Jet A-1, and JP-8P2). The densities of JP-8C and HRI-MD are 0.84 and 0.92 g/cm^3, respectively. The basic information of these fuels is presented in Table 1, and the properties of the samples are discussed in the following sections.

Thermal analysis. The simulated distillation experiments were carried out with fuel contained in a hermetically sealed aluminum crucible with a pierced lid (hole diameter about 100 μm) in TG50 thermobalance (METTLER). Samples of about 7 mg were used in each measurement and a purge gas (N_2) flow of 200 cm^3/min was used. The temperature was programmed from 25 to 425 °C at a heating rate of 10 °C/min.

The apparatus used for the measurement of the oxidation onset temperature was a Mettler high-pressure differential scanning calorimeter Model DSC 27HP, which is usable from ambient pressure up to 7 MPa. It should be noted that it is necessary to operate the instrument under elevated pressure to avoid problems associated with the evaporation of the fuels. DSC was carried out under the following conditions. About 2 mg of each of the fuels was placed in an uncovered standard aluminum crucible, and was heated from 50 to 600 °C at a rate of 10 °C/min in the DSC system which was under 3.5 MPa of air pressure. The system was continuously purged with 50 cm^3/min air.

Apparatus and procedures of thermal stressing. Thermal stressing of the jet fuels and middle distillates were studied in tubing bomb reactors at 450 °C for a heating period of 0-8 hours under 0.79 MPa of ultra high purity (UHP; 99.999%) N_2. A 5 ml sample was confined in a leak-tested reactor. The sample was deoxygenated through repetitive (6 times) pressurization to 6.9 MPa with UHP-N_2 and purging to remove oxygen/air in the reactor or dissolved in the sample. The reactor was pressurized to the desired starting pressure of 0.79 MPa with UHP-N_2 before

being immersed into a fluidized sand bath which has been preheated to 450 °C. After the experiment was started, the reaction pressure was closely monitored. The experiment was ended after the desired stressing time by removing the reactor from the fluidized sand bath and immediately quenching in a cool water bath. The products were separated into gases, liquids, and solid deposits.

Product chemical analysis. The gas samples were analyzed for their compositions and quantities by using a Perkin-Elmer Autosystem GC. Two detectors, a flame ionization detector (FID) and a thermal conductivity detector (TCD), were used to analyze the gas composition. The FID was used to detect hydrocarbon gases from C_1 to C_6. The TCD was used to determine CH_4, C_2H_2, C_2H_4, and C_2H_6 as well as non-hydrocarbon gases such as H_2, CO, and CO_2. The GC columns used were a 6 feet long, 1/8 inch diameter stainless steel column packed with 80/100 Chemipack C 18 for FID and a 10 feet long, 1/8 inch diameter stainless steel column packed with 100/120 Carbosieve SII (Supelco) for TCD. The compounds in the liquid products were identified by an HP 5890 Series II GC coupled with an HP 5971A Mass Selective Detector (MSD) and quantified by a Perkin-Elmer GC 8500. The column used was a 30 m, 0.25 mm i.d., DB-17 Fused Silica Capillary Column (50% phenyl, 50% methyl silicone) with a film thickness of 0.25 μm. The solid deposits are operationally defined as the materials which are not soluble in the resulting liquid co-products and pentane (washing solvent). The solid deposits were analyzed by Fourier transform infra-red spectroscopy and NMR spectroscopy.

Results and Discussion

Simulated distillation by TGA. Figure 1 shows the simulated distillation curve for JP-7 by TGA as well as the data determined by GC in our laboratory [5] for the same fuel. It can be seen that for JP-7 the results from TGA compare fairly well with that from GC. The simulated distillation curves by TGA are also presented in Figures 2 and 3 for five petroleum-derived and four coal-derived fuels, respectively. Table 2 summarizes the simulated distillation temperatures of these ten fuels at 5, 10, 30, 50, 70, 90, 95 wt % points. The distillation data show that (1) compared to the other 8 fuels, Jet A-1 and JP-7 have much narrower boiling point range judged from the sharp increase of recovered weight near 200 °C and 220 °C for Jet A-1 and JP-7, respectively; (2) on the other hand, HRI-MD has the widest boiling point range; (3) JPTS and JP-8C have distillation curves of much lower initial boiling point; on the contrary WI-MD is heavier than the rest with few low boiling point compounds; (4) the two petroleum-derived JP-8 fuels from different sources have moderately different distillation curves with JP-8P2 boiling approximately 20-25 °C higher than JP-8P at lower distillation range (up to 20 weight % recovered); (5) Jet A and JP-8P align well with the JP-8P2 distillation curve beyond 40 weight % recovered; (6) compared to JP-8P, JP-8C contains more low boiling point compounds and thus

exhibits higher vapor pressure; the volatility of JP-8C is between JP-8P and JP-4, which is a wide-cut distillate with vapor pressure an order of magnitude above that of JP-8P.

Chemical composition of samples. All the fuels were analyzed by GC and GC-MS before and after thermal stressing, and they are all complex mixtures of hundreds of compounds. Because of the large number of compounds in the fuels, one way to visualize their compositions is employing the total ion chromatograms (TIC) and specific ion chromatograms (SIC) of GC-MS analysis. Figure 4 presents the TIC and SIC (ions of m/z 57, 83, 91, 105, and 142) of JP-8P2. The fragment ions of m/z 57, 83, and 142 are characteristics of long-chain paraffins, alkylcyclohexanes, and alkylnaphthalenes, respectively. The ions of 91 and 105 imply the presence of alkylbenzenes. From the resemblance between TIC and SIC of m/z 57, we can find that the dominant constituents in JP-8P2 are the long-chain paraffins with carbon-number ranging from C_8 to C_{17} with most falling between C_{10} and C_{15}. The alkylbenzenes (C_2- ~ C_6-, mainly C_3- ~ C_5-) content is about 14 weight %. JP-8P2 also includes 12% monocycloparaffins (C_2- ~ C_7-) and low concentrations of tetralins, indans, naphthalenes, and olefins.

JP-7, Jet A-1, JPTS, Jet A, JP-8P, and FT-MD are also paraffinic fuels derived from petroleum or coal (FT-MD only) with long-chain paraffins as the dominant constituents, but the overall compositions and paraffins distributions are somewhat different. Figure 5 shows the SIC (m/z 57) for six of the seven paraffinic fuels. We can see that JP-8P and Jet A are quite similar to JP-8P2 in terms of the long-chain paraffins distributions. Jet A-1 has a narrower band from C_{10} to C_{14} with most falling between C_{11} and C_{12}. JPTS has a band from C_9 to C_{15}. JP-7 has a band from C_{11} to C_{16} with an average carbon number of 12. FT-MD is also a paraffinic fuel, although derived from coal, having almost exclusively paraffins (C_9 ~ C_{21}). Table 3 summarizes the approximate compositions of the seven paraffinic fuels based on compound classes including three major hydrocarbon types found in fuels (paraffins, alkylbenzenes, monocycloparaffins) and other minors (such as decalins, tetralins, indans, naphthalenes, and olefins). The detailed compositions of the three major hydrocarbon types for the fuels in Table 3 are presented in Table 4.

JP-8C, WI-MD, and HRI-MD are all coal-derived fuels, but their compositions are quite different from petroleum-derived paraffinic fuels. JP-8C is composed mainly of monocyclic and bicyclic paraffins, and two-ring hydroaromatic compounds. The major components are alkyl-substituted cyclohexanes (about 40%), decalin (6.7%), alkyldecalins (7.8%), tetralin (3.6%), and alkyltetralins (5.4%). There are also about 10% each of paraffins and alkylbenzenes. HRI-MD is a heavy fuel, i.e., with many high molecular-weight components compared with the paraffinic fuels and JP-8C. HRI-MD consists of (alkyl) bicyclic paraffins, alkyl two-ring aromatic compounds and some alkylbenzenes. There are about 15% alkyl-substituted (mainly, C_0- ~ C_3-) cyclohexanes and 13% paraffins (ranging from *n*-butane to *n*-tricosane). There are also some (C_0- ~ C_2-) 3-ring or 4-ring aromatics. Regarding WI-MD, it is heavier (with carbon number $\geq$12) than

the other nine fuels with few light molecular weight compounds. It has very high content of aromatics (with ring size not less than 2). The most abundant peaks are pyrene (4%) and multi-hydropyrenes (total about 8%), and less than 10% paraffins ($C_{14} \sim C_{25}$).

Oxidative stability of fuels by DSC. Figure 6 shows the representative oxidation onset results determined from DSC curves for the oxidation of Jet A-1 and FT-MD. The oxidation onset temperature was defined as the intersection point of the two tangent lines. The oxidation starts at about 198 °C for Jet A-1 and 190 °C for FT-MD, respectively. Table 5 summarizes the quantitative results of the dynamic DSC experiments. At least two measurements were made on each fuel. Fuels that are more easily oxidized exhibit lower onset temperatures.

The onset temperature data show that the order of oxidative stability of the seven fuels in Table 5 is Jet A > JP-8P > Jet A-1 > JP-7 ≈ JPTS > FT-MD > JP-8C. Heneghan and Zabarnick [7] studied the oxidation of three jet fuels (JPTS, Jet A-1, Jet A) and showed that the more thermally stable fuels would not necessarily oxidize less easily; in fact, the more thermally stable fuels (JPTS > Jet A-1 > Jet A) were more easily oxidized, i.e., Jet A > Jet A-1 > JPTS for oxidation stability. This stability order for these three fuels from their study is consistent with what was observed in our present work. The inverse relation between oxidative stability (in terms of oxidation onset temperature) and thermal stability using deposition tendency as the thermal stability criterion, seems to in general hold also for the fuels in this study.

Thermal degradation product distributions. The relative thermal stabilities of hydrocarbons in fuels as well as the whole fuels themselves were identified based on the overall reaction products (gas, liquid, and solid) distributions and GC/GC-MS analysis of the liquid products. For the hydrocarbons in fuels, it was found that at 450 °C long-chain *n*- and *iso*-paraffins ($\geq C_{10}$), and *n*-alkylbenzenes (alkyl$\geq C_3$-) are some of the unstable compounds. Some compounds that are relatively more stable compounds include long-chain paraffins ($\leq C_7$), C_0- to C_3-cycloparaffins, and C_0- to C_2-benzenes. One example is shown in Figure 7, which presents the total ion chromatograms of the neat sample of, and the liquid products from, FT-MD after thermal stressing at 450 °C for 1-8 hours. Recall that FT-MD is a paraffinic fuel which has paraffins ranging from C_9 to C_{21}. We can clearly find that long-chain paraffins of C_{11} through C_{21} decompose quickly; the decomposition rate increases with increasing chain size. Table 6 presents the approximate compositions of JP-8P2 by compound class after 0-8 hours. It can be observed that the content of paraffins monotonically decreases with increasing time, but the yields of aromatics increase with increasing time. The quantitative results indicate that the main reactions occurring in the first 2.5 hours include cracking of the paraffins into lower paraffins and olefins, and cyclization to form alkylcyclic paraffins and olefins. The alkylcyclic compounds were then subjected to dehydrogenation to form alkylbenzenes. This observation is consistent with the mechanisms proposed by Song et al. [8] It is also important to notice that tetralins and decalins, which are

known H-donors, decrease with increasing time. The fact that decalins decrease at a slower rate than tetralins seems to imply that the former are not as active H-donors as the latter.

A typical quantitative presentation of how the three major hydrocarbon types (paraffins, alkylbenzenes, monocycloparaffins) change with time is shown in Figure 8-10 for JP-8P2 fuel stressed at 450 °C for 1-8 hours. The compounds were grouped together based on the carbon numbers; for example, the paraffins were divided into 9 groups based on the carbon numbers; each group consists of straight and branched paraffins with the same carbon number. Figure 8 shows that at 450 °C long-chain paraffins with carbon number no less than 11 (i.e., C_n, $n \geq 11$) are unstable. Long-chain paraffins ($\geq C_{14}$) decompose quickly and almost completely by 2.5 hours. Notice that the content of C_8 increases from the initial 0.6% to 1.8% at 1 hour and then decreases to 0.5% after 8 hours. The initial increase is contributed from cracking yield from longer chain paraffins, and the C_8 later decomposes and results in the decreasing C_8 fraction at later time. Similarly, the yields of C_0- to C_3-cycloparaffins also increase at early stage and then decrease with increasing time.

The yields of the gas components from JP-8P thermally stressed at 450°C for 1-8 hours are presented in Figure 11. Methane is always the most abundant gaseous product (in mmole) followed by ethane and propane over the stressing range; this is also true for all other nine fuels studied. Another common characteristic for the fuels is that the paraffinic gases (CH_4, C_2H_6, C_3H_8, and C_4H_{10}) increase with increasing time but the olefinic gases (C_2H_4, C_3H_6, C_4H_8) increase initially then decrease with increasing time. Continuous cracking accounts for the progressive increase of paraffinic gases and the initial increase of olefinic gases. Olefins are known to be less stable and highly reactive because of unsaturation; this results in the later decrease of olefinic gases.

Thermal stability comparison. The decomposition extents of the ten fuels are significantly affected by their compositions. Figure 12 shows the gas yields from the ten fuels stressed for 1-8 hours. The figure indicates that the three coal-derived non-paraffinic fuels, i.e., JP-8C, HRI-MD, and WI-MD, are more thermally stable than the other seven paraffinic fuels when gas formation tendency is considered as the stability criterion. The difference in stability in terms of the gas formation is attributed to the composition difference. Paraffinic fuels produce more gases because the major reaction for long-chain paraffins is cracking into lighter gases of paraffins and olefins. On the other hand, the compositions of the three coal-derived non-paraffinic fuels are quite different from the paraffinic fuels; they have low fraction of paraffins but are rich in cyclic paraffins and hydroaromatics. Thus the major reaction for them is dehydrogenation to form alkylbenzenes (liquid yields) instead of the formation of low molecular-weight gases. It can be seen that HRI-MD and FT-MD produce the gas the least and the most, respectively. For example, the gas yields for HRI-MD and FT-MD are respectively 3.3% and 17% at 1 hour, 10% and 33% at

4 hours, and 16% and 52% at 8 hours. The six petroleum-derived paraffinic fuels (JP-8P, Jet A, JP-7, FT-MD, JPTS, and Jet A-1) have similar gas yields (ranging from 37% to 40%) for 8-hour stressing. However, for 1- ~ 4-hour stressing, Jet A-1 has the lowest or second to the lowest gas yields; this is consistent with the fact that among the paraffinic fuels, Jet A-1 has the lowest paraffin content and the narrowest paraffin band (from C_{10} to C_{14}, with most falling between C_{11} and C_{12}).

The solid yields from the ten fuels stressed for 1-8 hours are presented in Figure 13. The figure shows that there is no solid formed after 1-hour stressing for all the ten fuels, and the solid starts to form between 1 and 2.5 hours. The induction time, which is the time period needed for the formation of solid precursors (such as polyaromatics) from reactive intermediates, differs for each fuel. It was found that fuels rich in hydrogen-donors (such as cyclic paraffins) have longer induction period and tend to have better stability. The hydrogen abstracted from hydrogen-donors stabilizes the reactive radicals; this in consequence inhibits the secondary radical reactions and suppresses solid formation [9]. Two of the three coal-derived non-paraffinic fuels, JP-8C and HRI-MD, have much better stability than other fuels in terms of much less solid formation. This is again attributed to the composition difference and the fact that JP-8C and HRI-MD have high concentration of hydrogen donors. Figure 13 also shows that JP-7 and JPTS have higher stability among the seven paraffinic fuels in terms of less solid formation. This is also attributed to their lower aromatics content and higher hydrogen-donor compounds.

WI-MD, on the other hand, does not have good stability in the long run, judging from its high solid formation at 8-hour stressing. Figure 14 presents the total ion chromatograms of the neat sample of, and the liquid products from, WI-MD after thermal stressing at 450°C for 1-8 hours. It can be seen that WI-MD has very high content of aromatics and hydroaromatics. The hydroaromatics decomposed quickly to form saturated aromatics through dehydrogenation, and these aromatic compounds subsequently form more polycyclic aromatic hydrocarbons and solid deposits. WI-MD seems to be stable in terms of low gas formation; however, GC-MS analysis of the liquid products shows that in fact WI-MD is quite unstable and decomposes quickly to form aromatics and precursors to solid. In short, WI-MD tends to form more solid than other fuels due to its high aromatic content nature, and it can not be a good jet fuel without further treatment.

Summary

The oxidative and thermal stability of the fuels is significantly affected by their chemical composition. The oxidative and thermal stability of ten fuels have been studied in a DSC and a tubing bomb reactor, respectively. The compositions of the stressed as well as neat fuels were all qualitatively and quantitatively characterized by GC-MS and GC. Besides, the simulated

distillation curves were also determined by TGA. All the information is useful in explaining and evaluating the thermal stability of fuels.

The order of oxidative stability is Jet A > JP-8P > Jet A-1 > JP-7 ≈ JPTS > FT-MD > JP-8C. There seems to be an inverse relation between oxidative stability (in terms of oxidation onset temperature) and thermal stability (in terms of less solid deposits formation). The relative thermal stabilities of hydrocarbons in fuels as well as the whole fuels themselves were also identified. The fuels with higher contents of 1-3 ring cycloparaffins and/or hydroaromatics are more stable than those with higher contents of long-chain paraffins in terms of less gas formation. The former includes JP-8C, HRI-MD and WI-MD, and the latter covers the remaining 7 fuels. Among the paraffinic fuels, higher stability in terms of less gas formation was observed for those fuels having narrower distribution of paraffins with relatively shorter chain, e.g., Jet A-1; those with lower aromatics content and higher hydrogen-donor compounds exhibits less solid formation . Overall, coal-derived JP-8C and HRI-MD have the best thermal stability among the ten fuels studied either in terms of less gas or solid formation.

References

1. Roquemore, W. M.; Pearce, J. A.; Harrison III, W. E.; Krazinski, J. L.; Vanka, S. P. *Prepr.-Am. Chem. Soc., Div. Pet. Chem.* , **1989**, *34* (4), 841-849.
2. Lai, W.-C.; Song, C. *Fuel* **1995**, in press.
3. Wood, C. P.; McDonell, V. G.; Smith, R. A.; Samuelsen, G. S. *J. Propulsion* **1989**, *5* (4), 399-405.
4. Martel, C. R. Military Jet Fuels, 1944-1987. Summary Report for period Oct. 85-Oct. 87, AFWAL-TR-87-2062, November **1987**, Wright-Patterson Air Force Base, Ohio.
5. Yu, J.; Eser, S. *Ind. Eng. Chem. Res.* **1995**, *34*, 404-409.
6. Song, C.; Eser, S.; Schobert, H. H.; Hatcher, P. G. *Energy & Fuels*. **1993**, *7*, 234-243.
7. Heneghan, S. P.; Zabarnick, S. *Fuel* **1994**, *73*, 35-43.
9. Song, C.; Lai, W.-C.; Schobert, H. H. *Ind. Eng. Chem. Res.* **1994**, *33*, 548-557.

2. Thermal Decomposition of n-Alkanes in Near-Critical and Supercritical Regions: Product Distributions and Reaction Mechanisms (Contributed by Jian Yu and Semih Eser)

Introduction

In the last quarterly report we presented some results from the thermal decomposition of *n*-alkanes in the near-critical and supercritical regions [1]. The kinetics and the effects of pressure on conversion were discussed. We also compared the results obtained from the glass tube reactors with those from the tubing bomb reactors and discussed the effect of oxygen on thermal decomposition. In this section the product distributions and reaction mechanism for the thermal decomposition of *n*-alkanes will be discussed.

Results and Discussion

In the following discussion, all the results were obtained from the experiments with the glass tube reactor, unless noted otherwise. The data from the tubing bomb experiments is identified as such.

1. Product Distributions. The product distributions were obtained from the thermal decomposition of *n*-C_{10}, *n*-C_{12}, and *n*-C_{14} under different loading ratios, temperatures, and conversions. All experiments were conducted using a fixed loading ratio of 0.36 except for those dealing with the effect of loading ratio.

The reaction products from the thermal decomposition of C_{10}-C_{14} *n*-alkanes under the near-critical and supercritical conditions can be divided into two categories: those from the primary reactions and those from the secondary reactions of the primary products. The primary products include *n*-alkanes from C_1 to C_{m-2} (m = number of carbon atoms in the reactant) and 1-alkenes from C_2 to C_{m-1}. The secondary products include internal alkenes (mainly *cis*- and *trans*-2-alkenes), *n*-C_{m-1}, *n*-C_{m+1}, and C_{m+2} to C_{2m-2} normal and branched alkanes. There are also small amounts of cyclopentanes and cyclohexanes. The yields of branched alkanes lighter than the reactant are not significant until high conversion. The relative yields of the primary and secondary products are dependent upon reaction conditions (loading ratio, temperature, and residence time or conversion). Figure 15 shows the chromatogram of liquid products from the thermal decomposition of *n*-C_{14} at 425 °C for 15 min at a loading ratio of 0.36.

Since the product distributions from the thermal decomposition of *n*-C_{10}, *n*-C_{12}, and *n*-C_{14} are very similar, the following discussion on the effects of loading ratio, temperature, and conversion will be focused on *n*-C_{14}. The effects of chain length will be discussed at the end of this section.

Figure 16 shows the change in the overall molar yield of C_6-C_{13} *n*-alkanes, C_6-C_{13} 1-alkenes, C_6-C_{12} 2-alkenes, and C_{14}^+ normal and branched alkanes with loading ratio from the

thermal decomposition of *n*-C_{14} at 425 °C for 15 min. The yields of the products are expressed as the number of moles based on 100 moles of the reactant converted. It can be seen that the overall yield of C_6-C_{13} *n*-alkanes increases and that of C_6-C_{13} 1-alkenes decreases as loading ratio increases. While the overall yield of C_6-C_{13} *n*-alkanes is lower than that of corresponding 1-alkenes at low loading ratio, their overall yield exceeds that of C_6-C_{13} 1-alkenes at high loading ratio. The overall yields of C_6-C_{12} 2-alkenes and C_{14}^+ alkanes are low at low loading ratio, but their yields become significant as loading ratio increases. Since it is desirable to know the effects of pressure on the product distributions, the product yields in Figure 16 were plotted as the functions of pressure, as shown in Figure 17. One can see from Figure 17 that the large changes in product distributions with pressure occur in the near-critical region. This result can be attributed to the large pressure dependence of density or concentration in this region, resulting in a significant change in reaction mechanism. Figure 18 shows the similar changes in the molar yields of individual C_6-C_{13} *n*-alkanes and 1-alkenes with loading ratio/pressure from the thermal decomposition of *n*-C_{14} at 425 °C for 15 min.

Figure 19 shows the carbon number distributions of *n*-alkane and 1-alkene products as functions of loading ratio from the thermal decomposition of *n*-C_{14} in the tubing bomb reactor at 425 °C for 30 min. It can be seen that while the yields of C_6-C_{13} *n*-alkanes increase, those of methane, ethane, and propane decrease as loading ratio increases. The yields of all olefinic components decrease as loading ratio increases. Among the gaseous products, the yields of C_2-C_3 gases decrease significantly while the yield of methane remains within a narrow range as loading ratio increases. The yield of methane is always lower than those of ethane and propane and the yield of ethylene is always lower than that of propylene in the range of loading ratio examined. At the lower loading ratio, the yields of ethane, propane, and propylene are high and equivalent while those of methane and ethylene show intermediate values. In the supercritical region (loading ratio > 0.15), ethylene is formed in the lowest yield as compared to other gaseous products and very low ethylene yield is obtained at high loading ratio. The low ethylene yield indicates that the reaction mechanism under the conditions used in this study is different from that under low-pressure and high-temperature pyrolysis conditions which give very high ethylene yield [2-7]. Examination of Figures 15–19 reveals that the major reaction products from *n*-C_{14} thermal cracking are *n*-alkanes with carbon number from C_1 to C_{m-3} and 1-alkenes with carbon number from C_2 to C_{m-2}. While *n*-C_{m-2}, *n*-C_{m-1}, and 1-C_{m-1} are also present in the products, their yields are considerably lower than those of the major products. The same conclusions can be drawn for the thermal decomposition of *n*-C_{10} and *n*-C_{12}.

Figure 20 shows the product distribution as a function of carbon number from the thermal decomposition of *n*-C_{14} at two temperatures and for similar conversions. At similar conversions the formation of 1-alkenes is favored at the higher temperature while the production of *n*-alkanes is

facilitated at the lower temperature. Figure 21 shows that the selectivity for *n*-alkanes is affected by temperature more significantly at higher conversion.

Figure 22 shows the effects of conversion on the overall product distributions from *n*-C_{14} thermal cracking at 425 °C. While the overall yields of C_6-C_{13} *n*-alkanes and C_{14}^+ alkanes increase gradually, that of C_6-C_{13} 1-alkenes decreases rapidly with increased conversion. The overall yield of C_6-C_{12} 2-alkenes increases quickly at lower conversion and then remains at a stable level as conversion increases. Figure 23 shows a similar change in the molar yields of individual C_6-C_{13} *n*-alkanes and 1-alkenes with conversion from the thermal decomposition of *n*-C_{14} at 425 °C.

Figure 24 shows the carbon number distributions of *n*-alkane and 1-alkene products as functions of conversion from the thermal decomposition of *n*-C_{14} in the tubing bomb reactor at 425 °C. The relationship between the yield of liquid component and conversion is consistent with that observed in the glass tube reactor experiments, that is, the higher the conversion, the higher the yields of C_6-C_{13} *n*-alkanes and the lower the yields of C_6-C_{13} 1-alkenes. The yields of C_1-C_3 gases decrease with increased conversion. In the conversion range examined, the yields of gaseous products decrease in the order of propane > propylene > ethane > methane > ethylene.

Figure 25 shows the effect of chain length on the product distribution from the thermal decomposition of C_{10}-C_{14} *n*-alkanes at 425 °C for similar conversions. It can be seen that the yields of *n*-C_{m-1}, *n*-C_{m-2}, and 1-C_{m-1} are significantly lower than those of other *n*-alkane and 1-alkene products. The yields of individual *n*-alkane and 1-alkene with the same carbon number, except for *n*-C_{m-1}, *n*-C_{m-2}, and 1-C_{m-1}, increase as chain length decreases. This is because the number of components in the products from the thermal cracking of the lighter reactant is less than that from the heavier reactant. Therefore, at similar conversions the yield of the same component would be higher from the thermal cracking of the lighter reactant than from that of the heavier reactant.

2. Reaction Mechanism for Thermal Decomposition of *n*-Alkanes. The thermal decomposition of *n*-alkanes can be described by the free-radical mechanism. According to the product distributions and the changes in product composition with reaction conditions, the following mechanism has been developed for the thermal decomposition of *n*-alkanes under near-critical and supercritical conditions:

$$n\text{-}C_mH_{2m+2} \rightarrow R_i^{1\bullet} + R_j^{1\bullet} \qquad (1)$$

$$R_i^{1\bullet} + n\text{-}C_mH_{2m+2} \rightarrow n\text{-}C_iH_{2i+2} + R_m^{x\bullet} \qquad (2)$$

$$R_m^{x\bullet} \rightarrow R_m^{y\bullet} \rightarrow 1\text{-}C_kH_{2k} + R_n^{1\bullet} \quad (y\text{-}x \geq 4;\ 2 \leq k \leq m\text{-}1;\ n \leq m\text{-}2) \qquad (3)$$

$$R_n^{1\bullet} + n\text{-}C_mH_{2m+2} \rightarrow n\text{-}C_nH_{2n+2} + R_m^{x\bullet} \quad (4)$$

$$R_n^{1\bullet} \rightarrow C_2H_4 + R_{n-2}^{1\bullet} \quad (3 \le n \le 5) \quad (5a)$$

$$R_n^{1\bullet} \rightarrow R_n^{x\bullet} \rightarrow 1\text{-}C_kH_{2k} + R_{n-k}^{1\bullet} \quad (n \ge 6;\ x \ge 5) \quad (5b)$$

$$R_n^{1\bullet} + 1\text{-}C_kH_{2k} \rightarrow R_{n+k}^{x\bullet} \quad (6)$$

$$R_m^{1\bullet} + 1\text{-}C_kH_{2k} \rightarrow R_{m+k}^{x\bullet} \quad (7a)$$

$$R_m^{x\bullet} + 1\text{-}C_kH_{2k} \rightarrow R_{m+k}^{b\bullet} \quad (x \ne 1) \quad (7b)$$

$$1\text{-}C_kH_{2k} \rightarrow 2\text{-}C_kH_{2k} \quad (8)$$

$$R_n^{1\bullet} + R_m^{x\bullet} \rightarrow \text{products} \quad (9)$$

where $R_n^{1\bullet}$ is the primary radical with a carbon number of n, $R_m^{x\bullet}$ is the primary or secondary parent radical with a free electron at site x of carbon skeleton, $R_{m+k}^{x\bullet}$ is the heavy normal alkyl radical, and $R_{m+k}^{b\bullet}$ is the heavy branched alkyl radical.

The initiation reaction occurs by homolytic carbon-carbon bond cleavage to produce two primary radicals (eq 1). These radicals then abstract hydrogen from surrounding reactant molecules to form various parent radicals (eq 2), of which most are secondary radicals, since the formation of a secondary radical by hydrogen abstraction requires a lower activation energy. The parent radical isomerizes and then decomposes by β-scission to form an 1-alkene and a lower primary radical (eq 3). This lower primary radical could undergo one of these reactions: hydrogen abstraction from the reactant molecule (eq 4), decomposition to form an 1-alkene and a smaller primary radical (eqs 5a and 5b), and, except for fairly low conversion, addition to the terminal carbon of an 1-alkene to give a higher radical (eq 6). For the radical with carbon number larger than five, isomerization occurs before decomposition. Under the conditions used, the following reactions also occur: the addition of a primary parent radical or a secondary parent radical to an 1-alkene to produce a heavy *n*-alkyl radical (eq 7a), or a heavy branched alkyl radical (eq 7b), and the double bond isomerization of 1-alkene to 2-alkene (eq 8). The termination reaction occurs mostly by the recombination of a lower primary radical and a parent radical (eq 9). The recombination reactions between lower primary radicals and between parent radicals are less important because of relatively low concentrations of the lower primary radicals and low oriented collision frequencies between the parent radicals.

It should be mentioned that the isomerization of the lower primary radicals, which are produced by the β-scission of the parent radicals (eq 3), only occurs as an intermediate step during their decomposition (eq 5b). This assumption is reasonable according to the observed product distributions. If the isomerization of these lower primary radicals occurred immediately after their formation, one would expect much more lower secondary radicals than lower primary radicals before they underwent further reactions, according to the R-K mechanism [8]. If this were the case, one would observe significant amounts of lighter branched alkanes ($< C_m$) in addition to heavy ones because the addition reactions between these lower secondary radicals and 1-alkenes could also occur. The results shown in Figure 15 clearly indicate the absence of significant amounts of lighter branched alkanes.

The final product distributions are dependent upon the reaction conditions. At high temperatures and low pressures (low loading ratios), unimolecular radical decomposition reactions (eqs 5a and 5b) are favored over bimolecular reactions such as hydrogen abstraction (eq 4) and radical addition (eq 6) because of higher activation energies than bimolecular reactions and low reactant and product concentrations. At low temperatures and high pressures (high loading ratios), bimolecular reactions are favored over radical decomposition reactions. According to the elementary kinetic parameters given by Ranzi et al. [9] for the thermal decomposition of long-chain *n*-alkanes, the relative rates of radical decomposition to hydrogen abstraction can be estimated. For a heavier primary radical in the system of n-C_{14} as a reactant, for example, the estimated rate parameters for β-scission are $A = 10^{14.0}$ 1/s and $E_a = 30.0$ kcal/mol while those for hydrogen abstraction are $A = 10^{8.3}$ L/(mol s) and $E_a = 12.0$ kcal/mol. At 425 °C and a loading ratio of 0.36, the rate ratio of radical decomposition to hydrogen abstraction would be 0.84:1. This means that about 54% of the larger primary radicals formed from β-scission of the parent radicals would tend to be stabilized by hydrogen abstraction from the surrounding reactant molecules rather than undergoing further decomposition. This would result in the formation of significant amounts of higher *n*-alkanes. Since the hydrogen abstraction would gradually be favored as loading ratio increases, the yields of higher *n*-alkanes would increase and correspondingly those of 1-alkenes would decrease with increased loading ratio (Figures 16–19). Also, the depressed radical decomposition rate would result in lower yields of C_1-C_3 gases at higher loading ratio (Figure 19).

The formation of C_{m+2} to C_{2m-2} heavy normal and branched alkanes clearly indicates that significant addition reactions between parental radicals and 1-alkenes occur. This can be further confirmed from the literature. Ford [10] found significant amounts of C_{18}-C_{30} branched and normal alkanes in the liquid-phase thermal decomposition of *n*-hexadecane. Khorasheh and Gray [11] observed similar results in a study of high-pressure thermal cracking of *n*-hexadecane. Ford [10] identified all heavy alkanes as alkyl hexadecanes and attributed their formation to the addition reactions between parent *n*-hexadecyls (secondary or primary) and 1-alkenes. The results obtained

in this study are consistent with Ford's suggestion. As shown in Figure 26 for the thermal decomposition of *n*-C_{14} at 425 °C for 15 min, the heavy alkanes with the same carbon number are composed of seven different compounds, that is, one normal alkane and six alkyl tetradecanes with branch at sites 2 to 7 of the carbon skeleton, which were identified based on their retention orders by analogy with those reported by Ford [10]. The seven different compounds are produced for each carbon number because there are only seven different C_{14} radicals. The C_{16} to C_{26} normal and branched alkanes are formed (Figure 15) since the addition reactions occur between primary and secondary C_{14} radicals and C_2 to C_{12} 1-alkenes, which are primary products of thermal decomposition. There are negligible amounts of C_{27} alkanes because of low concentration of 1-C_{13}.

In the reaction products from the thermal cracking of *n*-C_{10}, *n*-C_{12} and *n*-C_{14}, we also noted the presence of *n*-C_{m-1} and *n*-C_{m+1}. The same observation was obtained by Khorasheh and Gray [11] in the high-pressure thermal decomposition of *n*-hexadecane. The formation of *n*-C_{m-1} and *n*-C_{m+1} in the thermal cracking of *n*-C_m can be explained by the addition reactions between low primary radicals and 1-alkenes (eq 6). For example, the addition of 1-pentyl radicals to the terminal carbons of 1-C_{m-6} and 1-C_{m-4} results in the formation of secondary C_{m-1} and C_{m+1} radicals, which then abstract hydrogen atoms from surrounding reactant molecules to produce the corresponding *n*-alkanes.

The addition reactions between alkyl radicals and 1-alkenes have activation energies as low as 7 to 8 kcal/mol [12] and thus are favored at lower temperatures as used in this study. As long as the concentrations of 1-alkenes reach some extent, this secondary reaction could occur significantly. Since the radical addition reactions are enhanced as loading ratio and/or conversion increases because of increased 1-alkene concentrations, the yields of heavy normal and branched alkanes would be expected to increase with increased loading ratio and/or conversion, as observed in Figures 16 and 22.

It is interesting to note that the mole yields of C_6-C_{m-1} *n*-alkanes increase as conversion increases (Figures 22 to 24). Intuitively the mole yields of C_6-C_{m-1} *n*-alkanes should decrease with increased conversion because of increased rates of addition reactions between C_6-C_{m-1} radicals and 1-alkenes (eq 6) (due to increased concentrations of 1-alkenes), and increased rates of addition reactions between parent radicals and 1-alkenes (eqs 7a and 7b). The latter factor would result in decreased formation of primary products (C_1 to C_{m-2} *n*-alkanes and C_2-C_{m-1} 1-alkenes) per 100 mol of reactant converted because the percent of parent radicals which can not undergo decomposition would increase as conversion increases. One possible explanation for the increased molar yields of C_6-C_{m-1} *n*-alkanes with increased conversion is that addition reactions are heavily weighted toward small radicals and small 1-alkenes because of higher oriented collision frequencies [13]. As conversion increases, the addition rates between small radicals and small 1-

alkenes would increase much faster than those between larger radicals and larger 1-alkenes. As a result, the yields of higher *n*-alkanes (e.g., C_6-C_{13}) increase while those of lighter ones (C_1 to C_4) decrease with increased conversion (Figure 24). The other possible explanation is that the rates of hydrogen abstraction reactions (eq 4) increase as conversion increases. In the closed reactor, pressure would increase with increased conversion because of the increased product concentrations. Since pressure increase would increase the rate constant of bimolecular hydrogen abstraction reaction and suppress that of unimolecular radical decomposition, the yields of higher *n*-alkanes would be expected to increase and those of 1-alkenes and light *n*-alkanes would decrease with increased conversion.

The double bond isomerization, which results in the formation of 2-alkenes, can be explained by the following mechanism suggested by Shabtai et al. [14]:

$$R\bullet + R'CH_2CH{=}CH_2 \rightarrow RH + R'\dot{C}HCH{=}CH_2 \qquad (10)$$

$$R'\dot{C}HCH{=}CH_2 \leftrightarrow R'CH{=}CH\dot{C}H_2 \qquad (11)$$

$$R'CH{=}CH\dot{C}H_2 + RH \rightarrow R'CH{=}CHCH_3 + R\bullet \qquad (12)$$

Since the concentrations of C_6-C_{12} 1-alkenes increase as loading ratio or conversion increases, the mole yields of corresponding 2-alkenes would increase with increased loading ratio or conversion, as shown in Figures 16 and 22. Other internal alkenes can also be formed by the similar mechanism. It can be expected that after a certain conversion a balance would be reached so that the mole yields of 2-alkenes would no longer increase with further increase in conversion (Figure 22).

Although the mechanism presented above provides good explanations for the observed experimental results, it is difficult to estimate whole product distributions quantitatively because the kinetic parameters for secondary reactions are not known. However, if we focus our attention on low conversions, it is possible to predict primary product distributions because we can neglect secondary reactions.

The following calculations were performed for the thermal decomposition of *n*-C_{14} at 425 °C and at different loading ratios, on the basis of the method suggested by Fabuss et al. [15]. In order to determine the distributions of initial C_{14} parent radicals, it is assumed that the activation energy for the formation of a secondary C_{14} parent radical is 2 kcal/mol lower than that for the formation of a primary C_{14} parent radical [8]. The C_{14} parent radicals initially formed are assumed to undergo isomerization in such a way that any radical can only isomerize into a free radicals in which the radical position is four or more carbon atoms away from the original position. For

example, the 2-tetradecyl radical can only isomerize into one of these radicals in which the radical positions can be found from 6 to 14. For the isomerization of the initial parent radicals, it is assumed that the secondary radicals are 4 kcal/mol more stable than the primary radicals [8].

The various C_{14} parent radicals formed after isomerization can decompose by β-scission into an 1-alkene and a lower primary radical. When two positions are available for β-scission, the relative rates for rupture are assumed to be equal if both processes give ethyl or higher primary radicals. The rupture to yield a methyl radical is assumed to require an activation energy of 1.5 kcal/mol higher than the rupture to produce a higher primary radical [9].

Under the conditions used in this study, some of the lower primary radicals formed from the decomposition of parent radicals would isomerize and then immediately decompose according to the same rules used above. The rest of the radicals would abstract hydrogen from surrounding reactant molecules to produce an *n*-alkane and a parent radical because secondary reactions are negligible at low conversion. The relative rates of radical decomposition to hydrogen abstraction increase with increased radical size [13]. To account for observed product distributions, it is assumed that the rate ratio of radical decomposition to hydrogen abstraction doubles as the carbon number of the radical increases for one. For the thermal decomposition of *n*-C_{14} at 425 °C and at a loading ratio of 0.357, this ratio is taken as one for C_{10} radicals. The rate ratio for other radicals can be calculated according to the above assumption. For the reactions carried out at other loading ratios, the rate ratio of decomposition to hydrogen abstraction for any radical can be obtained from the corresponding value at 0.357 loading ratio multiplied by a factor which is equal to 0.357 divided by the loading ratio examined. The small radicals formed from the decomposition of those lower radicals are assumed to be stabilized by abstracting hydrogen from surrounding reactant molecules and no longer undergo further decomposition.

Figures 27 to 29 show the comparisons between predicted product distributions by the method stated above and experimental results from the thermal decomposition of *n*-C_{14} at 425 °C for three different loading ratios and at lower conversions. Taking into account the assumptions made on the decomposition of those lower radicals, the agreement between predicted and experimental product distributions is quite satisfactory. In order to predict the product distributions at higher conversion, a much more sophisticated calculation is required because of significant secondary reactions.

References

1. Schobert, H. H.; Eser, S.; Song, C.; Hatcher, P. G.; Boehman, A.; Coleman, M. M. *Advanced Thermally Stable Jet Fuels.* Technical Progress Report (January 1995 - March 1995), June **1995**, The Pennsylvania State University.

2. Kunzru, D.; Shah, Y. T.; Stuart, E. B. Thermal Cracking of *n*-Nonane. *Ind. Eng. Chem. Process Des. Dev.* **1972**, *11*, 605-612.

2. Kunzru, D.; Shah, Y. T.; Stuart, E. B. Thermal Cracking of *n*-Nonane. *Ind. Eng. Chem. Process Des. Dev.* **1972**, *11*, 605-612.

3. Depeyre, D.; Flicoteaux, C.; Blouri, B.; Ossebi, J. G. Pure *n*-Nonane Steam Cracking and the Influence of Sulfur Compounds. *Ind. Eng. Chem. Process Des. Dev.* **1985a**, *24*, 920-924.

4. Depeyre, D.; Flicoteaux, C.; Chardaire, C. Pure *n*-Hexadecane Thermal Steam Cracking. *Ind. Eng. Chem. Process Des. Dev.* **1985b**, *24*, 1251-1258

5. Billaud, F.; Freund, E. *n*-Decane Pyrolysis at High Temperature in a Flow Reactor. *Ind. Eng. Chem. Fundam.* **1986**, *25*, 433-443.

6. Voge, H. H.; Good, G. M. Thermal Cracking of Higher Paraffins. *J. Am. Chem. Soc.* **1949**, *71*, 593-597.

7. Rebick, C. H_2S Catalysis of *n*-Hexadecane Pyrolysis. *Ind. Eng. Chem. Fundam.* **1981**, *20*, 54-59.

8. Kossiakoff, A.; Rice, F. O. Thermal Decomposition of Hydrocarbons, Resonance Stabilization and Isomerization of Free Radicals. *J. Am. Chem. Soc.* **1943**, *65*, 590-595.

9. Ranzi, E.; Dente, M.; Pierucci, S.; Biardi, G. Initial Product Distributions from Pyrolysis of Normal and Branched Paraffins. *Ind. Eng. Chem. Fundam.* **1983**, *22*, 132-139.

10. Ford, T. Liquid-Phase Thermal Decomposition of Hexadecane: Reaction Mechanisms. *Ind Eng. Chem. Fundam.* **1986**, *25*, 240-243.

11. Khorasheh, F.; Gray, M. R. High-Pressure Thermal Cracking of *n*-Hexadecane. *Ind. Eng. Chem. Res.* **1993**, *32*, 1853-1863.

12. Allara, D. L.; Shaw, R. A Compilation of Kinetic Parameters for the Thermal Degradation of n-Alkane Molecules. *J. Phys. Chem. Ref. Data*, **1980**, *9*, 523-559.

13. Dente, M. E.; Ranzi, E. M. Mathematical Modeling of Hydrocarbon Pyrolysis Reactions. In *Pyrolysis: Theory and Industrial Practice*; Albright, L. F., Crynes, B. L., Corcoran, W. H., Eds.; Academic Press: New York, 1983; pp 133-175.

14. Shabtai, J.; Ramakrishnan, R.; Oblad, A. G. Hydropyrolysis of Model Compounds. *Adv. Chem. Ser.* **1979**, *183*, 297-328.

15. Fabuss, B. M.; Smith; J. O.; Satterfield, C. N. Thermal Cracking of Pure Saturated Hydrocarbons. *Adv. Petro. Chem. Refin.* **1964**, *9*, 157-201.

3. The Use of Site-Specific ^{13}C-labeling to Examine the Thermal Degradation of Jet Fuel Components (Contributed by Daniel E. McKinney, Jacqueline M. Bortiatynski, and Patrick G. Hatcher)

Introduction

As discussed in a previous report, a strong case was made for the use of site-specific ^{13}C-labeling to examine the reactions of target components in complex mixtures such as jet fuel (Schobert et al.). The ^{13}C label serves as a flag for tracing of chemical transformations that occur in complex organic matrices (McKinney et al., 1993; Schobert et al., 1994; Burnham et al., 1995). Two analytical approaches have been used to examine the ^{13}C isotope flags and determine the structural changes that occur during thermal stressing. The method developed by Burnham et al. (1995) utilizes doubly-^{13}C-labeled substrates and gas chromatography-mass spectrometry to examine thermal stressing reaction kinetics. The second method utilized by McKinney et al. (1993) employs ^{13}C-labeling in combination with ^{13}C NMR to examine the reaction pathways and kinetics of the thermal stressing of 1-phenyl-1-^{13}C-hexane in a JP-8C jet fuel. As also discussed in this previous report was that the primary draw back of these studies is the cost of obtaining site specific ^{13}C-labeled substrates to carry out the reactions. The focus of this report is an update of the progress that has been made to obtain additional ^{13}C-labeled jet fuel components for future thermal stressing experiments.

Experimental

1. General Reaction Scheme. Reagent grade chemicals were purchased from Aldrich Chemicals and each reaction was carried out first without any ^{13}C-labeled precursor to optimize the reaction conditions for each of the steps shown in Scheme 1 (Schobert et al., 1994). The $K^{13}CN$ was purchased from Isotech Inc. and will be employed using the optimized reaction conditions.

2. Synthesis of 6-^{13}C-Dodecane. A detailed description of the optimized reaction conditions will appear in a future report, since the refinement of reaction conditions is currently in progress.

3. Synthesis of 1-Cyclohexyl-1-^{13}C-Hexane. A detailed description of the optimized reaction conditions will appear in a future report, since the reactions have not yet been carried out.

Scheme 1

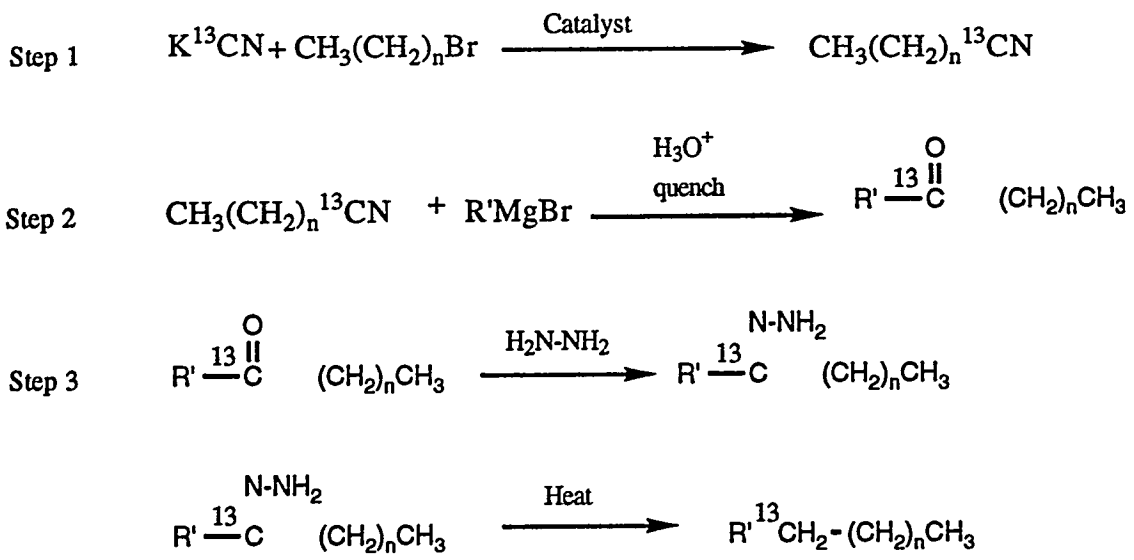

4. Thermal Stressing 1-Phenyl-1-^{13}C-Hexane for Isotope Ratio Monitoring Mass Spectrometry. Pyrolysis experiments for 1-phenyl-1-^{13}C-hexane were carried out in a 15 mL tubing bomb reactor at 400°C for heating periods of 1, 2, 4, and 6 hours under an initial inert pressure of 6.9 MPa UHP-N_2 (cold). The details of the tubing bomb thermal pyrolysis protocol has been discussed elsewhere (Song et al., 1993, 1994). Briefly, the 15 mL stainless steel reactor were loaded with 5 mL of JP-8C and 0.05 mL of 1-phenyl-1-^{13}C-hexane and purged repetitively with 6.9 MPa UHP-N_2 (3 times) to remove oxygen/air in the reactor or dissolved sample. Following reaction, the reactor was removed from the fluidized sand bath and quenched in a cool water bath. Only the liquid product was collected from the reaction and each bomb was examined by gas chromatography.

5. Instrumentation. Quantitative gas chromatography (GC) was carried out on each sample using a Hewlett-Packard 5890 II gas chromatograph with flame ionization detection (FID) equipped with a J&W DB-5 fused silica column (30 m, 0.25i.d., 0.25um film thickness).

Results and Discussion.

The synthesis of 6-^{13}C-dodecane is currently being carried out. Each step is being optimized with unlabeled materials to ensure that the maximum amount of ^{13}C-labeled product is produced. Following the synthesis of 6-^{13}C-dodecane a set of thermal stressing experiments will be carried out in JP-8C in an identical manner to those performed on 1-phenyl-1-^{13}C-hexane (Schobert et al., 1994). The products and kinetics of the pyrolysis reactions will be determined by gas chromatography and ^{13}C NMR.

The determination of the optimal synthetic protocol for 1-cyclohexyl-1-^{13}C-hexane will be carried out concurrently with the thermal stressing experiments discussed above. Once synthesized, thermal stressing experiments and product analysis will be carried out on the 1-cyclohexyl-1-^{13}C-hexane using the conditions established for the ^{13}C-labeling experiments (Schobert et al., 1994).

In an effort to obtain additional information concerning the thermal stressing of jet fuel components, a second set of pyrolysis experiments were carried out on 1-phenyl-1-^{13}C-hexane. Isotope ratio monitoring experiments will be used to examine all the products that carry the ^{13}C-label. This method of analysis is extremely sensitive and will allow for the identification of products that will be difficult with ^{13}C NMR methods due to their very low concentrations. Once identified, a more complete picture of the reaction pathways of the ^{13}C-labeled components can be established.

References:

1. Burnham, A.K.; Gregg, H.R.; Braun, R.L. *Energy Fuels* **1995**, 9, 190.
2. McKinney, D.E.; Bortiatynski, J.M.; Hatcher, P.G.; *Energy Fuels* **1993**, 7, 578.
3. Schobert, H.H.; Eser, S.; Song, C.; Hatcher, P.G.; Walsh, P.M.; Coleman, M.M. *Advanced Thermally Stable Jet Fuels* Technical Progress Report, 92PC92104-TPR-6, January, 1994.
4. Schobert, H.H.; Eser, S.; Song, C.; Hatcher, P.G.; Walsh, P.M.; Coleman, M.M. *Advanced Thermally Stable Jet Fuels* Technical Progress Report, 92PC92104-TPR-6, January, 1994.
5. Hatcher, P.G.; Walsh, P.M.; Coleman, M.M. Advanced Thermally Stable Jet Fuels Technical Progress Report, 92PC92104-TPR-9, July, 1994.
6. Song, C.; Eser, S.; Schobert, H.H.; Hatcher, P.G. *Energy Fuels* , **1993**, 7, 234.
7. Song, C.; Lai, W.C.; Schobert, H.H. *Ind. Eng. Chem. Res.*, **1994**, 33, 534.

Task 2. Investigation of Incipient Deposition

Deposit Growth During Heating of Coal-Derived Aviation Gas Turbine Fuels (Contributed by Prashant C. Sanghani and Andre Boehman)

In a previous report, we compared deposit growth on surfaces and in the bulk during pyrolysis of mixtures of tetradecane and coal derived jet fuel (JP8C). An improved analysis technique to quantify the species concentration was mentioned. Detailed quantification of various species is not yet complete.

Previously [1] we were able to correlate decomposition of tetradecane with formation of solids on the wall (which also means that tetradecane is the only contributor to solid formation). This simple model was unable to simulate the induction period for the onset of significant deposition. The actual fuel contains hundreds of components and any one of these compounds could contribute to solid formation by undergoing decomposition and forming an active radical.

Pyrolytic studies of pure compounds at 450°C and under a nitrogen environment have been performed by our group [2]. The compounds studied were *n*-decane, *n*-butylbenzene, *n*-butylcyclohexane, decalin, tetralin, naphthalene, *t*-butylbenzene, ethylcyclohexane and tetradecane.

The formation of solids from decane depends strongly on temperature. Figure 30 shows that treatment of decane at 400°C for 72 hours produced only 45mg of solids whereas heating at 450°C produced 460 mg solids in 10 hours. Since fuel degradation reaction occurs through free radical reaction and at 400°C the rate of initiation of free radical reaction is negligible, because of this a negligible radical pool exists to trigger the solid formation at 400°C and therefore no deposit forms at 400°C. Heating of butylbenzene at 450°C produced a significant amount of solid. Liquid products from *n*-butylbenzene obtained at 450°C for 4 hours included compounds such as alkylbenzenes, naphthalene and alkylnaphthalenes, biphenyl and alkyl biphenyls, bibenzyl, phenanthrene and terphenyl. *n*-Butylcyclohexane was found to be fairly stable and produced very little solids. Ethyl cyclohexane was more stable than *n*-butylcyclohexaane and produced apparently no solids. Since pyrolysis of alkylated benzenes produced significant quantity of naphthalene and alkylated naphthalenes, it is necessary to know the behavior of naphthalene. Treatment of naphthalene at 425 and 450°C for 48 hours did not produce solids. Similarly, decalin, which is one of the major components of coal-derived jet fuel, did not produce solids for 24 hours at 450°C. Figure 31 shows plot of solid produced from decane and decalin at 425°C and 450°C. Tetralin was found to give no solids for 48 hours at 450°C. *t*-Butyl benzene was found to have an induction period of 5 hours when stressed alone.

Knowing the results of individual compound pyrolysis can help understand the behavior of actual fuel. However, when the compound is in a complex mixture it does not necessarily behave in the same manner as it behaves during individual pyrolysis. The reason we could correlate the

tetradecane decomposition with deposit growth might be because tetradecane produced the most solids of any compound in the individual compound studies.

We have mentioned in a previous report the idea of grouping the species in terms of their tendency to form solids, based on a statistical analysis of compound variations during stressing. Since there are so many compounds and many of them coelute in the GC column and many of them ionize to a different extent, calculating the ratio of ion abundance and combining it with GC-FID results will not always work. Because of this, the known mixture in several different relative concentrations needs to be injected. After incorporation of this technique, we will present further development of kinetic model for incipient deposition and results of fuel pyrolysis.

References

1. H.H. Schobert, et al, Advanced Thermally Stable Jet Fuels, Technical Progress Report, January 1994 - March 1994.
2. S. Eser et al, Annual Progress Report July 1989- June 1990.

Task 3. Characterization of Solid Gums, Sediments, and Carbonaceous Deposits

2. *Effects of High Surface Area Activated Carbons on Thermal Stressing of Model Compounds (contributed by Katia Gergova, Rathnamala Arumugam, and Semih Eser)*

In our previous work we studied the effect of high surface area activated carbon PX-21 (BET surface area 2090 m^2/g) addition on thermal decomposition reactions. It has been established that activated carbon addition promoted a variety of reactions during thermal treatment of jet fuels and model compounds. The reactivity of an activated carbon depends on the nature of the carbon surface, presence of carbon-oxygen surface groups, availability of the active sites and surface areas. It has been shown that the activated carbon surface area is an important parameter which determines to a large extent, the effectiveness of added carbon in suppressing solid deposition during thermal stressing at high temperatures [1].

In this study we used three new high surface area activated carbons Maxsorb provided by the Kansai Coke and Chemicals Company, Ltd. Two granulated carbons were used in our study Maxsorb 94-06 and Maxsorb 94-20 and one powdered carbon Maxsorb 92-11A. Activated carbons have the following BET surface area:

Maxsorb 94-20	2080 m^2/g
Maxsorb 94-06	2320 m^2/g
Maxsorb 92-11A	3190 m^2/g

We also studied the effect of hydrogen donor, decalin, in addition to high surface area activated carbon PX-21 during thermal stressing. The activated carbon addition appears to promote H-transfer reactions during thermal stressing [2]. There seems to be synergistic effect between activated carbon and decalin addition in suppressing the thermal degradation reactions.

In the present work, 5% decalin was also added to dodecane and the mixture was stressed with 100 mg of each Maxsorb carbon at 450°C for 1h. Initially colorless, all dodecane samples turned yellow after thermal stressing. The darkest was the color of liquid stressed with Maxsorb 91-11A followed by Maxsorb 94-20, and Maxsorb 94-06.

All liquids stressed with activated carbons were lighter in color than the liquids stressed without carbons which appear to have brown color. There was no deposit formation on the reactor walls after thermal stressing of dodecane +5% decalin in contrast to 20 mg deposit on the reactor walls after thermal stressing without carbon.

Gas Chromatography(GC) of liquid samples was conducted using Perkin Elmer 8500 GC with a fused silica capillary column. Compounds in the liquid products were identified by capillary gas chromatography-Mass spectrometry (GC-MS) using a Hewlett-Packard 5090 II GC coupled with HP 5971 A mass selective detector.

Figure 1 shows the concentration of dodecane in the stressed liquids and indicates that the addition of Maxsorb carbons inhibits decomposition of dodecane. The most effective carbon is Maxsorb 94-06, followed by Maxsorb 94-20 and Maxsorb 92-11A. The liquids obtained after thermal stressing of dodecane+decalin with Maxsorb carbons have 10-11% higher dodecane concentration than the liquids stressed without carbons.

Figure 2 shows the ability of activated carbons to promote H-transfer reactions during thermal stressing. The concentration of naphthalene in the stressed liquids increased considerably in the presence of Maxsorb carbons. The highest is the concentration of naphthalene in the liquid obtained after thermal stressing of dodecane + 5% decalin mixed with Maxsorb 92-11A, followed by Maxsorb 94-06, and Maxsorb 94-20. We assumed in our previous study that part of the naphthalene in the liquids obtained after stressing with PX-21 is a result of decomposition reactions rather than H-transfer reactions. One can see (Figure 2) that the naphthalene concentration is lower for the liquid stressed with Maxsorb 94-20 than the liquid stressed with Maxsorb 92-11A. These results suggest that Maxsorb 94-20 is the most effective between the investigated Maxsorb carbons in preventing decomposition reactions and stabilizing free radicals.

The lower temperature (425°C) and longer time (5h) was also used to study the effect of 50 mg Maxsorb activated carbon added during thermal stressing of dodecane + 5% decalin and the results are compared with the effect of PX-21 carbon. The appearance of liquids obtained after stressing with Maxsorb carbons is similar (yellow in color) to this of PX-21 carbon. Darker is the color of the liquid obtained from stressing with Maxsorb 92-11A. The liquid stressed without carbon at the same conditions showed dark brown color and produced 30 mg deposit at 425°C for 5h.

Figure 3 shows the dodecane concentration after thermal stressing . Maxsorb 92-20 has the largest effect on preventing degradation of dodecane. The comparison of Figure 3 and Figure 1 (dodecane concentration after thermal stressing at 450°C for 1h) suggests that:

- Dodecane + 5% decalin mixture is more stable at lower temperature (425°C) even for longer period of time (5h compared to 1h) than at higher temperature (450°C).
- Maxsorb activated carbons have a more strong effect on thermal stability of dodecane+5% decalin during stressing at 450°C for 1h than at 425° for 5h. This temperature dependence can be attributed to more effective H-transfer reactions on carbon surfaces at a higher temperature.

Figure 4 shows the naphthalene concentration of the liquids obtained after thermal stressing at 425°C for 5h. The results are comparable to these from Figure 2 (450°C, for 1h). The naphthalene concentration increases considerably in the presence of carbons because of the H-transfer reactions. Figure 4 confirmed the higher activity of Maxsorb 94-20 compared to other two carbons. The naphthalene concentration of the liquids stressed with granulated Maxsorb 94-20 and Maxsorb 94-06 for both temperatures is lower than the naphthalene concentration of the liquid

stressed with powdered Maxsorb 92-11A. This is an indication that granulated activated carbons are more effective in preventing thermal degradation reactions.

The effect of extraction on the activity of Maxsorb carbons during thermal stressing of model compounds at 450°C for 1h In our previous study we determined that the extraction of PX-21 with toluene proved the presence of some aromatic hydrocarbons which possibly diminish the activity of PX-21 during thermal stressing [3]. The Maxsorb activated carbons were extracted in Soxhlet apparatus using 300 ml toluene and 5g sample for 24h. Dodecane +5% decalin were stressed at 450°C for 1h in the presence of extracted carbons.

Figure 5 compared the dodecane concentration of liquids in the presence of original and extracted carbons. One can see clearly that extracted carbons have up to 10% higher dodecane concentration depending on carbon used. The greatest is the effect of extracted carbon Maxsorb 94-06 which appears to be also very effective in stabilizing thermal degradation of dodecane+decalin when is used in its original form.

Figure 6 shows the naphthalene concentration of the liquids obtained from thermal stressing of dodecane +5% decalin in the presence of original and extracted carbons. As different from dodecane concentration, naphthalene concentration in the stressed liquids decreases when extracted carbons were used. These demonstrated that some of naphthalene compounds identified in the liquids after thermal stressing are due to thermal degradation and not only H-transfer reactions. The stronger the effect of activated carbon added, the lower the concentration of naphthalenes which are precursors of carbonaceous solids.

Microstructure of used Maxsorb carbons after thermal stressing with model compounds at 425°C for 5h. In our previous report we studied the microstructure of used PX-21 carbon [3]. The long tubular carbonaceous solids were observed on the overlayer which covered the used PX-21 carbon and obviously were formed during the second thermal stressing of the used carbon.

The scanning electron microscope (SEM) ISI model SX 40-A was used to study the microstructure of Maxsorb carbons 94-20 and 92-11A stressed subsequently with dodecane and decalin mixture at 425°C for 5h. The SEM micrographs of stressed carbons are shown in Figure 7a,b. The tubular deposits shown in Figure 7a,b were observed in various areas of stressed carbons and they usually appear to have hoop band structure (Figure 7a). It is interesting that there are more of these structures on the granulated used carbon Maxsorb 94-20 (Fig 7a) than on the surface of powdered used carbon Maxsorb 92-11A (Fig7b). Most probably this is due to the larger surface of granulated carbon which provided more suitable conditions for the tubular growth. The deposit shown on the surface of Maxsorb carbons on the carbonaceous overlayer as well as the deposits on the carbonaceous overlayer of PX-21 carbon formed during thermal stressing at relatively low temperature of 425°C.

Conclusions

The high surface area activated carbons Maxsorb 94-20, 94-06, and 92-11A were stressed with the model compounds dodecane and 5% decalin at 450°C for 1h and 425°C for 5h. It appears that they suppress the carbon deposition and help retard the degradation of dodecane. These carbons showed the same effect as PX-21 carbon which was used in our previous work. The considerable difference in the surface area of Maxsorb carbons (1000 m^2/g) does not effect the performance of activated carbons during thermal stressing. This is an indication that surface area higher than 2000 m^2/g does not increase the catalytic effect and the ability of carbon to suppress carbon deposition during thermal stressing.

The concentration of naphthalene in the stressed liquids depends on both H-transfer reactions and degradation processes that took place during thermal stressing.

The toluene extraction of activated carbons before thermal stressing resulted in an increase in the effectiveness of activated carbon added before thermal stressing.

Unusual tubular deposits were formed on the carbonaceous overlayer of Maxsorb carbons as well as PX-21 carbon after they were stressed subsequently with dodecane and decalin at 425°C.

References:

1. H. H. Schobert, S. Eser, C. Song, P. G. Hatcher, P. M. Walsh, M. M. Coleman, Advanced Thermally Stressed Jet Fuels, Technical Progress Report, P2PC92104- TPR-2, November-January 1993.

2. H. H. Schobert, S. Eser, C. Song, P. G. Hatcher, A. Boehman, M. M. Coleman, Advanced Thermally Stressed Jet Fuels, Technical Progress Report, P2PC92104- TPR-9, July 1994.

3. H. H. Schobert, S. Eser, C. Song, P. G. Hatcher, A. Boehman, M. M. Coleman, Advanced Thermally Stressed Jet Fuels, Technical Progress Report, P2PC92104- TPR-11, January - March 1995.

Task 4. Coal-based Fuel Stabilization Studies

Further Studies on Potential Jet Fuel Stabilizers. (Contributed by Emily M. Yoon, Michael M. Coleman, and Chunshan Song)

Introduction

In a previous report, we demonstrated that THQ (1,2,3,4-tetrahydroquinoline) was an effective thermal stabilizer for jet fuels for temperatures 400-500°C [1]. Understanding why THQ is an outstanding thermal stabilizer at high temperatures is important, and a number of compounds compounds (listed below) were evaluated as potential additives in the model compound dodecane. It was also a goal of these studies to enhance our understanding of the underline mechanisms involved in thermal stability of jet fuels and the like.

Results and Discussions

The compounds evaluated were 5,6,7,8-tetrahydroquinoline (**2**), 1,2,3,4-tetrahydro-isoquinoline (**3**), 5,6,7,8-tetrahydroisoquinoline (**4**), 1,2,3,4-tetrahydronaphthalene (**5**), 1,2,3,4,5,6,7,8-octahydrophenanthrene(**6**), 9,10-dihydrophenanthrene (**7**) with structures shown in Scheme 1, along with 1,2,3,4-tetrahydroquinoline (**1**), benzyl alcohol (**8**), and 1,4-benzenedimethanol (**9**).

Scheme 1

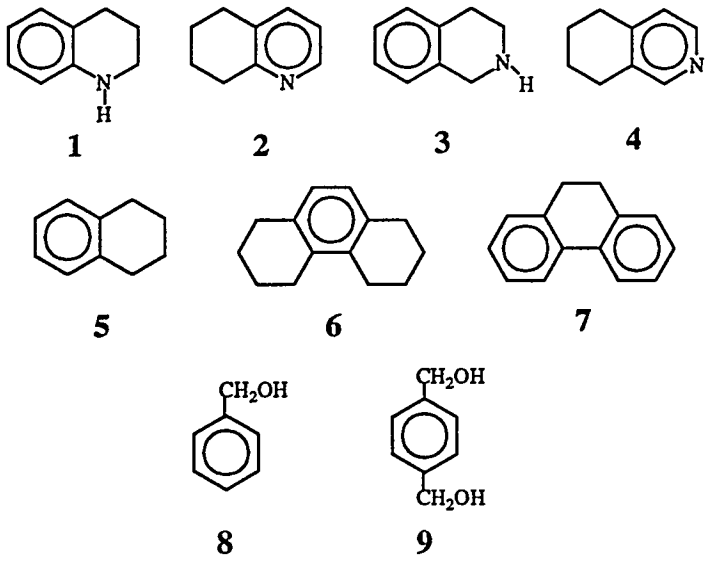

Thermal stressing was performed on 10 mL dodecane samples containing the additive (10 mol% with respect to dodecane) at 425°C for various periods of time (3–9 hrs). The total weight of gases formed upon thermal stressing was obtained by measuring the weight difference of the reactor before and after venting the gases upon thermal stressing. The liquid products were analyzed using a Perkin-Elmer GC with a FID detector. The reaction products were analyzed using GC/MS.

Isomers of THQ (**2, 3, 4**) were evaluated to study the effect of N atom position in the ring. Tetralin (**5**), which has a structure similar to THQ, but without the N atom in the ring was studied in order to probe the effect of N atom on hydrogen transfer. In a similar vein, the importance of the number of transferable hydrogens and the type of ring system present was probed using the compounds **6–9**. Figures 39 and 40 show respectively the yield of gas results obtained from the 3 and 6 h thermal stressing experiments of dodecane at 425°C. Based upon the amount of gases formed after 3 h at 425°C, THQ (compound **1**) is the most effective thermal stabilizer. Additives **5, 6, 7,** and **9** appear reasonable while additives **2, 3, 4,** and **8** are poor. After 6 h at 425°C (Fig. 40), only THQ (compound **1**) and possibly compound **7** are superior thermal stabilizers at a concentration of 10 mol%.

Figures 41 and 42 show mole% dodecane remaining in the recovered liquid after 3 h and 6 h of thermal stressing at 425°C, respectively. Compound **7** (9,10-dihydrophenanthrene) was not soluble in dodecane even after thermal stressing and therefore the liquid analysis data is not feasible. Similarly, data for compound **9** (1,4-benzenedimethanol) was not obtained after 3 h thermal stressing because of its insolubility in dodecane. Returning to Figure 41, approximately 96 mol% of dodecane remains in the presence of THQ after 3 h at 425°C. In contrast, the dodecane mixtures containing additives 2, 3, 4, 5, 6, and 8 have only about 65– 85 mol% dodecane remaining. This effect is more dramatic after 6 h at 425°C as illustrated in Figure 42. Now approximately 90 mol% of dodecane still remains in the presence of THQ, while only between approximately 35–55 mol% of dodecane remains in the presence of the other additives.

The relative thermal stabilities of the additives and the reaction products formed from them during thermal stressing were determined by GC and GC/MS and are reported in Table 7. By analyzing these products, the superior thermal stability of THQ as an additive over the other compounds can be rationalized. Although compounds **1–4** have the same number of hydrogens available for hydrogen transfer, the results indicate that the position of N atom in the ring system is important. Compound **3** (1,2,3,4-tetrahydroisoquinoline) is not as stable as compound **1** (THQ), because the ring opens to form 1,2-dimethylbenzene, 1-ethyl-2-methyl- benzene, 1-ethenyl-2-methylbenzene, *o*-ethylbenzonitrile, and isoquinoline. When compound **3** loses the H-atom from the N–H bond, the resultant radical is not resonance stabilized

whereas the radical from compound **1** (THQ) is resonance stabilized by delocalization through the aromatic ring. Compounds **2** and **4** are not stable at 425°C as they convert quickly to quinoline and isoquinoline, respectively. In compounds **2** and **4**, the hydrogen transfer occurs from the C–H bond, where the bond dissociation energy of C–H is 96–99 kcal/mol while compound **1** (THQ) loses a H-atom from the N-H bond which has the bond dissociation energy of 84 kcal/mol [2]. Consequently, it is more difficult to abstract H-atoms from compounds **2** and **4** compared to compound **1** (THQ). Compound **5** (tetralin) also is not stable at 425°C as it forms methyl indene, methyl naphthalene and naphthalene. Since compound **5** (tetralin) does not have a N-atom in the ring, the hydrogen transfer in this case once again occurs from C–H bond. Therefore, compound (tetralin) is not as effective as a thermal stabilizer as compound (THQ).

Although compound **6** (OHP) has eight hydrogens available for hydrogen transfer, it is not stable at 425°C; in addition to its dehydrogenation products like 1,2,3,4-tetrahydro-phenanthrene and phenanthrene, it degrades to form products like alkyl naphthalenes and alkyl benzenes. Compounds **8** and **9** are effective stabilizers, but when they are compared to compound **1** (THQ), they are not stable as THQ at high temperatures. Compound **8** (benzyl alcohol) produced benzene, methylbenzene, ethylbenzene and benzaldehyde. Compound **9** (1,4-benzenedimethanol) is a more effective stabilizer than compound **8** (benzyl alcohol), primarily because the doubling of the transferable hydrogens.

We conclude, therefore, that compound **1** (THQ) is a superior additive in inhibiting the thermal degradation of dodecane because: (a) it has four transferable hydrogens, (b) it is relatively stable at 425°C, (c) the N–H bond is weaker than the C–H bond, and (d) the radicals formed are stabilized by delocalization through the aromatic ring.

References

1. Yoon, E.M.; Coleman, M.M.; *Advanced Thermally Stable Jet Fuels*, Technical Progress Report, 92PC92104-TPR-10, February 1995.
2. March, J., Advanced Organic Chemistry, Wiley, 1992.

Task 5. Exploratory Studies on the Direct Conversion of Coal to High-Quality Jet Fuels.

1. Novel Approaches to Low-Severity Coal Liquefaction and Coal/Resid Co-processing using Water and Dispersed Catalysts. (Contribution by Russell Byrne and Chunshan Song).

Introduction

Previous work in our laboratory has demonstrated a remarkable synergism between water and a dispersed molybdenum sulfide catalyst for promoting liquefaction of Wyodak subbituminous coal at relatively low temperature (350–375°C) [1-5]. Based on these encouraging results with Wyodak coal, we have embarked on a more in-depth fundamental and exploratory study on the promotional effects of water on coal hydroliquefaction using dispersed catalysts. One of our current interests is to determine whether this potentially significant phenomenon is a rank-dependent characteristic.

In our last report, preliminary results from work using Pittsburgh #8 high-volatile bituminous coal were presented which indicated a similar marked improvement in coal conversion at 350°C through co-use of water with dispersed molybdenum sulfide catalyst. The overall improvement in conversion observed for the higher-rank coal, however, was somewhat less dramatic than that for Wyodak coal. Reactions performed at two different temperatures (350 and 400°C) were discussed in light of our earlier results for Wyodak coal.

We are presently completing a more thorough study of the effects of reaction temperature range (350–425°C) on the water-promoted catalytic liquefaction of Pittsburgh #8 coal. In the present report, we have constructed a temperature versus conversion profile with the data obtained to date for Pittsburgh #8 coal runs with ammonium tetrathiomolybdate (ATTM) and ATTM + water, as has previously been done by Song and Saini [1,5] for Wyodak coal runs. Notable trends and similarities between the conversion profiles for these two coals of different rank are discussed, in terms of the optimum temperature windows in which water-dispersed catalyst synergistic interaction is maximized. Effects of reducing the catalyst loading level from 1.0 wt% to 0.1 wt% Mo to dmmf coal are also discussed for the reactions of Wyodak coal at 350°C.

Experimental

The coals used were Wyodak subbituminous coal and Pittsburgh #8 high-volatile bituminous coal. These are Department of Energy Coal Samples (DECS-8 and DECS-12, respectively) maintained in the DOE/Penn State Coal Sample Bank, ground to ≤ 60 mesh, and stored under argon atmosphere in heat sealed, argon-filled laminated foil bags consisting of three layers. Wyodak subbituminous coal contains 28.4% moisture, 32.4% volatile matter, 29.3% fixed

carbon and 9.9% ash, on as-received basis; 75.8% C, 5.2% H, 1.0% N, 0.5% S, and 17.5% O, on dmmf basis. Pittsburgh #8 high-volatile bituminous coal contains 2.4% moisture, 35.2% volatile matter, 52.4% fixed carbon and 10.0% ash, on as-received basis; 84.8% C, 5.7% H, 1.4% N, 0.8% S, and 7.4% O, on dmmf basis. Both fresh raw coals, and coals pre-dried in a vacuum oven (vd) at 100°C for 2h were used. Reagent grade ammonium tetrathiomolybdate (ATTM, obtained from Aldrich with 99.97% purity) was employed as the dispersed catalyst precursor. The water-soluble inorganic salt ATTM is expected to generate molybdenum sulfide particles on the coal surface upon thermal decomposition at ≥ 325°C. ATTM was dispersed onto either the raw coal or vacuum-dried coal samples by incipient wetness impregnation from its aqueous solution. The metal loading was kept constant at 1 wt% Mo on dmmf coal basis, unless otherwise specified. Following impregnation, the coal samples were dried in a vacuum oven at 100°C for 2h prior to use.

Liquefaction experiments were carried out in 25 mL tubing bomb reactors with around 4g of coal at the desired temperature for 30 min (plus an additional 3 min for reactor heat-up time). For both thermal and catalytic experiments with added water, the weight ratio of water to dmmf coal was kept at around 0.46. All reactions described in this paper were performed in the absence of any organic solvent. The reactors were purged several times with H_2 and finally pressurized with 6.9 MPa H_2 (cold). A fluidized sandbath maintained at the desired temperature was used as the heater. After the desired reaction time, the reactors were removed from the sandbath and quenched in a cold water bath to rapidly bring down the temperature < 150°C, then were allowed to cool down to ambient temperature in air. The reactors were vented and the mass of product gases (including residual H_2) determined. Gaseous products were analyzed by GC, with the aid of gas standards for quantitative calibration of GC responses of CO_2, CO, H_2 and C_1–C_4 hydrocarbon gases. H_2 consumption was determined by subtracting the mass of residual H_2 found in the product gases (determined by GC) from the mass of H_2 initially charged. The liquid and solid products were carefully recovered from the reactor and transferred to an extraction thimble. The products were subsequently separated by sequential Soxhlet extraction into oil (hexane solubles), asphaltene (toluene soluble but hexane insoluble), preasphaltene (THF soluble but toluene insoluble), and residue (THF insoluble). Further experimental details may be found in the last quarterly report

Results and Discussion

Experimental results from the temperature versus conversion study for the catalytic solvent-free reactions of Pittsburgh #8 coal, performed in both the presence and absence of added water, are summarized in Table 8. These averaged results are also represented in a temperature versus conversion profile shown in Figure 43. For comparative purposes in the following discussion,

earlier temperature versus conversion data for Wyodak coal obtained by Song and Saini [1,5] are illustrated in Figure 44. All reactions were performed using a catalyst loading of 1 wt% Mo to dmmf coal.

Effect of Temperature on Coal Conversion with H_2O and ATTM. Considering first of all, the effect of reaction temperature on conversion of Wyodak coal in the catalytic runs with added water (Figure 44), it can be seen that there is a definite temperature window (325-375°C) where increasing temperature significantly increases coal conversion. At 375°C, maximum conversion (77.6 wt%) of Wyodak coal is attained for the catalyst + water system. As temperature is further increased beyond 375°C, coal conversion begins to fall dramatically to around 54 wt% at 425°C. Compared to the catalytic runs without water (also shown in Figure 44), the strong promotional effects of added water on low temperature catalytic liquefaction of Wyodak coal are clearly apparent in the temperature range 325–375°C. As the temperature approaches 400°C, water begins to have a strong inhibiting effect on the catalytic liquefaction of Wyodak coal when compared to using ATTM alone.

Referring now to Figure 43 for Pittsburgh #8 coal, it can be seen that for the catalytic runs with added water, conversion again increases with increasing temperature up to 375°C. At 375°C, maximum conversion (58.0 wt%) of Pittsburgh #8 coal is attained for the ATTM + water system. Beyond 375°C, conversion then falls slowly but steadily with increasing temperature to 425°C. When compared to the catalytic runs of Pittsburgh #8 coal without water, it can be seen that water addition has a promotional effect on conversion at lower temperatures. At around 400°C, however, the beneficial effects of water addition are lost for this coal, and conversion is similar for catalytic runs both with and without water at this temperature. Unfortunately, data for the catalytic run without water at 425°C is not yet available.

There are several particularly interesting points which arise when comparing the temperature versus conversion profiles for Wyodak coal and Pittsburgh #8 coal. For both coals, water addition has a promoting effect on catalytic liquefaction at lower temperatures (≤375°C). Significantly, both coals display maximum conversion at 375°C for the ATTM + water system. For the lower-rank coal (Wyodak), the promoting effect of water addition at low temperature is more pronounced than that observed for the higher-rank coal Pittsburgh #8. Similarly, the inhibiting effect of water on catalytic liquefaction of Wyodak coal at higher temperatures is also more dramatic than that for Pittsburgh #8. It is indeed intriguing that both these coals exhibit the same transitional temperature of 375°C for the catalyst + water runs, below which, conversion increases with increasing temperature and above which, conversion decreases with increasing temperature. This raises the obvious question, "what is the significance of this temperature in terms of the interaction between catalyst and water on promoting coal conversion?" Could it be that above this temperature water deactivates the dispersed molybdenum sulfide catalyst generated from ATTM in

some way? Could it be simply that at this temperature the chemical/physical properties of super-heated water change? Could it be a consequence of the relative interplay between water-promoted ionic versus catalyst-promoted radical cleavage mechanisms within the depolymerizing coal structure with temperature?

Effect of Catalyst Loading on Conversion of Wyodak Coal at 350°C. Table 9 summarizes conversion data for Wyodak coal at 350°C obtained using a reduced catalyst loading of 0.1 wt% Mo on dmmf coal basis. These data are also represented in Figure 45. Compared to original data obtained at a loading of 1 wt% Mo on dmmf coal basis (Figure 46), it is apparent that this reduction in the catalyst concentration significantly reduces the overall effectiveness of the catalyst for promoting conversion of Wyodak coal, both in the catalytic runs and catalytic runs with added water. For the catalytic runs, conversion fell from 29.8 wt% to 20.5 wt%. In the case of catalytic runs with added water, conversion fell from 66.5 wt% to 40.3 wt%. This latter observation indicates that the magnitude of the promotional effect arising through co-use of water and ATTM is not only sensitive to reaction temperature and water/coal ratio, but is also dependent upon the catalyst concentration employed. We are currently investigating the relative effectiveness of a catalyst loading of 0.5 wt% Mo on dmmf coal basis, in an attempt to identify the minimum catalyst concentration threshold required for maintaining optimum conversion.

Summary

We have found that there are strong synergistic effects between water and dispersed molybdenum sulfide catalyst (1 wt% Mo on dmmf coal basis) for promoting the low temperature ($\leq$ 375°C) liquefaction of both Wyodak subbituminous and Pittsburgh #8 bituminous coals. We have constructed a temperature versus conversion profile for both the water-promoted catalytic and catalyst-only runs of Pittsburgh #8 coal, similar to that previously constructed for Wyodak coal. Comparison of these profiles for the two coals of different rank reveals certain distinct similarities. Water addition to the catalytic runs of both coals has a promotional effect on conversion at low temperature ($\leq$ 375°C). The promoting effects of water are more pronounced for the lower-rank subbituminous coal (Wyodak) than for the high-volatile bituminous coal (Pittsburgh #8). Both coals display a maximum conversion at 375°C in the catalyst + water runs. At higher temperatures ($\geq$ 400°C), water has a negative impact on the catalytic liquefaction of both coals. The inhibiting effect of water at higher temperatures is more dramatic for Wyodak subbituminous coal than for Pittsburgh #8 high volatile bituminous coal.

Now we have established that 375°C appears to be the optimum temperature at which water -dispersed catalyst synergistic interaction is maximized for conversion of both coals, we next plan to perform a series of experiments at this specific temperature using various water/coal weight

ratios. In this way we hope to establish the optimum water/coal ratios for maximizing conversion of both of these coals during catalytic liquefaction using ATTM.

We observed that dropping the catalyst loading, from 1.0 wt% to 0.1 wt% Mo on dmmf coal basis, had an adverse effect on conversion for Wyodak coal at 350°C, both for catalytic runs and catalytic runs with added water. The latter finding demonstrates that the magnitude of the promotional effects arising through co-use of ATTM and water is dependent upon the catalyst concentration employed. We are presently investigating the relative effectiveness of a 0.5 wt% Mo catalyst loading, these results will be discussed in the next quarterly report.

References

1. Song, C.; Saini, A.K. *Energy & Fuels*, **1995**, 9, 188.

2. Song, C.; Schobert, H.H.; Saini, A.K. *Am. Chem. Soc. Div. Fuel Chem. Prepr.* **1993**, 38, 1031.

3. Song, C.; Schobert, H.H.; Saini, A.K. *Energy & Fuels.* **1994**, 8, 301.

4. Song, C.; Saini, A.K. *Am. Chem. Soc. Div. Fuel Chem. Prepr.* **1994**, 39, 1103.

5. Song, C.; Saini, A.K.; Mc Connie, J. *Proc. of 8th Int. Conf. Coal Science,* Oviedo, Spain, Sept 10-15, **1995**, in press.

2. Exploratory Studies on the Possibility of Non-Radical Hydrogen Transfer under Low Temperature Liquefaction Conditions. (contributed by Shona Martin)

Introduction

The pathways by which coal macromolecules can be depolymerised to give lighter products have long been sought by coal scientists and the precise roles of individual functional groups in the reactions which occur during liquefaction are still not clear. Generally, radical reactions for hydrogen incorporation are dominant at temperatures ≥350°C. Recently, however, the existence of non-radical pathways has been proposed, due to the observation that gaseous hydrogen reacts with coals under low temperature conditions in preference to hydrogen from donor solvents like tetralin [1]. Indeed, the polar functionalities in coals may play a key role in ionic reaction processes. For example, phenolic groups, present in concentrations of up to 10 wt% in low rank coals, are believed to exert major influences on both product yield and quality [2,3]. It has been proposed that phenols may be one such species which may participate in concerted reactions, whereby phenols are converted to ketones via an enol intermediate; this mechanism has been proposed to be facilitated by molecular hydrogen, thus being the basis of a possible non-radical hydrogenation of coal.

Preliminary studies were conducted on Wyodak coal, known to be rich in phenolic species, in an attempt to observe if such mechanisms occur under low temperature liquefaction conditions: 350°C, 1000 psi H_2, 30 min [4]. However, no definite conclusions were drawn from this work, other than that under the conditions employed, no significant ketone formation was observed. Indeed, the reactions observed were proposed to be the result of thermal activity. In light of this, tests were conducted to examine the possibility that the reaction with H_2 may be a mineral matter catalyzed reaction.

Demineralization is based on the premise that it is possible to isolate the kerogen by dissolution of the mineral matter phase; this is commonly facilitated by consumption of carbonates, sulphides, oxides and hydroxides in HCl, followed by silicates in HF. Demineralization is typically carried out at a temperature sufficient to dissolve the carbonates but not high enough to oxidate the organic matter, *ca* 60°C.

Experimental.

1. Demineralization Wyodak coal (DECS-8) was obtained from the Penn State coal bank and demineralised according to the standard method [5]. The first stage is an HCl wash (10 mL per gram of coal) to remove any rare earths which would form insoluble fluorides at the HF wash stage. This is stirred at 50°C overnight, then filtered and washed. In the second stage, a 40% HF

solution (20 mL per gram of coal) is left stirring at room temperature for approximately 4 hours to ensure complete digestion; the subsequent filtration step utilizes Teflon membranes. The final sample was thoroughly washed with distilled water to ensure removal of residual HF. Further, the filtrate was tested with $AgNO_3$ which indicates the presence of chloride ions.

2. Liquefaction The demineralised coal samples were dried in a vacuum oven at 100°C for 2 hours prior to use. Liquefaction was carried out in a 25 mL tubing bomb with *ca* 4 g coal, at 350°C for 30 min. As standard practice, the reactors were purged several times with H_2 and finally pressurized to 6.9 MPa H_2 (cold). When solvent was present, the coal:solvent ratio was 1:1 w/w. On completion, the bombs were quenched in water, reducing the temperature to 150°C and thus halting the reaction, before being allowed to cool to room temperature. The gaseous products were collected and analyzed by GC; mass of product gases (including residual H_2) was attained, thus allowing H_2 consumption to be determined. The liquid and solid products were recovered and separated by sequential Soxhlet extraction into *n*-hexane solubles (oils), toluene solubles (asphaltenes) and THF solubles (preasphaltenes). The THF-insoluble residue was washed with acetone followed by n-pentane to remove any residual THF. All recovered products were finally dried under vacuum at 100°C for *ca* 10 hours. The conversion of coal into soluble products and gases was calculated on the basis of recovered THF-insoluble residue.

It must be noted that the yield of isolated product, i.e. oils, asphaltenes, preasphaltenes and gas, were marginally greater than that calculated from the overall conversion based on the mass of THF-insoluble residue; typically of the order 2–3 wt%. Further, the data presented in Table represents the average values from two or more duplicate runs.

3. FTIR Fourier Transform Infrared (FTIR) spectra of the demineralised coal and liquefaction residues were recorded on a Digilab FTS-60 spectrometer by co-adding at least 200 scans at a resolution of 2 cm^{-1}. The samples were prepared as KBr discs; the KBr was dried at 110°C overnight in a vacuum oven prior to sample preparation. The predried sample (2±0.01 mg) was mixed with KBr (300±0.01 mg) in a Perkin Elmer Wig-L-Bug grinder-mixer for 120 s. All the spectra were baseline corrected.

4. ^{13}C NMR Solid state ^{13}C NMR spectra were recorded on a Chemagnetics M-100 NMR spectrometer using the cross polarization magic angle spinning (CP-MAS) technique. The measurements were carried out at a carbon frequency of 25.1 MHz.

Results and Discussion.

Results for the reactions, both in the presence and absence of solvent, are reported in Table 10. In light of the fact that a complete set of data has not been completed to date, for purposes of initial comparison, these will be discussed with respect to previously published data with untreated Wyodak coal [1].

Initial results would seem to indicate a comparative level of conversion between the two sets of data, suggesting that the thermal reactions undergone at 350°C are not mineral matter catalyzed. The seemingly higher conversion reported for the demineralised coal in the absence of solvent compared to the untreated coal may be due to water present in the sample due to insufficient drying; this is an area which requires further identification and is currently being explored. It is worth noting that for the demineralised coal reacted in the presence of the non-hydrogen donor solvent, i.e. 1-methylnaphthalene, C_1–C_4 gas production is greater by an order of magnitude than for the other reactions. However, reliance should not be placed on the GC results for gaseous products, as the reproducibility of the calculated product distribution was inconsistent. Furthermore, the net hydrogen consumption from tetralin was not calculated, which would better illustrate if non-radical pathways effectively participate during hydrogenation.

It would therefore be premature to draw any firm conclusions at this early stage as comparative data with untreated coal have yet to be completed for this set of experiments. However, suffice to say the level of conversion attained with the demineralised coal is comparable to the untreated coal. Further characterization was carried out on the parent demineralised coal and certain products by FTIR and NMR.

Solid State ^{13}C NMR. The ^{13}C CP-MAS spectra of the demineralised coal and products from the experiment conducted under H_2 are shown in Figure 47. The ^{13}C CP-MAS spectrum of the demineralised Wyodak displays many similarities to that of the untreated coal [1]. The region between 0 and 80 ppm consists primarily of aliphatic carbons, e.g. methoxy groups and the symmetry of this band should be noted. The second region of interest between 90 and 170 ppm is due to the presence of aromatic carbon. The shoulders present on the side of the aromatic band may be attributed to specific functionalities, e.g. catechol groups (at 142 ppm) and phenolic groups (at 152 ppm). The carboxylic functionality is prominant at 180 ppm, similarly for the carbonyl at *ca* 210 ppm. Upon liquefaction under H_2 without solvent, the primary features illustrated by the product are as follows. In the aliphatic band, the symmetry observed for the parent coal is lost, and the appearance of a shoulder at ≈25 ppm is observed. This may be attributed to a number of groups, including CH_3-Ar side chains (20-21 ppm) or CH_3-CO_2-R acetates (20–22 ppm). Furthermore, the distinct shoulders observed in the aromatic region have virtually disappeared, indicating a loss of oxygen functionalities.

FTIR. Comaparative FTIR spectra of the demineralised coal and certain products are shown in Figures 48 and 49. The spectrum of the whole demineralised coal indicates the presence of most of the groups of interest in this study.

Hydroxyl groups at	3300–3600 cm^{-1}
Aromatics	3030 cm^{-1} and associated bands at 1450–1600 cm^{-1}
Aliphatics	2920, 2850 cm^{-1}
Carboxylic acids	1710–1760 cm-1
Conjugated Ketones	1715 cm-1
Esters, Lactones	1712–1735 cm^{-1}
	(present as a shoulder on the C=O band)

After reaction under H_2 at 350°C, the most notable feature of the whole product spectrum is a decrease in hydroxyl concentration, in part attributed to a loss of H_2O. Further examination of the THF-insoluble residue from this experiment confirms the loss of OH functionality coupled with the disappearance of the ester shoulder. The FTIR spectrum of the THF-insoluble residue from the reaction conducted with tetralin displays somewhat contrasting features. The carboxyl stretching region is much broader; moreover, the ester shoulder is more pronounced and the carbonyl region is much more defined. It would be of interest to generate the difference spectrum between the demineralised coal and the respective products as this would better illustrate the changes in structure undergone during reaction.

Summary

These results to date on the demineralised coal lead to the suggestion that conversion to products at temperatures such as 350°C are not mineral matter catalyzed. In the immediate future, the aim is to complete liquefaction tests for the complete set of variables, i.e. coal (both treated and untreated), in the presence and absence of solvent. ^{13}C NMR and FTIR difference spectrum of the parent coal, whole and fractionated products should highlight any changes in product composition brought about by demineralised coal. This will hopefully point towards the verification, or otherwise, of the possibility of non-radical hydrogenation in coal liquefaction.

References:

1. Song, C., A.K. Saini, H.H. Schobert , Energy and Fuels **8**, 301 (1994)

2. Trewhella, M.J. , A. Grint , Fuel **67**, 1135 (1988)

3. Li, C.L.i, Z.R. Xu, Z.A. Cao and B.C. Gates, AIChE, J **31**(1), 170 (1985)

4. Martin, S.C., H.H. Schobert, Advanced Thermally Stable Jet Fuels, Technical Progress

Report, 92PC92104-TPR-11, p74

5. Durand, B. and C. Nicaise "Kerogen, Insoluble Organic Matter from Sedimentary Rocks" Editor B. Durand, Editions Technip Paris p35 (1980)

3. Low-temperature routes to hydrogenation of Pittsburgh No. 8 coal. (Contributed by Elena Korobetskaya).

Hydrogenation of coal with gaseous hydrogen at high pressure and temperature is a difficult process from the technological point of view, and consequently an expensive process. Conditions of this process require the building of thick-walled reactors. High pressure and temperature make the process of hydrogenation hazardous; the building of thick-walled reactors makes hydrogenation inconvenient and expensive. For these reasons, development of new methods using lower temperatures and pressures becomes desirable. The basic topic of the work on these problems is "hydrogenation of coal at temperature below 300^C". The first step of this work is the experiment presented in this report. A result of this experiment is the demonstration of the apparent necessity to use some kinds of catalysts or hydrogen-donor solvents in hydrogenation at temperature below 300°C.

Method

Pittsburgh # 8 (DECS-12) coal sample was used for the experiment. The experiment was carried out at 300°C. The starting pressure of hydrogen in the batch reactor was 1000 psi. Time of reaction was 30 min. No catalyst or solvent were used for the experiment. Changes of reaction pressure are presented in Table 11.

The residue was investigated by NMR and pyrolysis -GC/MS. Spectra are presented in Figures 51-53.

Results and discussion

It is quite obvious from the comparison of Fig.52 and Fig. 53 that nothing significant changes in the hydrocarbon structure of coal sample at 300°C. It means that the hydrogenation process does not occur at temperature 300°C and below in the absence of solvent or catalyst. These are the two common ways to reduce the temperature of hydrogenation. The next experiments with DECS-12 coal sample will be carried out in presence of hydrogen-donor solvent (9,10-dihydrophenanthrene).

There is another way to decrease temperature of hydrogenation and increase the rate of reaction of hydrogenation. T. Cablewski, A. Faux, C. Strauss [1] have shown that using microwave energy it is possible to increase the rates of some organic reactions in several times. On the other hand there are some works of Russian researchers who investigated coal using microwave energy (for instance I. A. Korobetskii, M. Y. Shpirt, N. Balabanova, B Georgiev, I. Mikhailov [2]). These works concern the oxidation of coal by oxygen plasma. The oxidation

occurs at 150°C. Using microwave energy decreases temperature of reaction. Also, it was noted that the rate of reaction is increased by influence of microwave energy.

In accordance with information cited above, it would be interesting to add the influence of microwave energy as a factor of increasing of the rate of hydrogenation and decreasing of temperature of reaction to the other factors (catalysts, solvents).

Conclusions

The present experiment demonstrates that hydrogenation does not occur in absence of catalysts or hydrogen-donor solvents. There are two common ways to decrease temperature of hydrogenation: to use catalysts or hydrogen-donor solvents (for instance, 9,10-dihydrophenanthrene). Probably, there may be other ways to attain the same goal of reducing the reaction severity for coal hydrogenation. One way might be to use the microwave energy as a factor of decreasing of temperature of hydrogenation.

4. Exploratory Studies on Coal liquids Upgrading using Mesoporous Molecular Sieve Catalysts (Contributed by Madhusudan Reddy Kondam and Chunshan Song)

Introduction

In the process of examining the mesoporous molecular sieve catalysts for upgrading the coal derived liquids to jet fuels, we reported in previous reports the successful synthesis of phase pure mesoporous molecular sieves, Al-MCM-41, with varying Si/Al ratios and using three different aluminum sources (aluminum isopropoxide, Catapal B alumina, and aluminum sulfate) [1,2]. The detailed characterization of those materials by various techniques (XRD, chemical analysis, surface area measurement, thermal analysis and solid state NMR) was performed, in order to understand their physico-chemical characteristics [1-3]. Then the catalytic evaluation of those materials was performed in model reactions of hydrogenation of naphthalene and phenanthrene and alkylation of naphthalene [5]. All the previous results indicated that source of aluminum used in the synthesis of Al-MCM-41 samples has a significant influence on their physico-chemical properties including their acid catalytic and supporting properties. In this report we present a) the synthesis of the same material with another aluminum source (sodium aluminate) and comparison of its acidity with earlier samples by temperature programmed desorption of *n*-butylamine on TGA and DSC, b) studies on crystallite size of Pt in the Pt supported Al-MCM-41 samples and c) catalytic test results of these new materials with another model reaction of 1,3,5-triisopropylbenzene hydrocracking.

Experimental

Synthesis of Al-MCM-41 with varying Si/Al ratio using sodium aluminate as aluminum source was synthesized similar to the procedure reported in scheme I of our earlier report [1] However, to keep the chemical composition of synthesis gel ($50SiO_2$-xAl_2O_3-$4.32Na_2O$-$2.19(TMA)_2O$-15.62(CTMA)Br-$3165H_2O$; where x=0.5, 1.0 and 2.0) same, the amounts of sodium silicate and fumed silica were varied. This was because of the fact that in sodium aluminate source there is sodium, has to be balanced in order to maintain the pH, which was absent in all other aluminum sources. The Al-MCM-41 samples synthesized using sodium aluminate were also calcined at similar conditions described elsewhere [1]. All the physico-chemical characterization (chemical analysis, XRD, acidity measurements and solid state NMR) was done similar to them used for earlier samples [1-3]. However, the acidity measurement of these new samples was also performed by DSC apart from TGA. The sample preparation with *n*-butylamine is done similarly which was used in earlier work [2]. The conditions for TGA were similar with the earlier work starting from 30°C to 700°C at rate of 10°C/min in nitrogen flow. The DSC was performed on a

Mettler DSC 27HP in the temperature range from 400°C to 600°C at 10°C/min. rate in nitrogen flow.

The crystallite sizes of Pt in Pt supported Al-MCM-41 were calculated from the XRD peak breadths using the Scherrer's equation [4].

$$L = K\lambda/\beta \cos\theta$$

wherein θ and λ have their usual meanings, L is the mean dimension of the crystallites composing the powder, β is the breadth of the pure diffraction profile on the 2θ scale in radians, and K a constant approximately equal to unity and related both to the crystallite shape and to the way in which β and L are defined. The breadth β of the pure diffraction profile is obtained by $\beta=(B-b)$, where B and b are the breadths of the diffraction profiles of actual sample and the silicon standard. The simplified equation of Scherrer's equation was derived using reflection anology and given as

$$L_{hkl} = 0.9\lambda/\beta_{hkl} \cos\theta$$
$$= 0.9 \text{ X } 1.542 \text{ X } 57.3/\beta_{hkl} \cos\theta$$

Prior to catalytic runs, MCM-41 samples were converted into protonic form and then in some cases Pt was loaded by wet impregnation. The detailed procedure is given elsewhere [2].

The hydrocracking of 1,3,5-triisopropylbenzene was performed in a batch reactor and product analyses were done according to the procedure identical to those reported earlier [2,3,5]. All the reactions were carried out in horizontal tubing-bomb reactors (with vertical shaking, 200 cycles per minute) with 0.1 g of catalyst, 1.0 g of reactant at 350°C for 2 hours under 1500 psi hydrogen pressure.

Results and Discussion

XRD patterns of the samples prepared with sodium aluminate with varying SiO_2/Al_2O_3 molar ratios clearly showed that they are pure MCM-41 type molecular sieves with good crystallinity. Like with all earlier Al-MCM-41 samples prepared with other sources, the crystallinity of the samples with sodium aluminate also decreased with reducing the SiO_2/Al_2O_3 molar ratio. The d-spacing values (Table 12) of the major XRD peak indicates that aluminum incorporation in the framework is as good as with aluminum isopropoxide source infact it seems slightly better than with all other sources studied.

The SiO_2/Al_2O_3 molar ratios of calcined MCM-41 samples prepared using sodium aluminate from the chemical analyses are presented in Table 12. Initial molar ratios taken while synthesizing samples (input) and the ratios obtained from the crystalline solid products (output) are compared. It is noticed that output ratios are smaller than the input ratios. Similar results were obtained with samples prepared using Catapal alumina and aluminum isopropoxide. This was attributed, as with many other high silica molecular sieves, that zeolites normally incorporate all of the aluminum present in the reaction mixture leaving varying amounts of silica or silicate in

solution according to other factors such as the hydroxide concentration and the presence of various inorganic and organic cations in the reaction mixture [6].

Thermal analyses of *n*-butylamine pre-adsorbed MCM-41 samples prepared with sodium aluminate with two different SiO_2/Al_2O_3 molar ratios are shown in Figure 52. It is observed from the TGA curves that most of n-butylamine is desorbing below 473 K like with all other earlier samples prepared with different aluminum sources. Figure 52 also shows that the samples with different SiO_2/Al_2O_3 molar ratios (50 and 25) show the different levels of *n*-butylamine desorption (22 and 26 wt%). This can explain the different levels of acidity due to different amounts of aluminum incorporation upon the variation of SiO_2/Al_2O_3 molar ratio from 50 to 25.

Figure 54 represents comparison of the TGA curves for all the samples prepared with four different aluminum sources. From the weight losses due to the *n*-butylamine desorption, as it was discussed in earlier reports, it is clear that MCM-41 samples prepared with different aluminum sources adsorbed different levels of *n*-butylamine. Especially the sample prepared with sodium aluminate shows more weight loss. This indicates that sample prepared with sodium aluminate source seems to be more acidic comparatively with all the samples prepared with other sources. This could be due to the improved aluminum incorporation in the framework and confirms the d-spacing values.

Figures 55 and 56 show the DSC curves for the *n*-butylamine adsorbed Al-MCM-41 samples prepared with sodium aluminate as aluminum source. Figure 57 represents the DSC curves obtained with and without 30 min. nitrogen flushing prior to the DSC measurements. The sample (Figure 54a) which was not flushed with nitrogen clearly shows three DSC endothermic peaks whereas other flushed samples show only two DSC endothermic peaks at about 100°C and 400°C (Figure 54b and 55). The extra peak below 50°C with unflushed sample could be due to the presence of physisorbed *n*-butylamine, which was removed by nitrogen flushing for other samples prior to the DSC measurement. The second and third peaks may be attributed to the desorption of n-butylamine from the weak and strong acid sites respectively. Figure 55 illustrates the DSC curves of *n*-butylamine desorption on Al-MCM-41 samples prepared with sodium aluminate with SiO_2/Al_2O_3 molar ratios 50 and 25. It is clear from the DSC curves that peak intensities for the sample of SiO_2/Al_2O_3 molar ratio 25 are high indicating the increased number of acid sites. The reason for the increased acidity is due to the increased amount of aluminum incorporation in the framework upon decreasing the SiO_2/Al_2O_3 ratio. Similar results were observed from TG analysis.

Figure 58 illustrate the ^{27}Al MAS NMR spectra of as-synthesized mesoporous molecular sieves, MCM-41, with different SiO_2/Al_2O_3 molar ratios (50 and 25) using sodium aluminate. It shows that both the samples exhibit only a peak at around 50 ppm. No peak at 0 ppm corresponding to octahedral Al species is detected in these samples, confirming that all the Al

atoms in the as-synthesized MCM-41 materials are present in a tetrahedral environment [7]. It also shows that decreasing the SiO_2/Al_2O_3 molar ratio from 50 to 25 did not change the Al symmetry, which indicates that it is possible to incorporate most of the aluminum even with increasing Al contents.

Figure 59 shows the XRD patterns of Pt supported Al-MCM-41 samples, which have shown different acidities and catalytic activities, prepared with three different aluminum sources. To confirm our earlier conclusion of the difference in catalytic activity was only due to difference in acidity but not due to the difference in the Pt crytallite sizes, here we studied the Pt crystallite sizes by XRD, calculated using Scherrer's equation and shown in Table 13 XRD peaks for Pt are sharp and very intensive indicating that Pt particles are quite large and their size distribution seems to be narrow. Pt crystallite sizes calculated from Scherrer's equation are about 1700 Å except for one sample being low. However, as the crystallites sizes are very large the values calculated using Scherrer's equation may not be accurate [4].

The preliminary catalytic and non catalytic test results for the reaction of 1,3,5-triisopropylbenzene hydrocracking on Al-MCM-41 sample (MRK9b), which was prepared using aluminum isopropoxide, with and without Pt loading are presented in Table 14. This model reaction was chosen in order to check the capability of converting the very large molecules as they are mesoporous materials with about 25-30 Å pores The first observation is that both catalysts (with and without Pt loading) are active (100 and 68% conversion) and almost no conversion (1%) without catalyst at similar conditions. However, reactions went non-selectively as expected, because of the no shape-selective nature of mesoporous materials with wide pores. The main products for the catalyst without Pt are diisopropyl and isopropylbenzenes, whereas Pt loaded catalyst further improved the hydrocracking activity and the products were mainly benzene and other lighter hydrocarbons.

In conclusion, our results in this report indicate that a) sodium aluminate is also a good source of aluminum to synthesize the mesoporous aluminosilicate molecular sieves with improved acidity, b) DSC can also be used to determine the relative acidity of molecular sieves, c) Pt loading on Al-MCM-41 samples by wet impregnation yielded large crystallites with good uniformity and d) these mesoporous molecular sieves are capable of converting large molecules like 1,3,5-triisopropyl benzene. On the basis of above results, we are now planning to prepare Al-MCM-41 molecular sieve catalysts in large quantities, evaluate them further with more model reactions and then coal liquids in our future work.

References

1. H. H. Schobert, S. Eser, C. Song, P. G. Hatcher, A. Boehman and M. M. Coleman, *Advanced thermally stable jet fuels*, 92PC92104-TPR-10, p. 90.

2. H. H. Schobert, S. Eser, C. Song, P. G. Hatcher, A. Boehman and M. M. Coleman, *Advanced thermally stable jet fuels*, 92PC92104-TPR-11, p. 49.

3. K. M. Reddy and C. Song, *Catalysis Letters*, submitted for publication, 1995.

4. H. P. Klug and L. E. Alexander, *X-ray Diffraction Procedures, For Polycrystalline and Amorphous Materials*, A Wiley-interscience Publication, New York, 1974.

5. K. M. Reddy and C. Song, *Preprints of ACS Symp.*, Chicago, 1995, submitted.

6. P. A. Jacobs and J. A. Martens, *Synthesis of high silica aluminosilicate zeolites*, Elsevier, 1987.

7. C.-Y. Chen, H.-X Li and M. Davis, *Microporous Mater.*, 1993, 2, 27.

APPENDIX I

Tables

Table 1. Coal- and Petroleum-Derived Jet Fuels and Middle Distillates.

	Fuel	Description	Received	Supplier/Source	Sample No.
Coal-Derived Fuels					
1)	JP-8C	Hydrotreated JP-8	5-30-89	WPAFB	89-POSF-2685 ?
2)	WI-MD	Middle distillates from coal liquefaction at Wilsonville	4-20-90	DOE PETC	259E MD
3)	FT-MD	Middle distillates from Fischer-Tropsch Synthesis	8-16-91	DOE PETC	PETC F-T
4)	HRI-MD	Middle distillates from coal liquefaction at HRI	11-26-91	WPAFB	83-POSF-0849
Petroleum-Derived Jet Fuels					
5)	JP-8P	Petroleum-Derived JP-8	5-30-89	WPAFB	
6)	JP-8P2	Petroleum-Derived JP-8	5-31-90	WPAFB/Tank S-15	
7)	JP-7	Petroleum-Derived JP-7	5-31-90	WPAFB/Tank S-16	
8)	Jet A-1	Commercial jet fuel	8-16-91	WPAFB/Tank S-7	90-POSF-2747
9)	JPTS	Thermally stable jet fuel	8-16-91	WPAFB	91-POSF-2799
10)	Jet A	Commercial jet fuel	8-16-91	WPAFB	90-POSF-2827

Table 2. Simulated Distillation Temperatures of Ten Fuels at Seven Different Weight Percent Points Obtained by TGA.

	Weight % distilled						
Fuel	5	10	30	50	70	90	95
JP-8C	127	150	187	211	233	260	270
WI-MD	252	277	314	330	344	362	370
FT-MD	201	225	260	281	302	322	328
HRI-MD	153	193	266	301	327	359	372
JP-8P	145	167	198	212	228	250	258
JP-8P2	173	193	209	219	230	247	255
JP-7	179	199	218	223	228	239	245
Jet A-1	156	176	197	202	207	216	222
JPTS	138	159	188	197	206	222	229
Jet A	153	175	207	221	234	251	257

Table 3. Approximate Compositions of Paraffinic Fuels by Compound Class.

	Fuel						
Compound class (wt%)	JP-8P	JP-8P2	JP-7	Jet A-1	JPTS	Jet A	FT-MD
Paraffins	61.3	59.3	69.8	50.7	67.4	61.9	96.0
Monocycloparaffins	13.5	11.5	17.0	15.5	13.6	12.8	
Decalins	0.9	1.7	4.3	3.3	1.5	1.6	
Alkylbenzenes	15.5	13.5	1.8	20.7	12.5	13.5	
Tetralins	0.4	2.0		0.8	0.1	0.9	
Indans	1.4	2.6	0.1	3.0	0.6	1.7	
Naphthalenes	3.0	2.5		0.7	0.1	2.3	
Olefins	1.5	3.3	4.1	3.1	2.2	2.7	0.4
Others							

Table 4. Detailed Compositions of the Three Major Hydrocarbon Types for Paraffinic Fuels.

	Fuel						
Compound (wt%)	JP-8P	JP-8P2	JP-7	Jet A-1	JPTS	Jet A	FT-MD
Paraffin (C_7)						0.2	
Paraffin (C_8)	1.5	0.6			0.2	0.9	
Paraffin (C_9)	6.8	3.5		0.1	2.7	3.8	0.7
Paraffin (C_{10})	11.8	7.5		7.6	10.9	9.5	7.6
Paraffin (C_{11})	11.3	12.0	16.9	25.1	25.1	13.9	11.8
Paraffin (C_{12})	10.1	11.9	25.2	12.4	17.3	10.6	13.7
Paraffin (C_{13})	8.8	9.1	19.1	4.8	4.7	9.1	11.1
Paraffin (C_{14})	6.4	8.7	6.0	0.5	4.4	7.7	10.4
Paraffin (C_{15})	3.1	4.3	1.7	0.1	1.3	4.8	10.4
Paraffin (C_{16})	1.5	1.8	0.9	0.1	0.7	1.4	8.7
Paraffin (C_{17})	0.1						5.5
Paraffin (C_{18})	0.1						6.9
Paraffin (C_{19})							4.7
Paraffin (C_{20})							4.1
Paraffin (C_{21})							0.5
Paraffin (C_{22})							0.1
Methylcyclohexane	0.1	0.0			0.2	0.3	
C_2-cyclohexane	1.0	0.6			0.7	0.8	
C_3-cyclohexane	3.9	1.7		0.5	2.9	2.4	
C_4-cyclohexane	4.3	2.9	0.9	7.8	5.2	3.7	
C_5-cyclohexane	2.1	3.0	7.3	5.6	2.7	3.0	
C_6-cyclohexane	1.4	2.1	5.9	1.4	1.2	1.7	
C_7-cyclohexane	0.6	1.0	2.6	0.2	0.5	0.7	
C_8-cyclohexane	0.1	0.1	0.4		0.1	0.2	
Toluene	0.2	0.0	0.0			0.2	
C_2-benzene	1.9	0.8			0.9	0.9	
C_3-benzene	5.5	4.3		4.3	6.5	4.2	
C_4-benzene	4.9	4.5	0.9	9.8	4.1	4.9	
C_5-benzene	2.3	2.9	0.8	5.8	1.1	2.6	
C_6-benzene	0.6	0.8	0.2	0.8		0.8	
C_7-benzene	0.1	0.2					

Table 5. Onset Temperature of Oxidation Exotherm from DSC for Seven Fuels.

	Fuel						
	JP-8P	JP-8C	JP-7	Jet A-1	JPTS	Jet A	FT-MD
Temperature (°C)	201.8	187.5	193.6	198.3	193.5	207.3	190.3

Table 6. Approximate Compositions of JP-8P2 by Compound Class after 0-8 Hours.

	Thermal stressing time (h)				
Compound class (wt%)	0.0	1.0	2.5	4.0	8.0
Paraffins	59.3	47.1	26.1	16.1	12.3
Monocycloparaffins	11.5	10.1	6.9	6.6	3.3
Decalins	1.7	1.4	0.9	0.3	0.2
Alkylbenzenes	13.5	18.7	23.7	24.9	21.5
Tetralins	2.0	1.2	0.2	0.07	0.04
Indans	2.6	2.4	2.7	2.8	2.1
Naphthalenes	2.5	4.0	7.5	8.7	6.1
Olefins	3.3	4.4	6.6	3.0	2.5
Others					

Table 7. Data for Thermal Stressing at 425°C for 3h and 6h.

Additives	Dodecane remaining (mol%)		Additive remaining (mol%)		Reaction Products	
	3h	6h	3h	6h	3h	6h
1 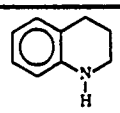	96.1	89.4	72.5	62.3	quinoline	quinoline
2 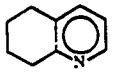	66.8	33.6	54.4	16.8	quinoline	quinoline
3 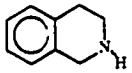	78.8	44.2	<0.1	<0.1	isoquinoline 1,2-dimethyl benzene 1-ethyl-2-methyl benzene 1-ethenyl-2-methyl benzene o-ethyl benzonitrile	isoquinoline 1-ethyl-2-methyl benzene 1-ethenyl-2-methyl benzene o-ethyl benzonitrile
4 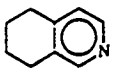	68.0	37.5	59.9	23.6	isoquinoline	isoquinoline
5 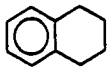	70.1	42.3	74.0	41.7	naphthalene methyl indene	naphthalene methyl naphthalene methyl indene
6 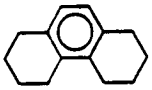	82.3	51.5	35.9	9.3	tetrahydrophenanthrene phenanthrene alkyl naphthalene	tetrahydrophenanthrene phenanthrene alkyl naphthalene alkyl benzene
8 	67.7	43.7	2.3	<1.0	benzene toluene benzaldehyde	benzene toluene benzaldehyde 1-ethyl benzene
9 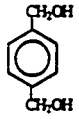	------	55.2	------	26.3	----------	benzene, toluene benzaldehyde benzyl alcohol methyl benzyl alcohol 1,4-benzaldehyde 1,4-dimethyl benzene 1-methanol-4-benzaldehyde

Table 8. Conversion Data and Product Yields for Catalytic Runs of Pittsburgh #8 Coal With ATTM and ATTM + Water.

Exp No.	13/16	15/26/29	28/31	27/30	18/24	17/25	32
Rxn Temp. °C	350	350	375	375	400	400	425
Time, min.	30	30	30	30	30	30	30
H_2O added	none	H_2O	none	H_2O	none	H_2O	H_2O
Catalyst	ATTM	ATTM	ATTM	ATTM	ATTM	ATTM	ATTM
H_2O/dmmf coal, wt	none	0.45	none	0.44	none	0.46	0.42
Mo/dmmf coal, wt%	1	1	1	1	1	1	1
dmmf % Coal Conversion	25.07	47.78	47.74	57.99	54.03	54.89	50.66
dmmf % yield Preasphaltene	24.86	42.56	39.12	38.22	36.37	29.26	26.02
dmmf % yield Asphaltene	2.06	3.93	3.91	11.65	7.00	15.50	8.91
dmmf % yield Oil (isolated)	2.18	1.49	3.25	8.92	4.89	7.92	10.83
dmmf % yield Oil (by diff.)	n/a	n/a	4.34	7.47	9.39	8.22	12.57
dmmf % yield Gas (GC)	0.27	0.42	0.38	0.64	1.27	1.91	3.16
dmmf % yield Gas (diff)	0.57	0.50	0.95	0.99	1.67	1.95	3.54
Gas comp, dmmf							
CO	0.04	0.01	0.05	0	0.06	0.01	0.02
CO_2	0.1	0.31	0.15	0.43	0.36	0.88	1.15
CH_4	0.04	0.04	0.11	0.11	0.43	0.44	0.99
C_2-C_4	0.06	0.05	0.08	0.10	0.43	0.58	1.00
% H_2 Consumption, dmmf	< 0.3	0.44	0.38	0.52	0.64	0.76	0.733

Table 9. Conversion Data and Product Yields for Non-Catalytic and Catalytic Runs (0.1 wt% Mo to dmmf Coal) of Wyodak Coal With and Without Added Water.

Exp No.	2	5/6	7/8	9/10
Rxn Temp. °C	350	350	350	350
Time, min.	30	30	30	30
H_2O added	none	H_2O	none	H_2O
Catalyst	none	none	ATTM	ATTM
H_2O/dmmf coal, wt	none	0.49	none	0.48
Mo/dmmf coal, wt%	0	0	0.1	0.1
dmmf % Coal Conversion	13.42	19.85	20.46	40.25
dmmf % yield Preasphaltene	3.87	8.27	5.22	20.03
dmmf % yield Asphaltene	1.99	0.85	2.34	1.61
dmmf % yield Oil (isolated)	3.17	3.80	4.85	5.91
dmmf % yield Oil (by diff.)	3.26	5.82	7.55	10.30
dmmf % yield Gas (GC)	5.02	7.84	5.36	8.32
dmmf % yield Gas (diff)	5.02	7.98	4.59	8.22
Gas comp, dmmf				
CO	0.29	0.14	0.34	0.12
CO_2	4.48	7.45	4.73	7.86
CH_4	0.15	0.13	0.16	0.16
C_2-C_4	0.09	0.12	0.12	0.16
% H_2 Consumption, dmmf	1.15	1.74	1.23	1.91

Table 10. Results of Non-Catalytic Liquefaction of Normal and Demineralised Wyodak Coal at 350 °C for 30 min. Under 6.9MPa H_2.

Coal	Pretreatment	Solvent	Gaseous Distribution			Liquid Distribution			Total Liquids	% Conv.
			CO	CO_2	C_1-C_4	Oil	Asph.	Preasph.		
Wyodak	-	-	0.2	4.5	0.2	2.1	2.6	4.5	9.2	12.5
"	demineralised	-	0.087	3.01	0.048	0.06	4.46	10.29	14.81	19.71
"	-	Tetralin	0.2	4.1	0.2	4.1	7.6	10.0	21.7	25.9
"	demineralised	"	0.07	2.0	0.035	2.83	3.38	9.79	16.0	21.52
"	-	1-MN	0.2	4.3	0.2	1.1	5.8	7.4	14.3	18.3
"	demineralised	"	0.095	1.9	0.485	2.14	6.30	11.73	20.16	15.01

Table 11. Changes of Reaction Pressure

Time [min]	Pressure [psi]
0	1000
1	1500
2	1510
3	1520
4	1525
5	1526
6	1532
8	1539
10	1540
15	1540
20	1539
25	1540
30	1540
Pressure after reaction	990

Table 12. Some characteristics of Al-MCM-41 samples prepared with sodium aluminate

Sample	SiO_2/Al_2O_3 molar ratio		d spacing (Å)
	Input	Output	
MRK13a	100	90	37.2
MRK13b	50	49	40.3
MRK13c	25	21	38.9

Table 13. Crystallite sizes of Pt in Pt/MCM-41 catalysts

Catalyst	Peak width of Si (111) b (2θ)	Peak width of Pt (111) B (2θ)	β = B-b (2θ)	Crystallite size L (Å)
Pt/MRK9b	0.2737	0.3385	0.0648	1275
Pt/MRK10b	0.2737	0.3214	0.0477	1732
Pt/MRK11b	0.2737	0.3208	0.0471	1754

Table 14. Hydrocracking of 1,3,5-triisopropylbenzene over MCM-41 catalysts

Reaction conditions: 0.1 g catalyst, 1.0 g triisopropylbenzene, 1500 psi H_2 pressure, 350 °C temperature and 2 hours reaction time

Catalyst	Product distribution (wt%)		
	no catalyst	H/MRK9b	Pt/MRK9b
1,3,5-Triisopropylbenzene Conv. (%)	1.02	67.69	100.0
isopropylbenzene	0.00	19.56	0.0
1,3-diisopropylbenzene	94.20	63.09	0.0
1,4-diisopropylbenzene	3.30	7.71	0.0
benzene and other lighter hydrocarbons	4.10	9.63	100.0

APPENDIX II

Figures

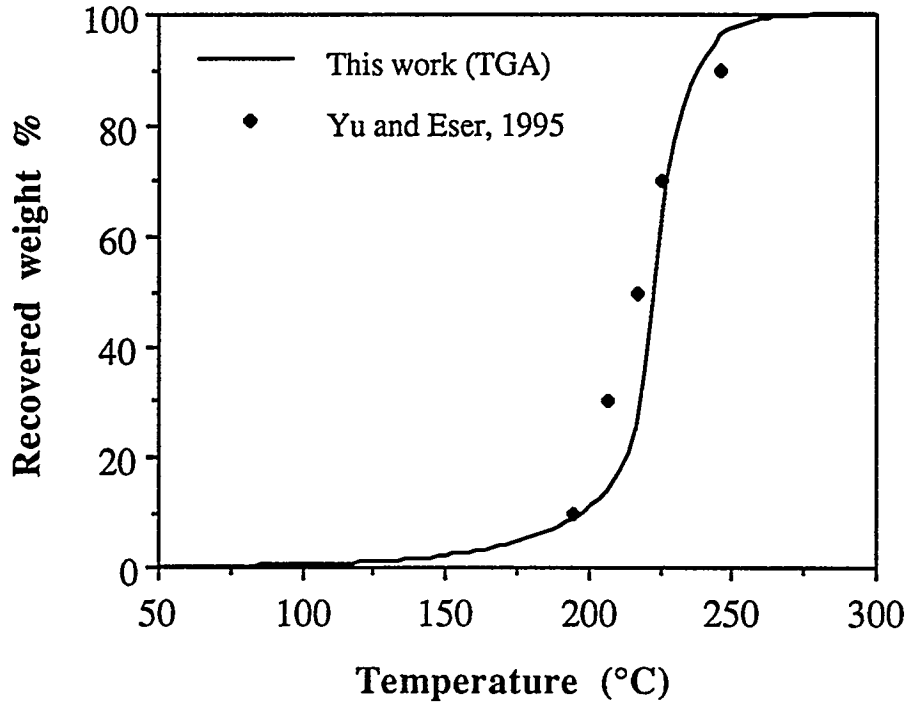

Figure 1. Simulated Distillation Curve for JP-7 by TGA (This Work) as well as the Data Determined by GC [Yu and Eser, 1995].

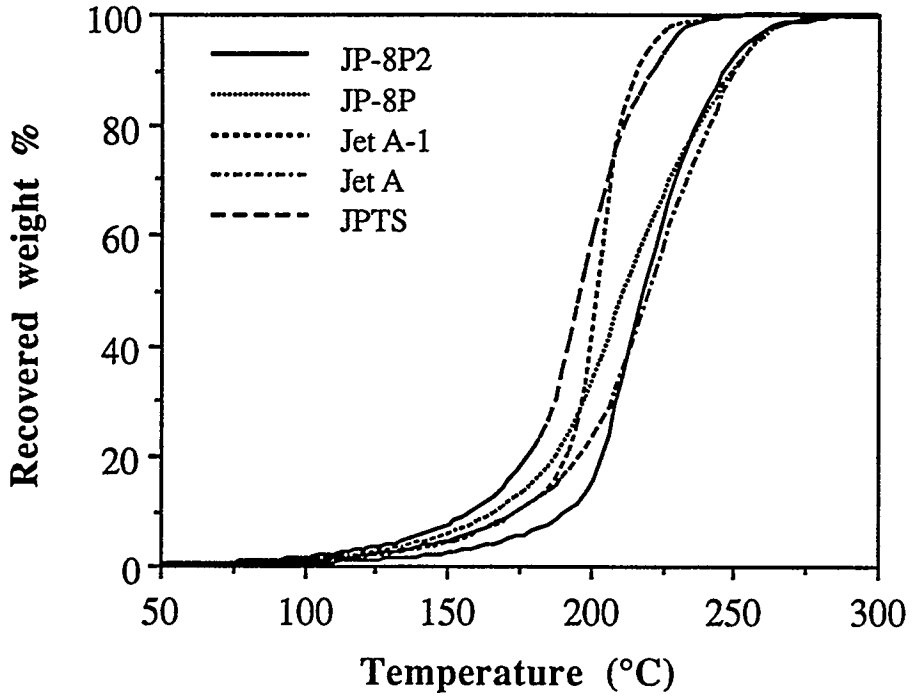

Figure 2. Simulated Distillation Curves for Five Petroleum-Derived Fuels by TGA.

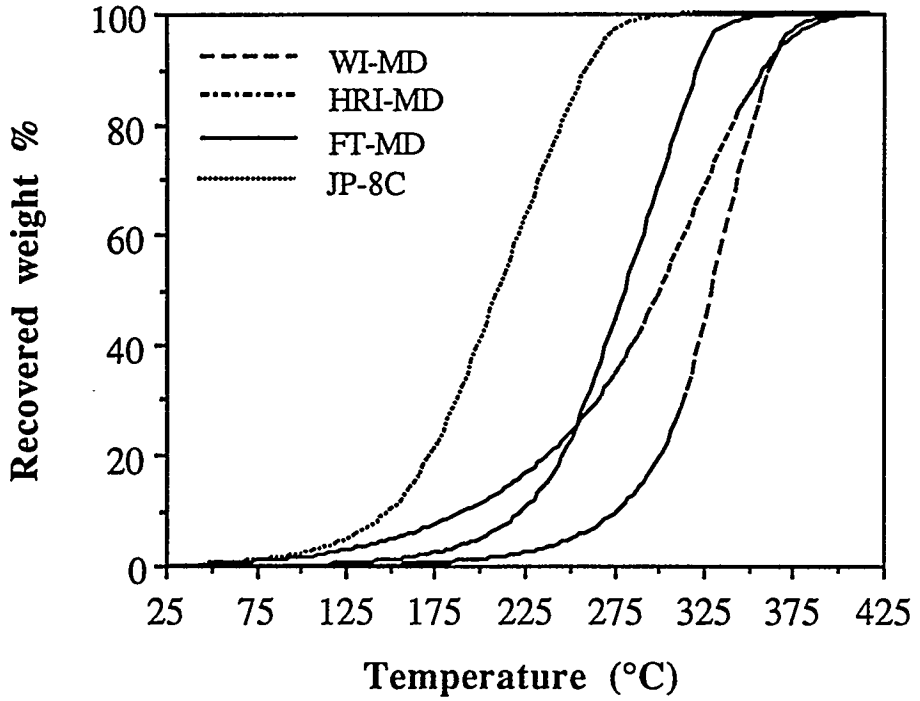

Figure 3. Simulated Distillation Curves for Four Coal-Derived Fuels by TGA.

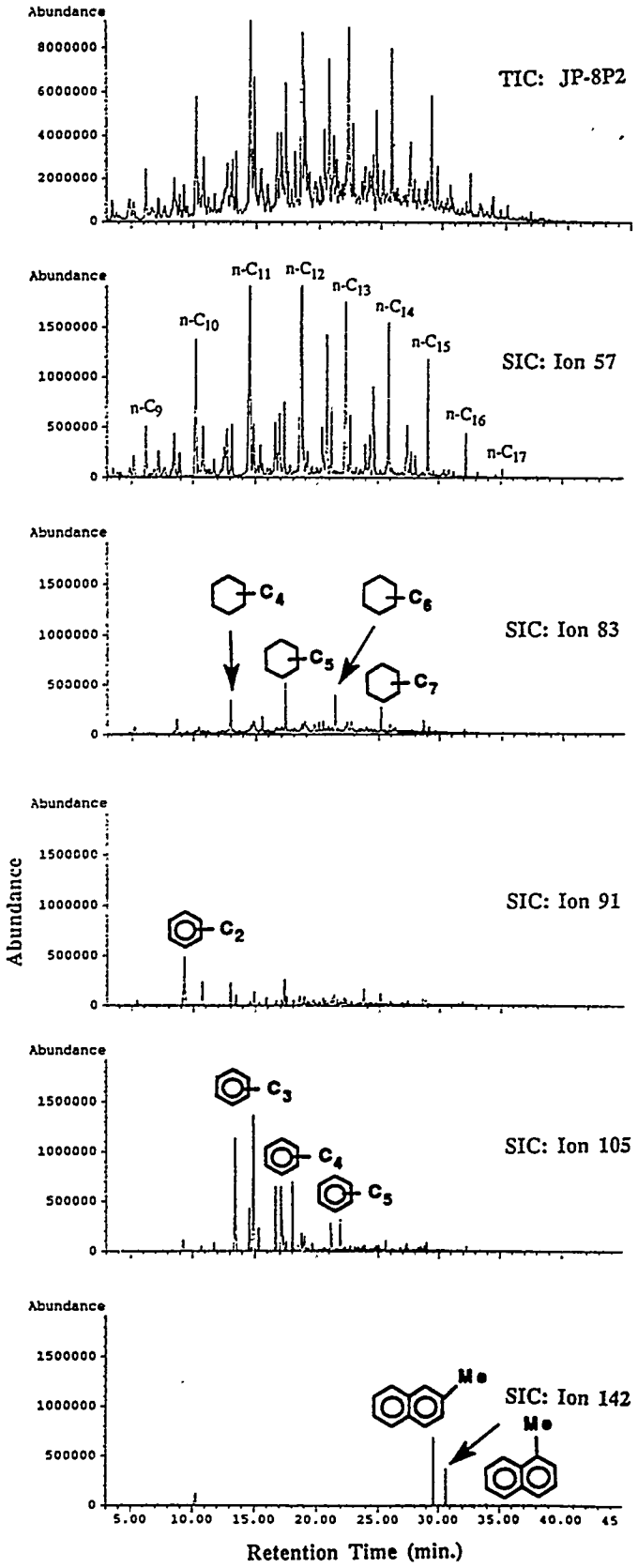

Figure 4. Total and specific ion chromatograms (ions of m/z 57, 83, 91, 105, and 142) of JP-8P2 from GC-MS analysis.

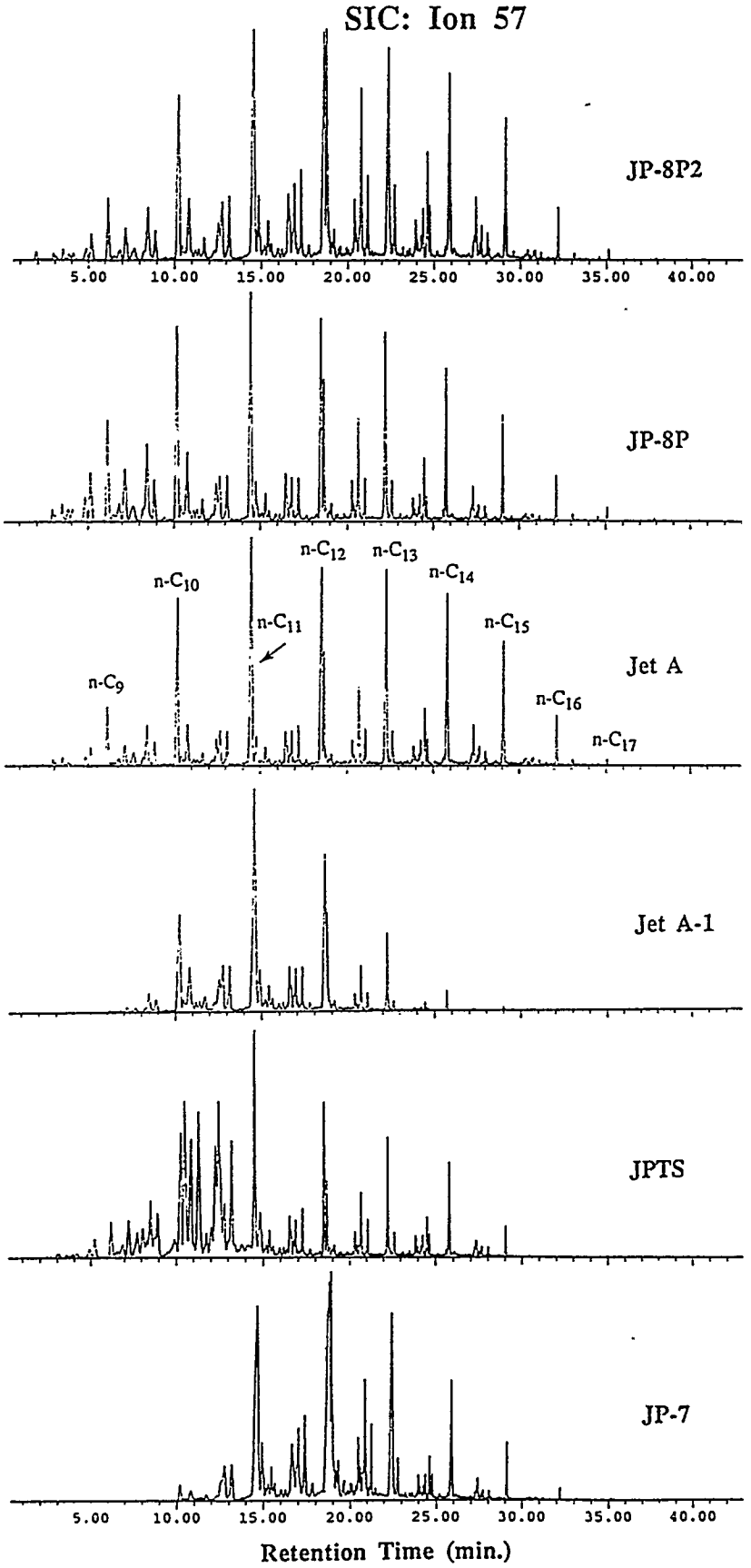

Figure 5. **Specific ion chromatograms (ion of m/z 57) of six paraffinic fuels.**

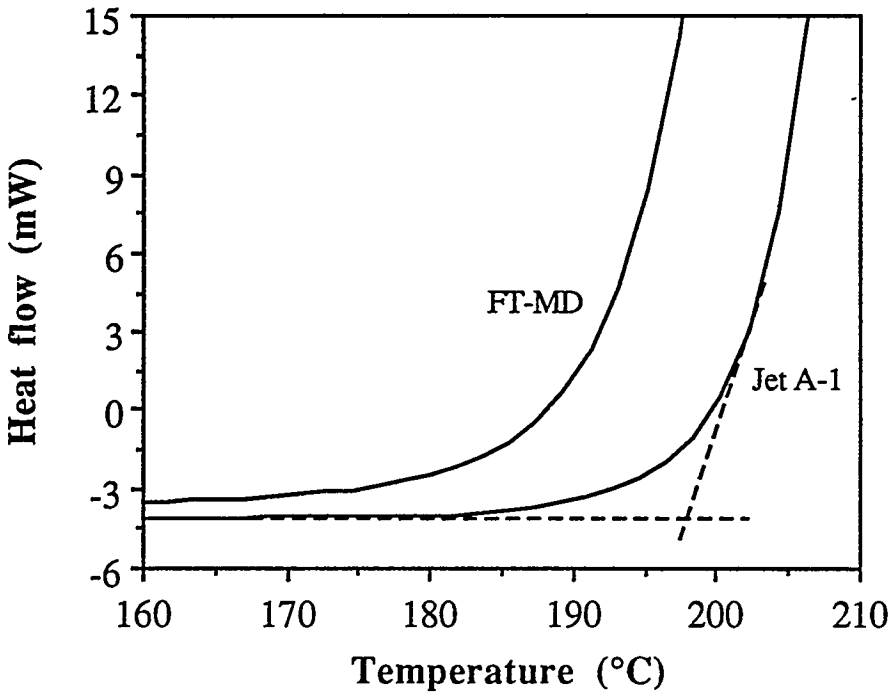

Figure 6. Onset of DSC Curves for the Oxidation of Jet A-1 and FT-MD.

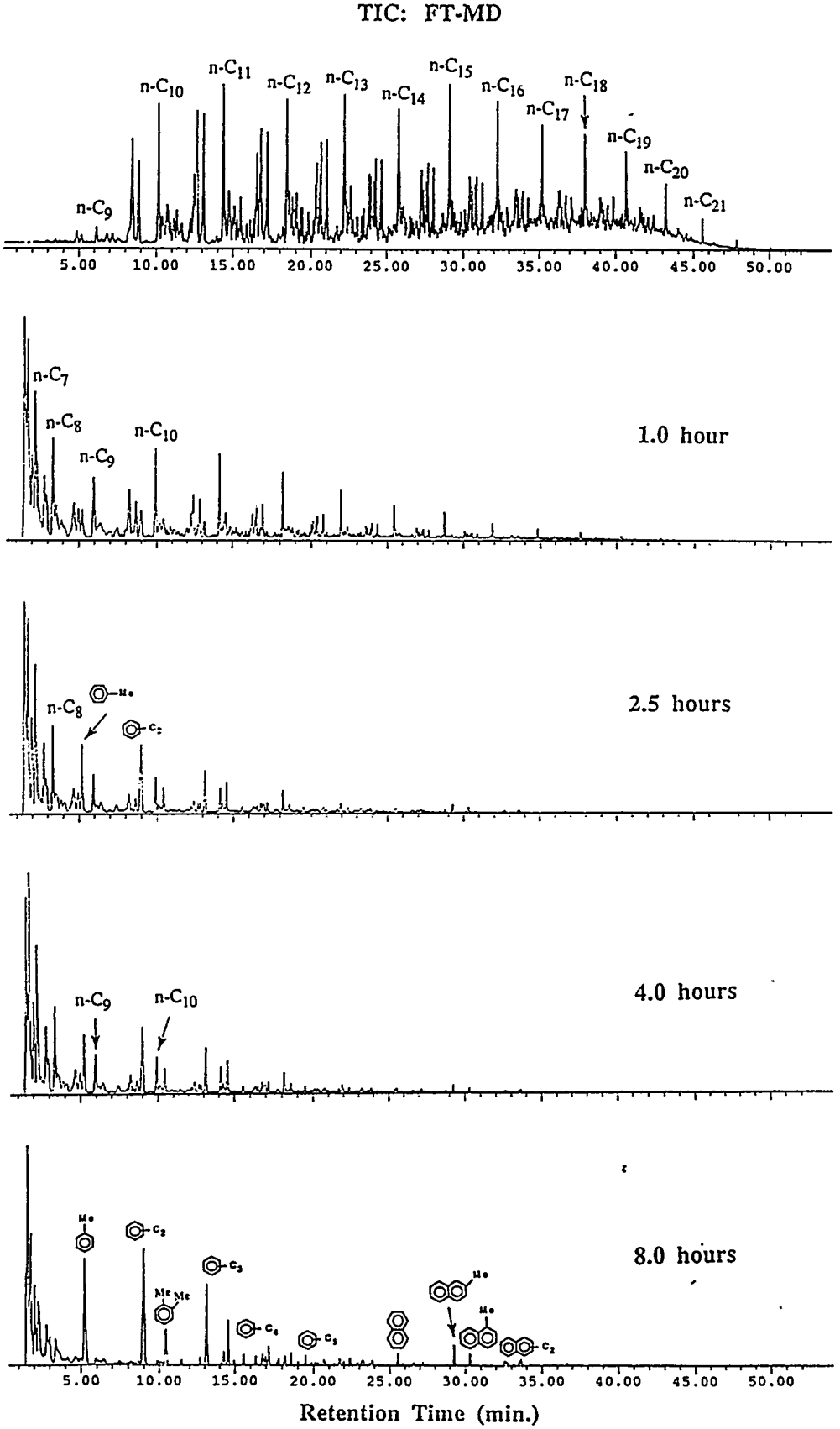

Figure 7. Total ion chromatograms of the neat sample of, and the liquid products from, FT-MD after thermal stressing at 450°C for 1-8 hours.

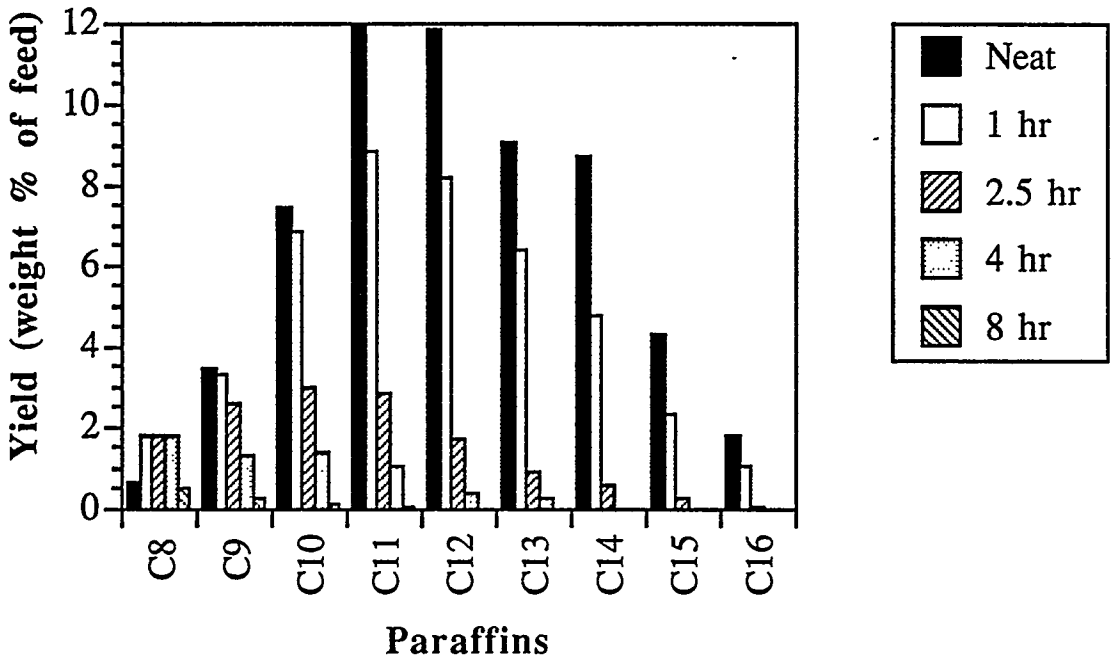

Figure 8. Paraffins Distribution of the Liquids from JP-8P2 at 450 °C for 0-8 h.

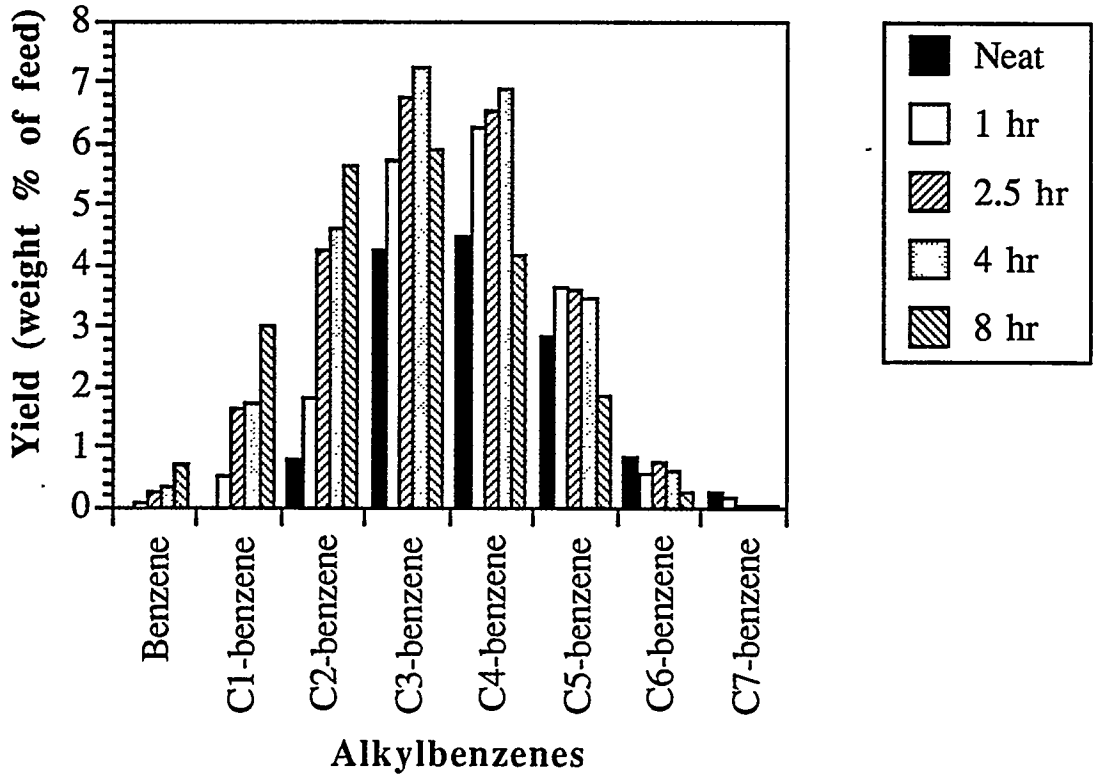

Figure 9. Alkylbenzenes Distribution of the Liquids from JP-8P2 at 450 °C for 0-8 h.

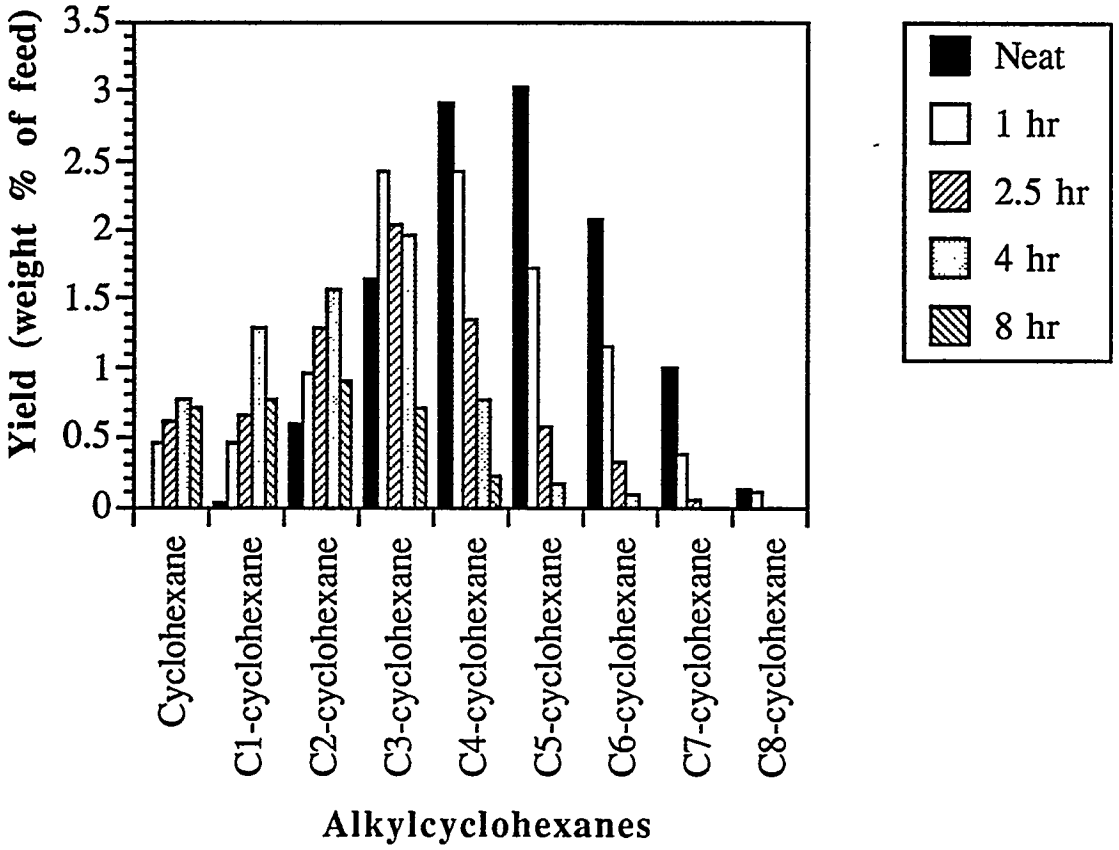

Figure 10. Alkylcyclohexanes Distribution of the Liquids from JP-8P2 at 450 °C for 0-8 h.

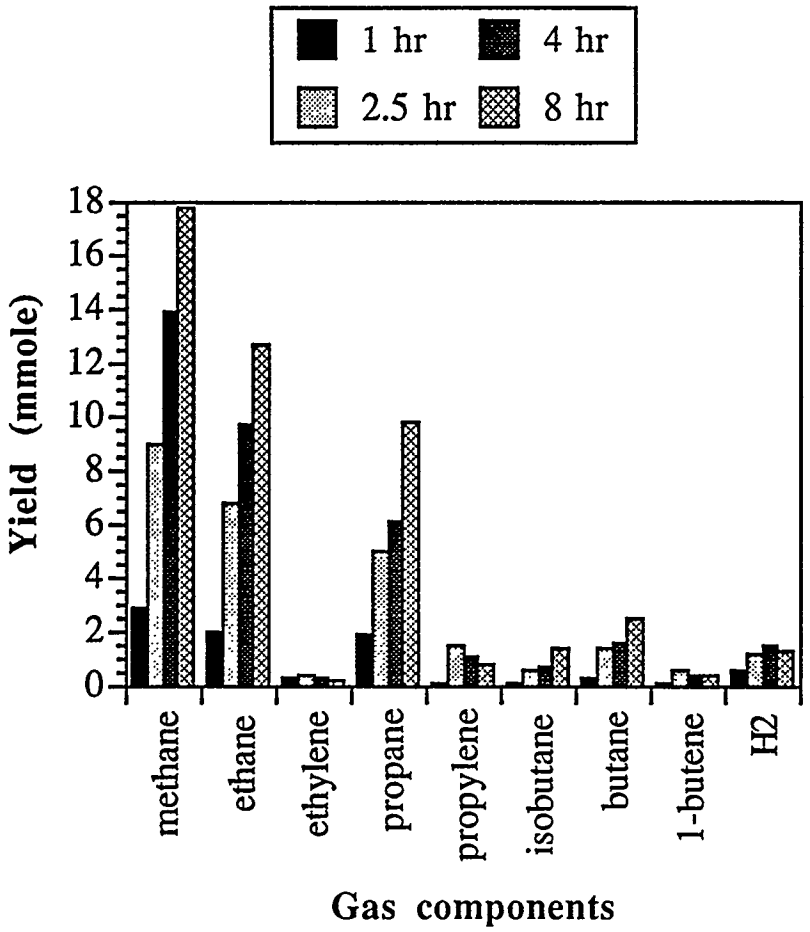

Figure 11. Yields of H_2 and $C_1 \sim C_4$ Gases from JP-8P.

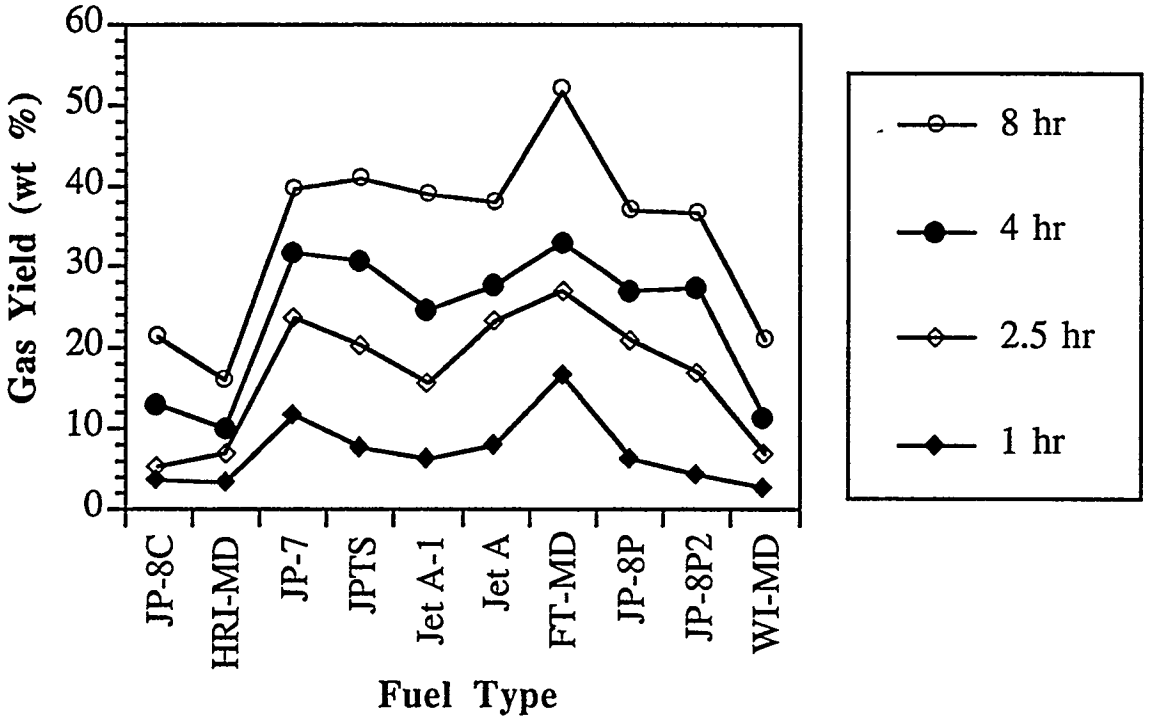

Figure 12. Yields of Gases at 450 °C for 10 Fuels.

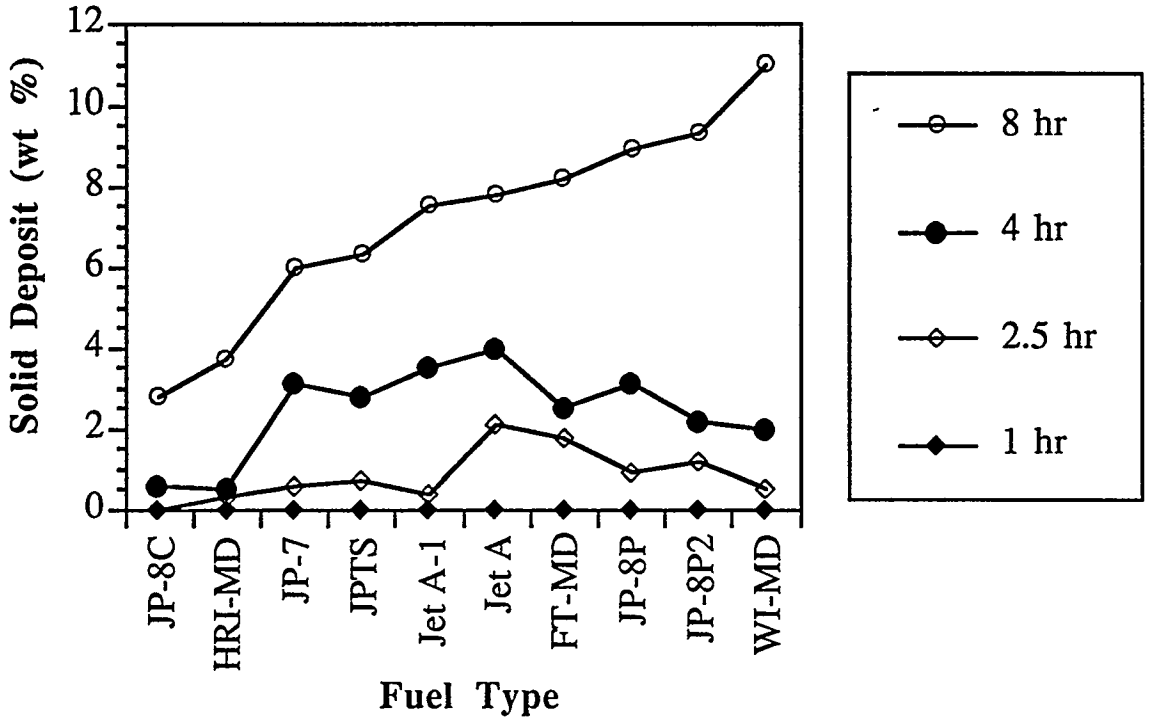

Figure 13. Yields of Solid Deposits at 450 °C for 10 Fuels.

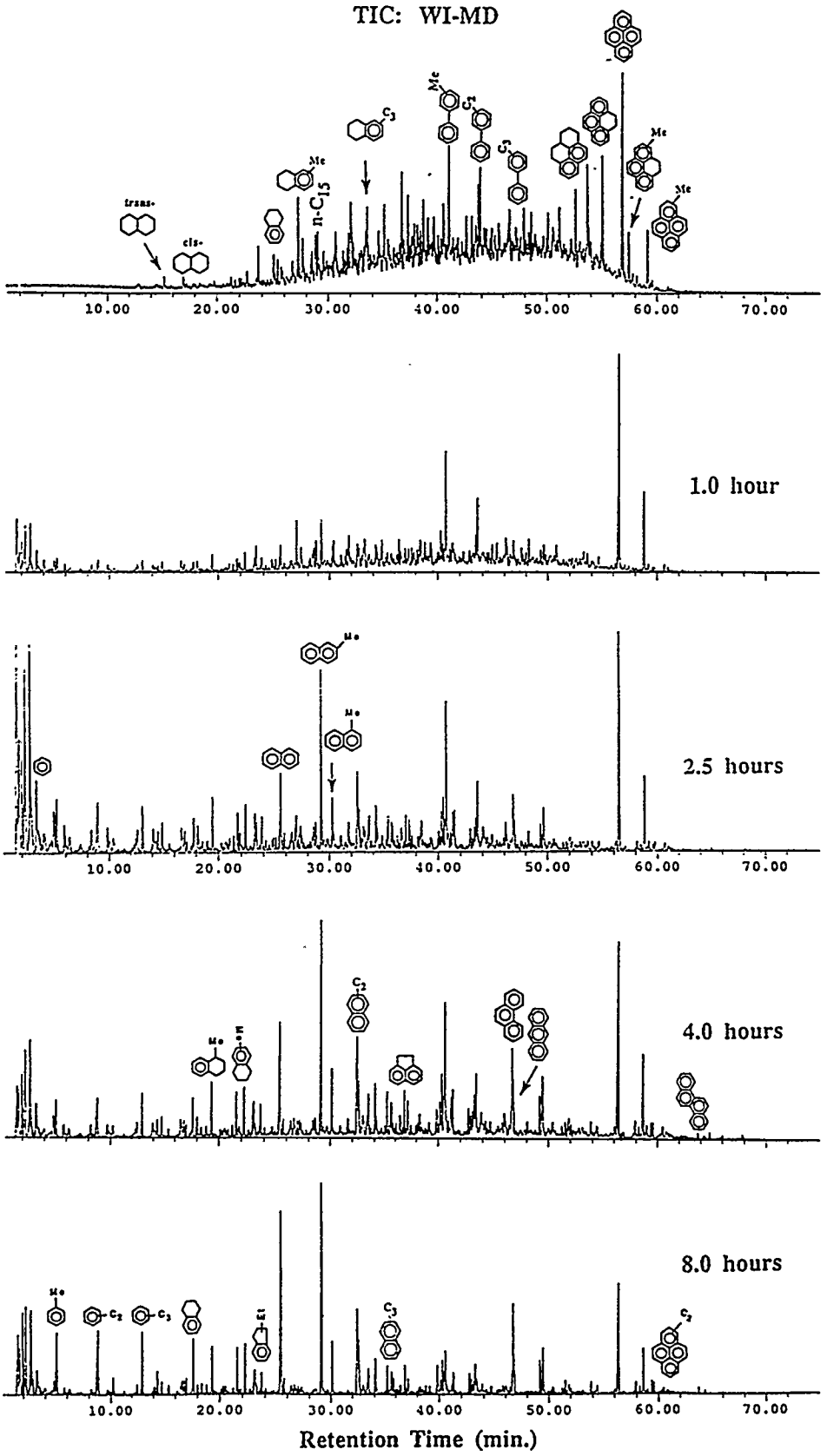

Figure 14. Total ion chromatograms of the neat sample of, and the liquid products from, WI-MD after thermal stressing at 450°C for 1-8 hours.

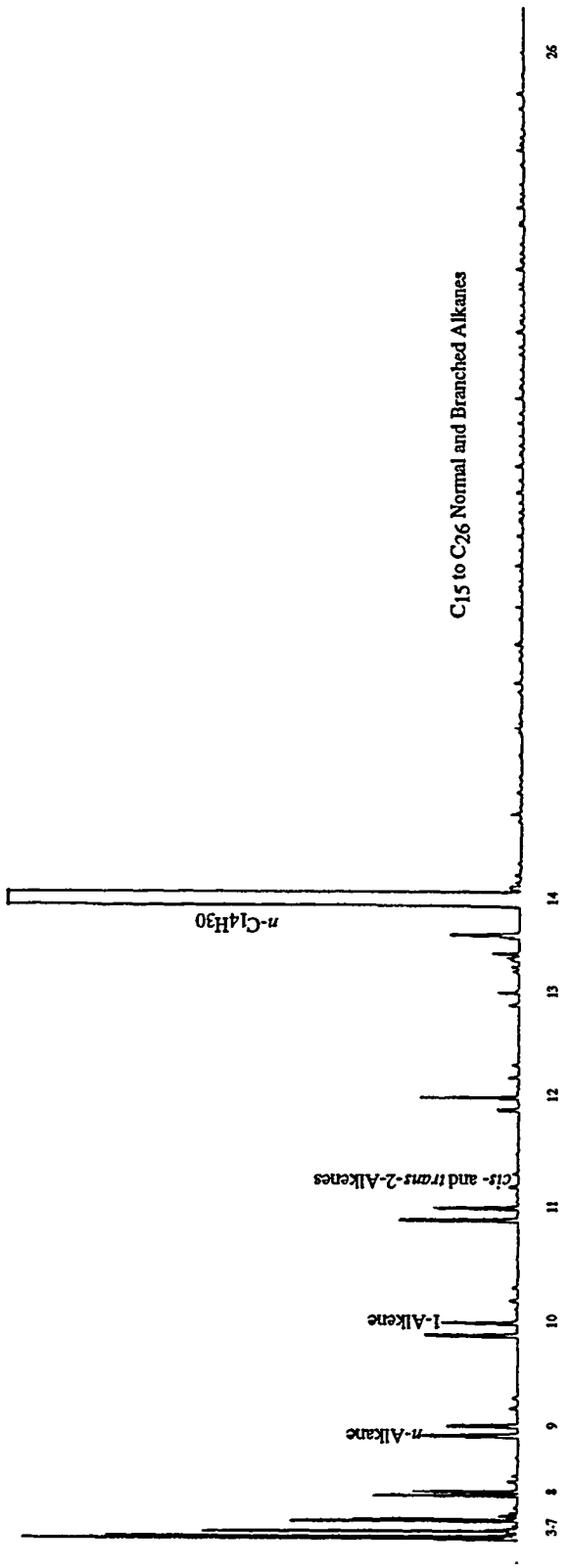

Figure 15. Chromatogram of Liquid Products from Thermal Decomposition of n-C_{14} at 425 °C for 15 min at a Loading Ratio of 0.36.

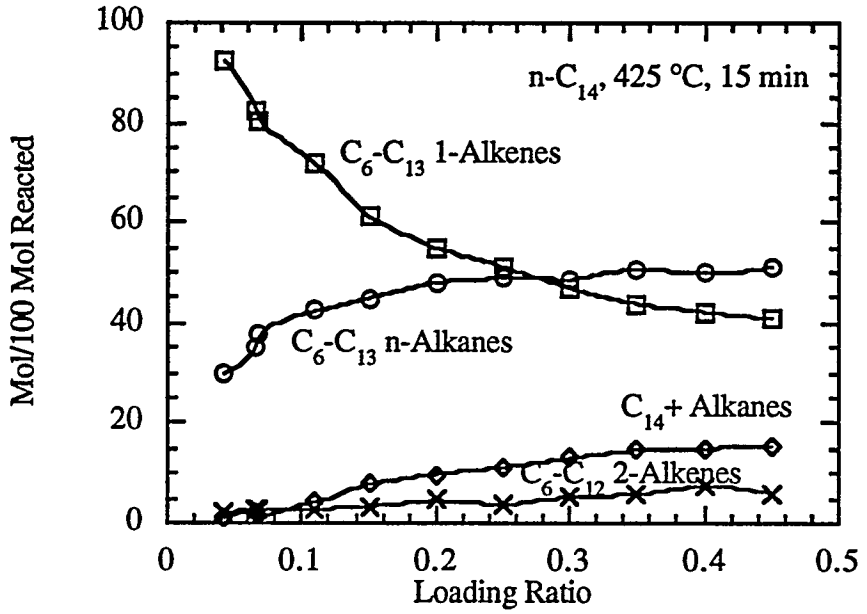

Figure 16. Overall Product Distributions as Functions of Loading Ratio from Thermal Decomposition of *n*-C_{14} at 425 °C for 15 min.

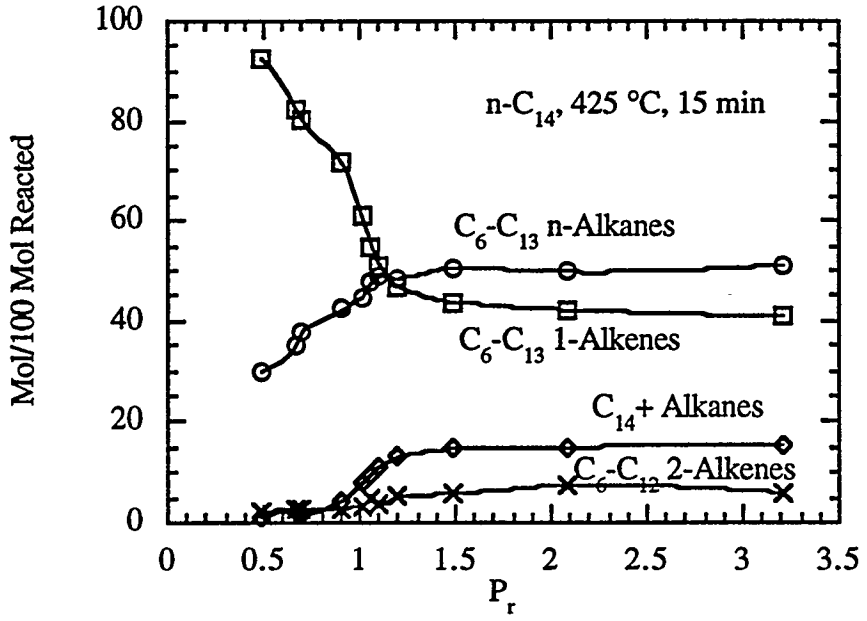

Figure 17. Overall Product Distributions as Functions of Reduced Pressure from Thermal Decomposition of *n*-C_{14} at 425 °C for 15 min.

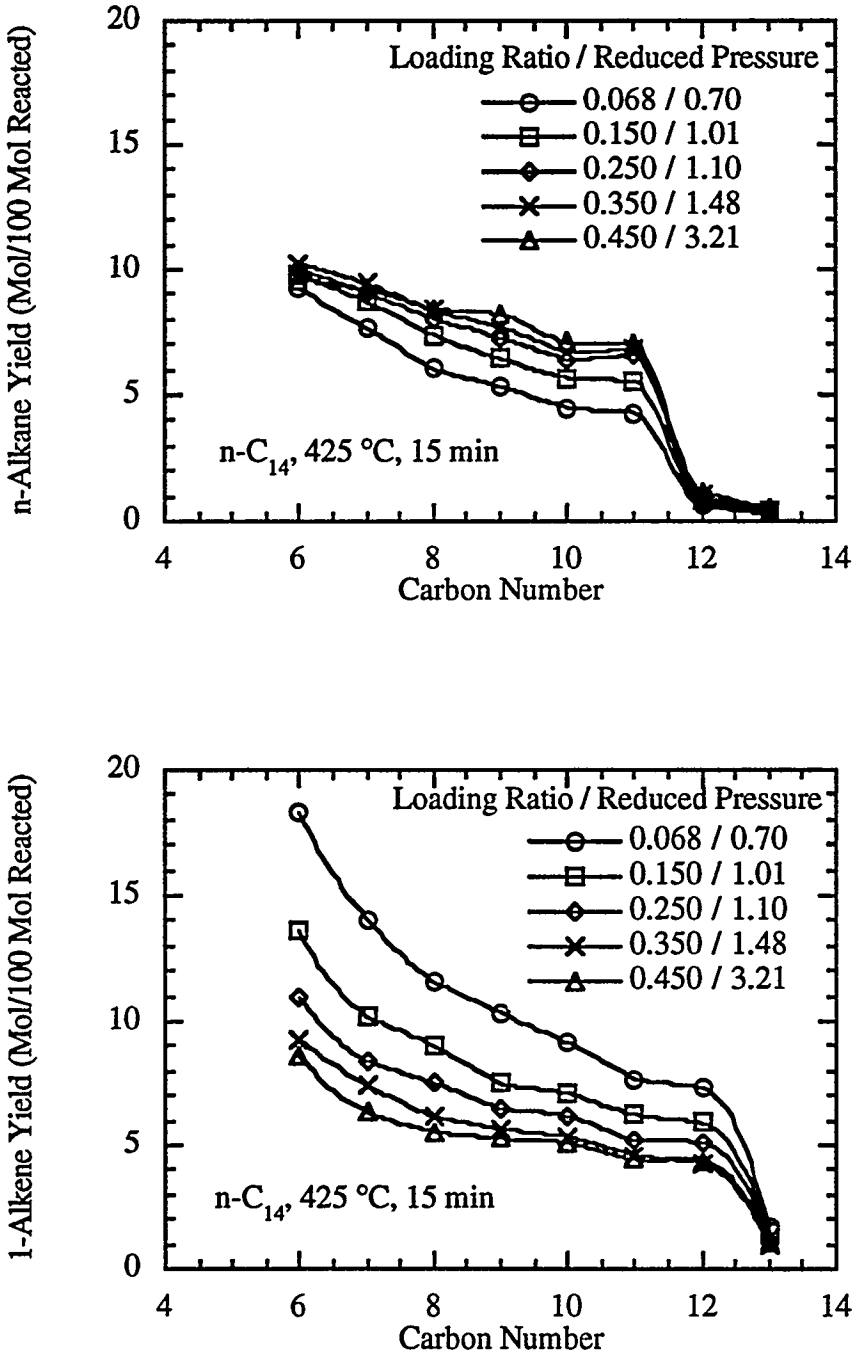

Figure 18. Effects of Loading Ratio on Product Distributions from Thermal Decomposition of *n*-C_{14} at 425 °C for 15 min.

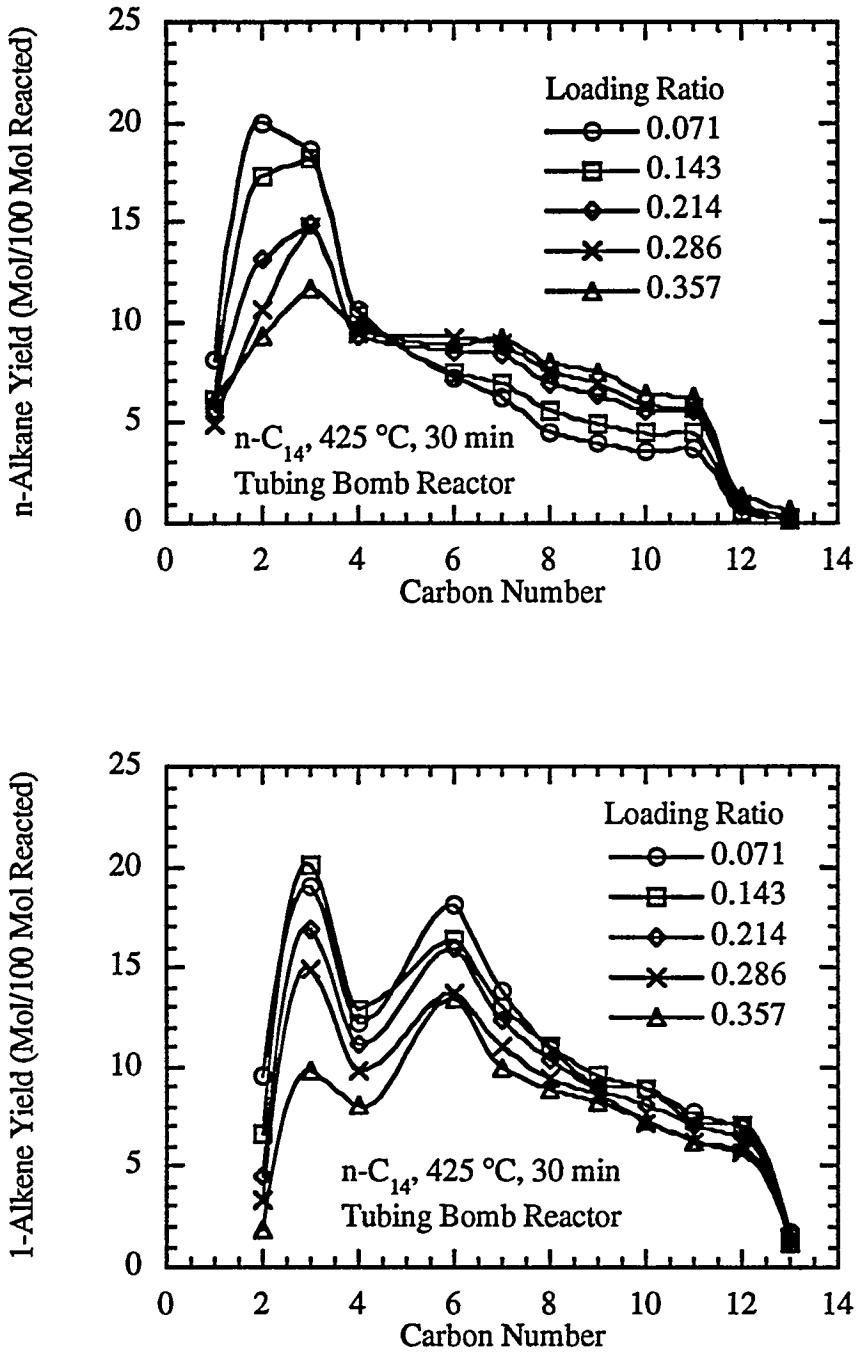

Figure 19. Effects of Loading Ratio on Product Distributions from Thermal Decomposition of *n*-C_{14} in Tubing Bomb Reactor at 425 °C for 30 min.

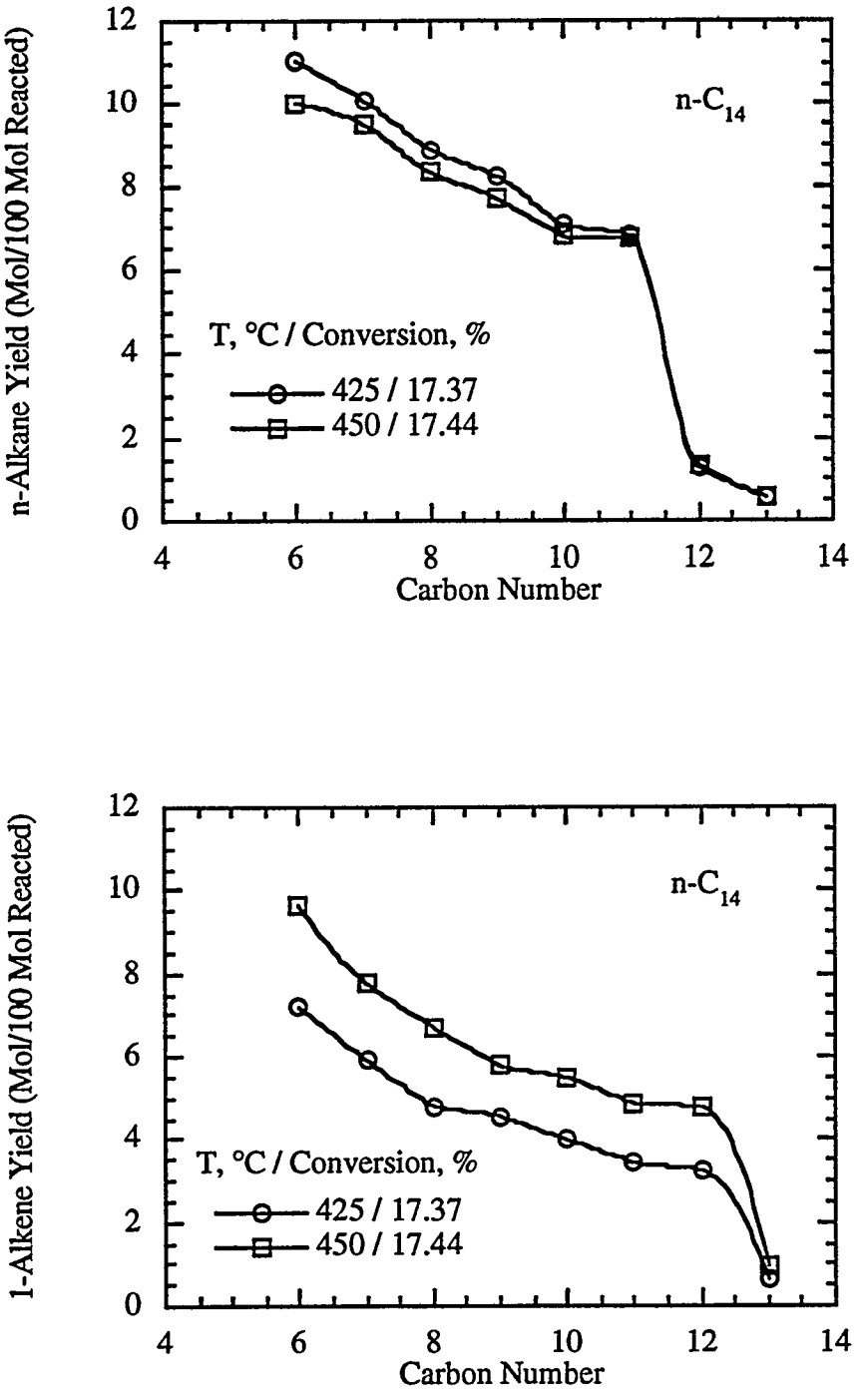

Figure 20. Effects of Temperature on Product Distributions from Thermal Decomposition of *n*-C_{14}.

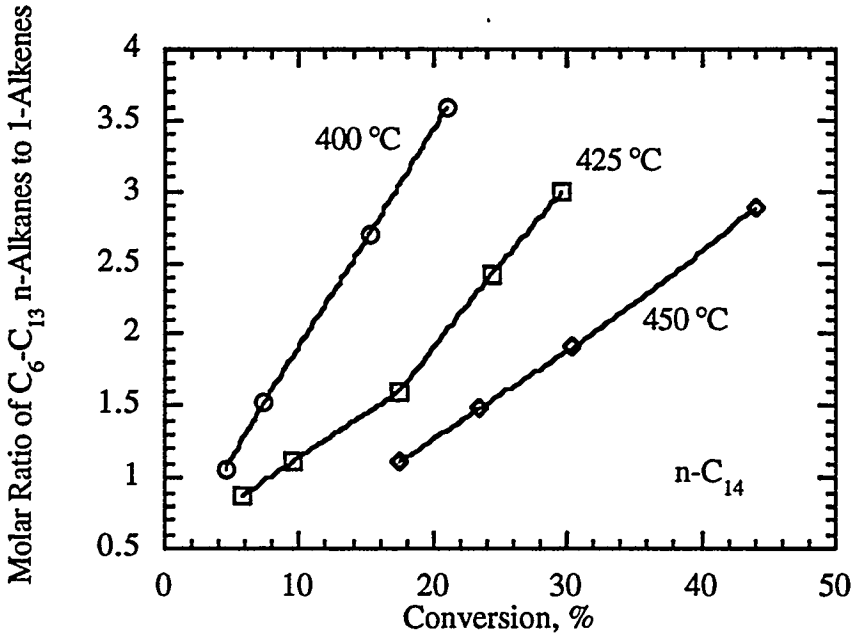

Figure 21. Effects of Temperature and Conversion on Molar Ratio of C_6-C_{13} *n*-Alkanes to 1-Alkenes from Thermal Decomposition of *n*-C_{14} at a Loading Ratio of 0.36.

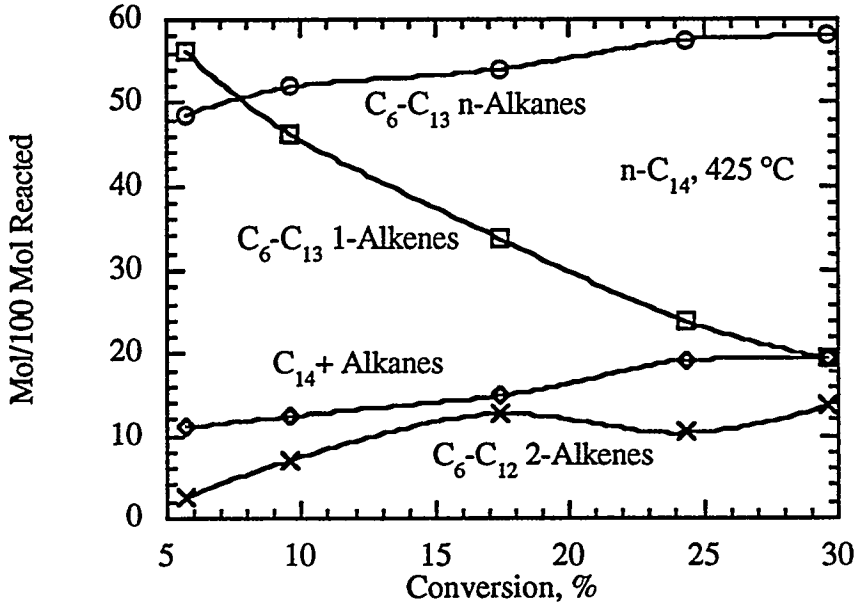

Figure 22. Overall Product Distributions as Functions of Conversion from Thermal Decomposition of *n*-C_{14} at 425 °C.

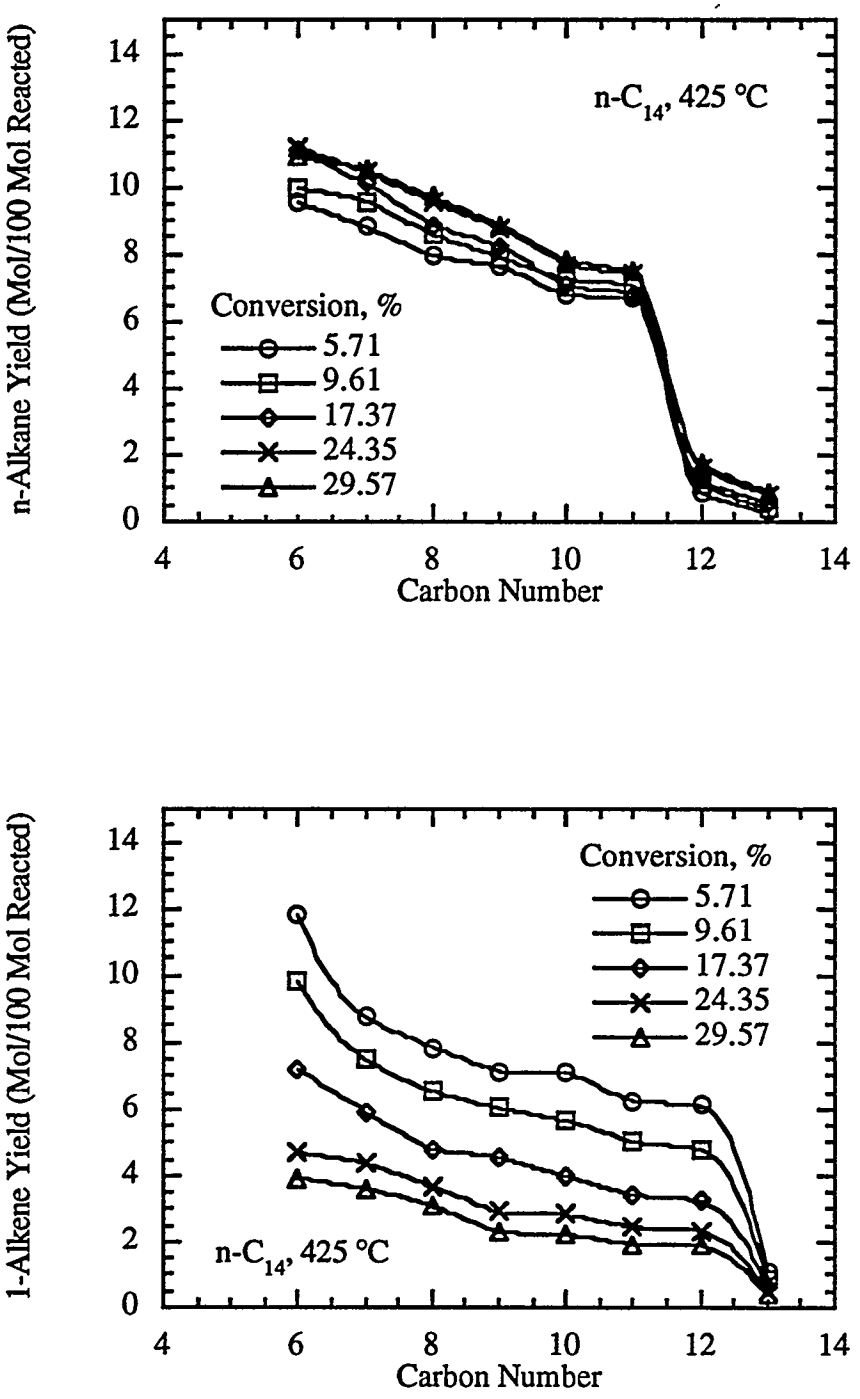

Figure 23. Effects of Conversion on Product Distributions from Thermal Decomposition of *n*-C_{14} at 425 °C.

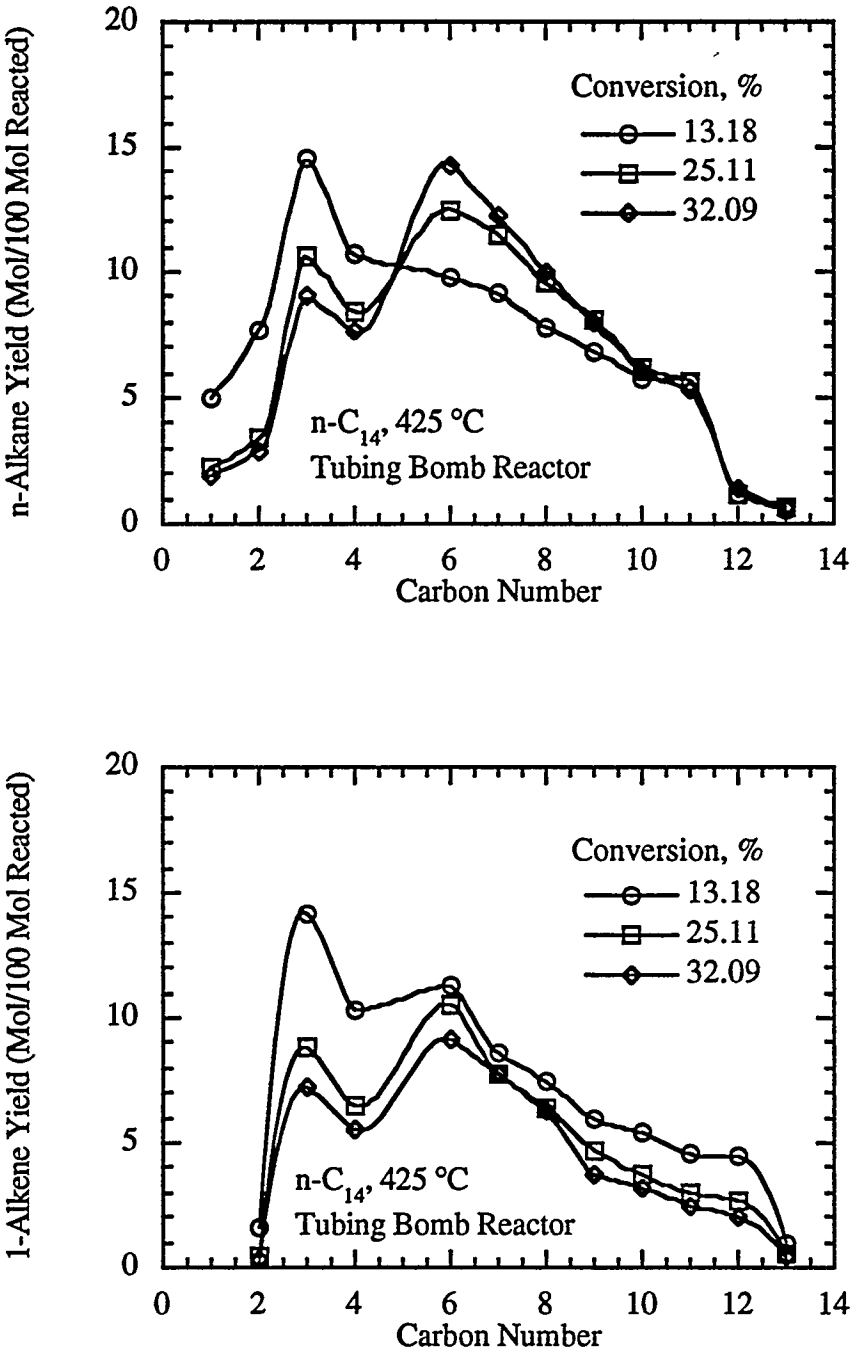

Figure 24. Effects of Conversion on Product Distributions from Thermal Decomposition of *n*-C_{14} in Tubing Bomb Reactor at 425 °C.

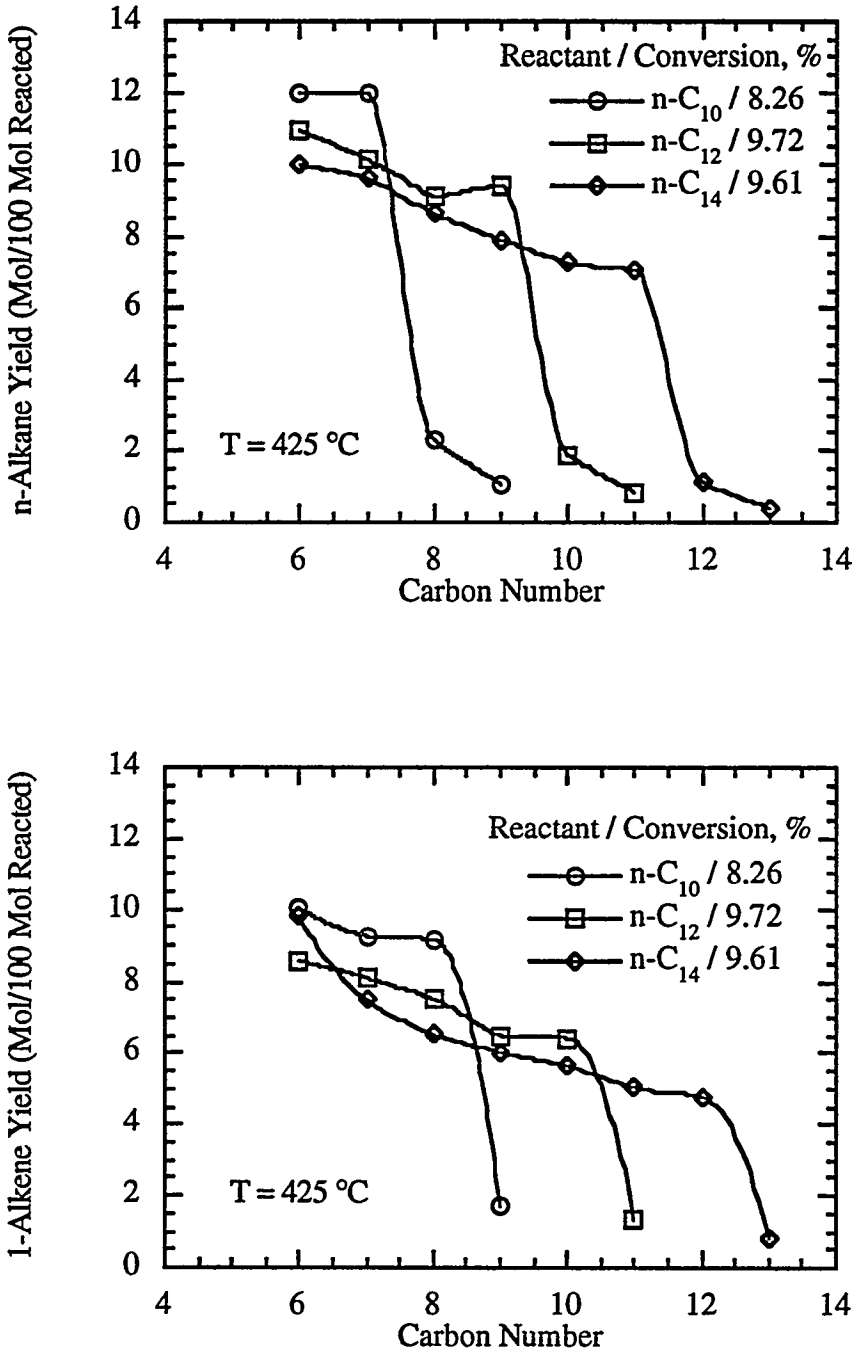

Figure 25. Effects of Chain Length on Product Distributions from Thermal Decomposition of *n*-Alkanes at 425 °C.

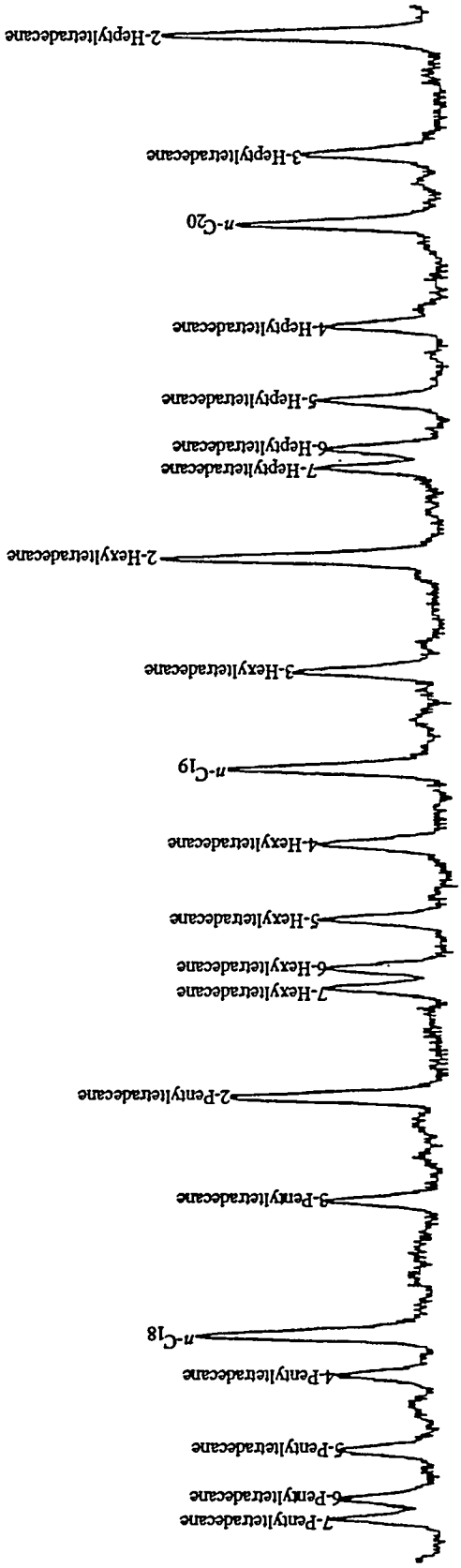

Figure 26. Expanded Chromatogram of Liquid Products from Thermal Decomposition of n-C_{14} at 425 °C for 15 min at a Loading Ratio of 0.36.

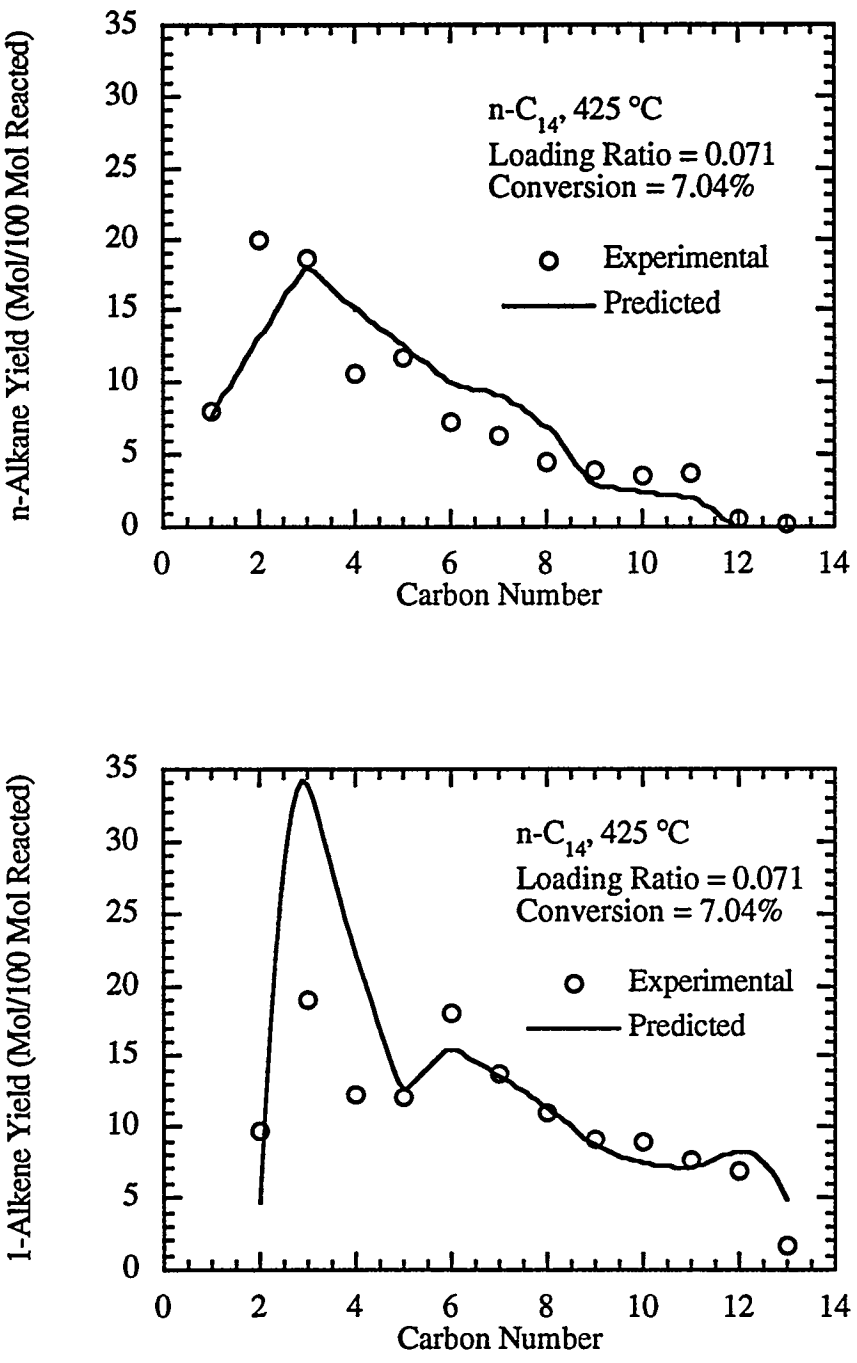

Figure 27. Comparison of Predicted Product Distributions with Experimental Data from the Thermal Decomposition of *n*-C_{14} at 425 °C and for a Loading Ratio of 0.071.

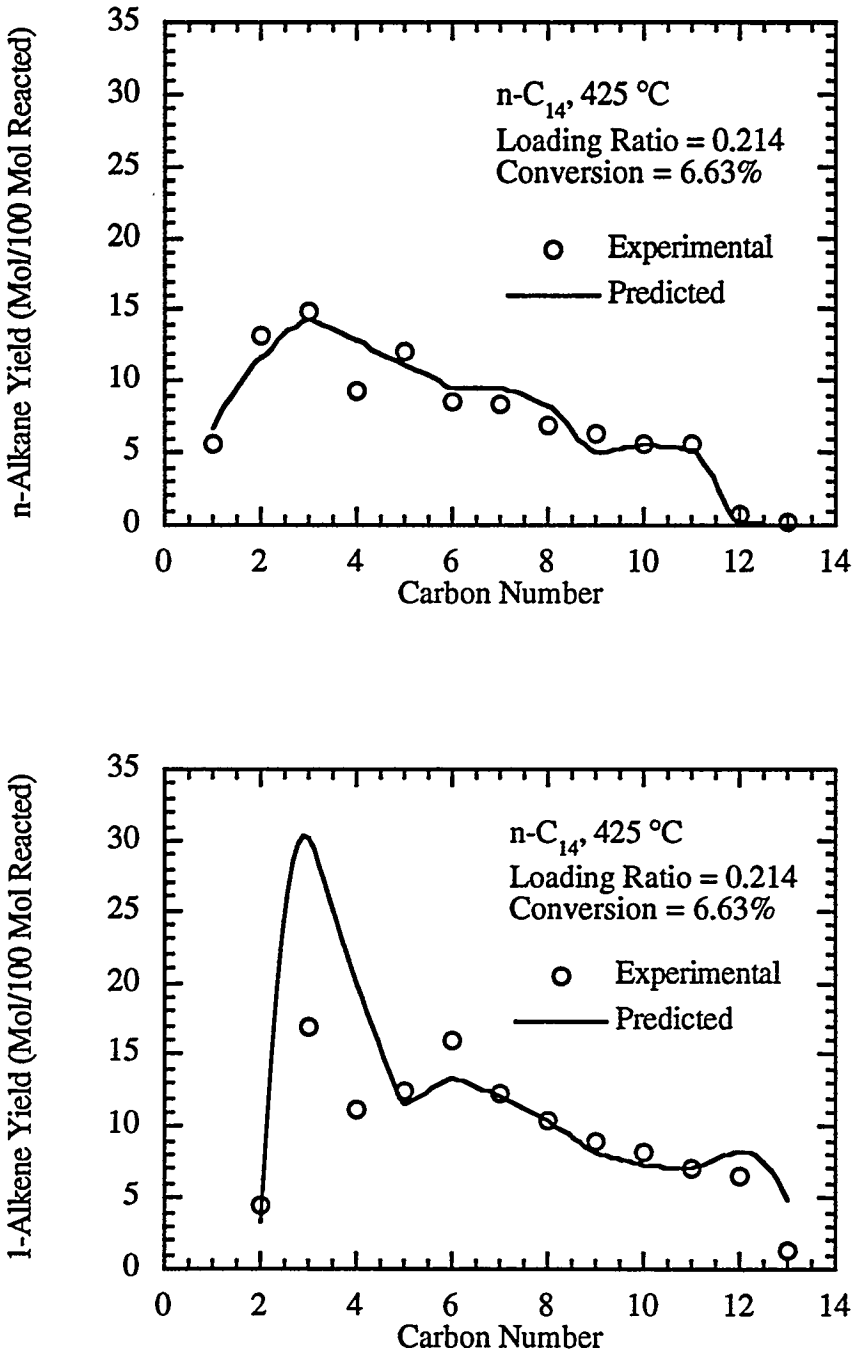

Figure 28. Comparison of Predicted Product Distributions with Experimental Data from the Thermal Decomposition of *n*-C_{14} at 425 °C and for a Loading Ratio of 0.214.

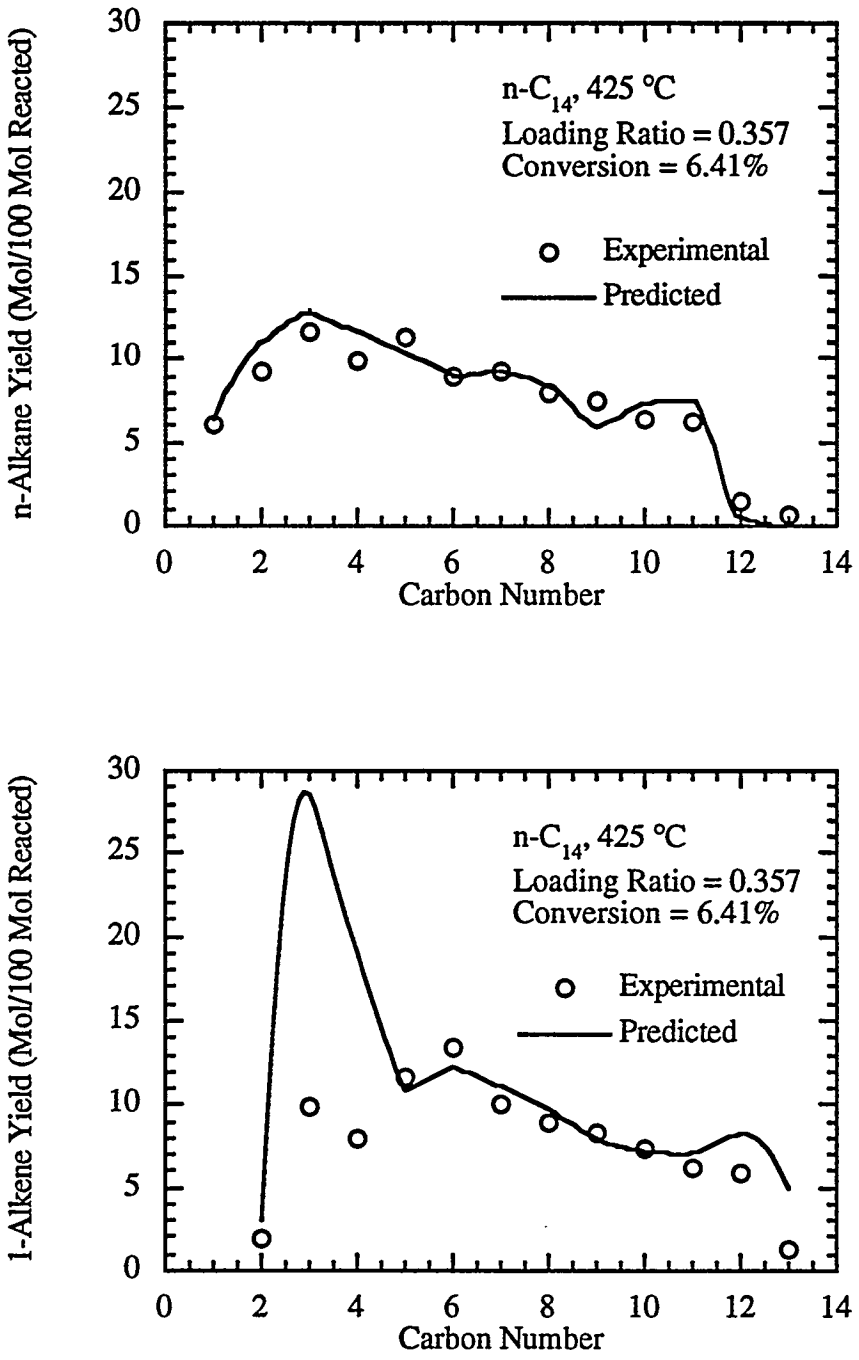

Figure 29. Comparison of Predicted Product Distributions with Experimental Data from the Thermal Decomposition of *n*-C_{14} at 425 °C and for a Loading Ratio of 0.357.

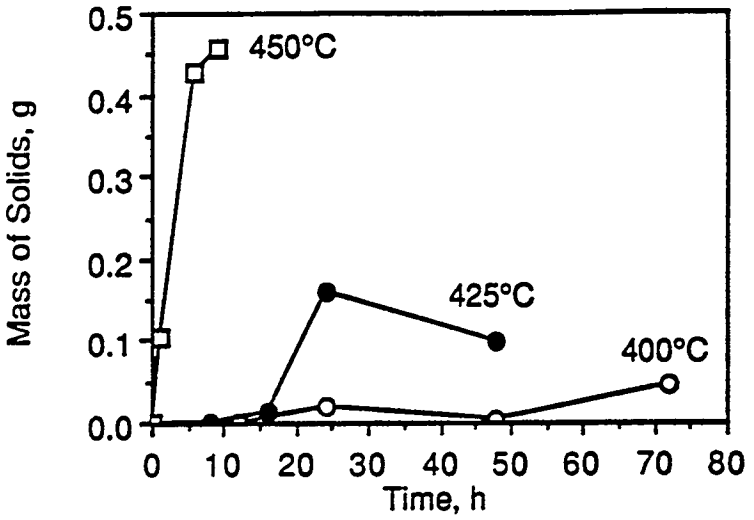

Figure 30. Formation of solids from n-decane at 400, 425, and 450°C.[2]

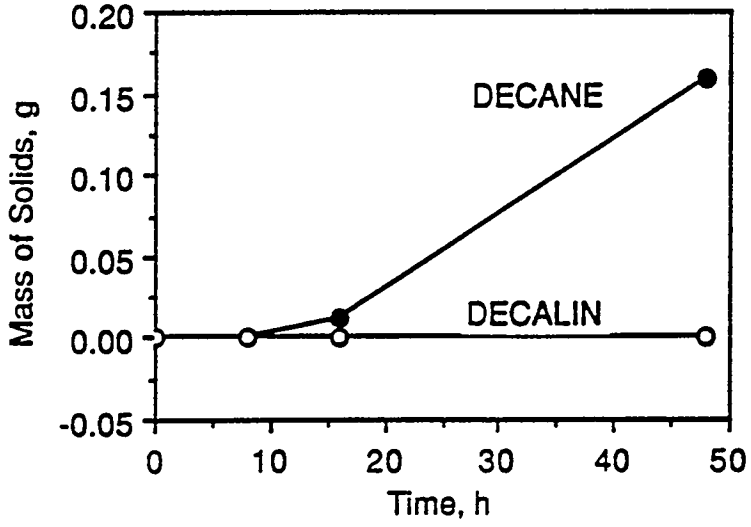

a

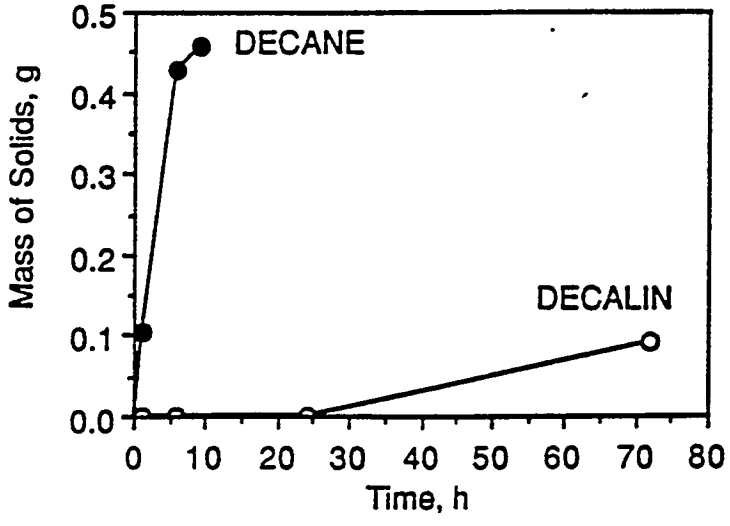

b

Figure 31. Solid formation from decane and decalin at 425°C (a) and 450°C (b).[2]

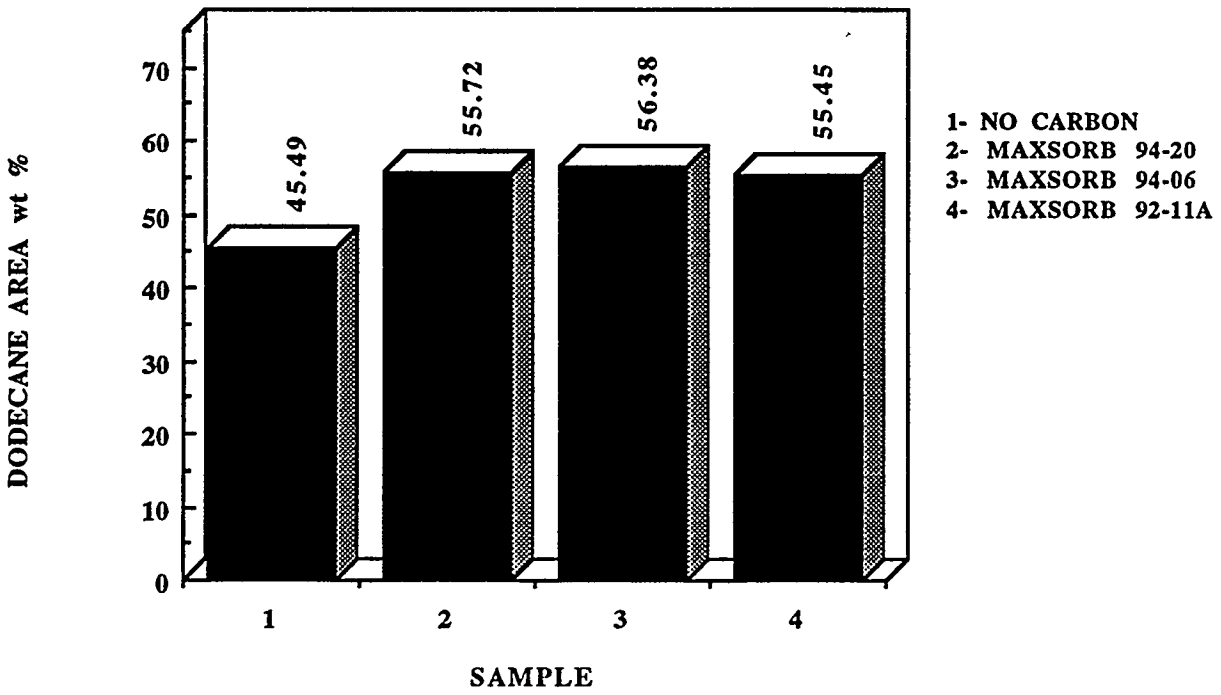

Figure 32. The Area Percent of Dodecane in the Liquids Obtained after Thermal Stressing of Dodecane + 5% Decalin + 100 mg Maxsorb Carbons at 450°C for 1h.

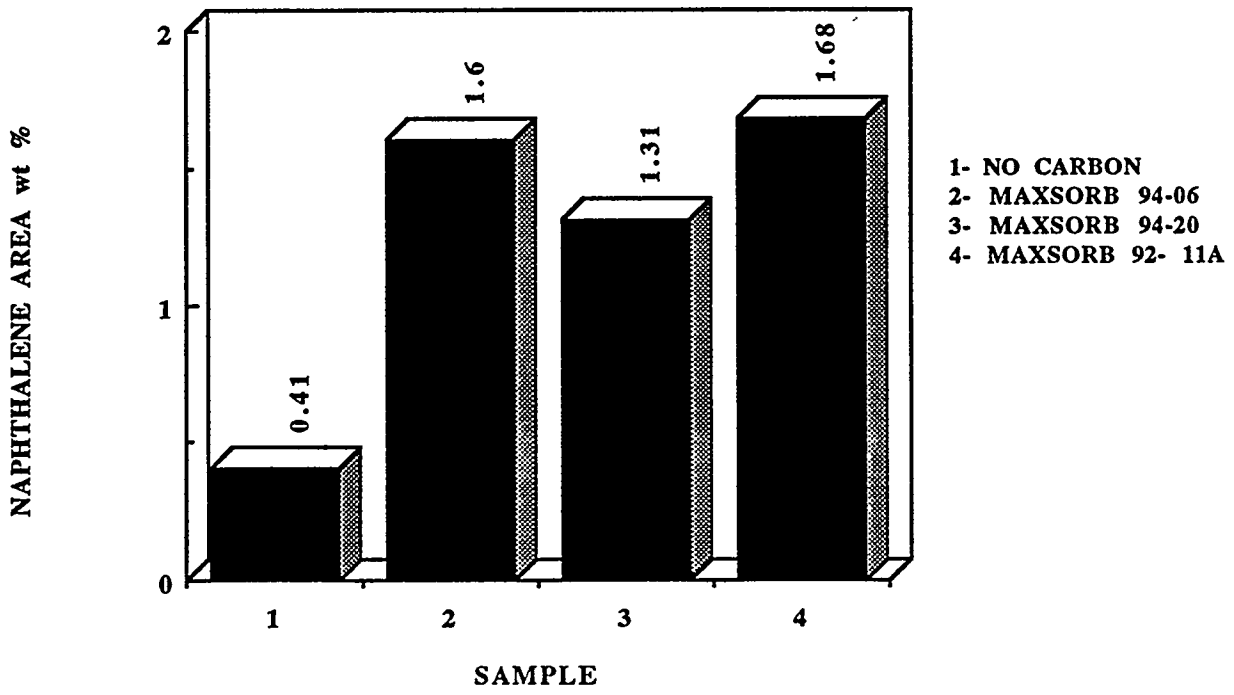

Figure 33. The Area Percent of Naphthalene in the Liquids Obtained after Thermal Stressing of Dodecane + 5% Decalin + 100 mg Maxsorb Carbons at 450°C for 1h.

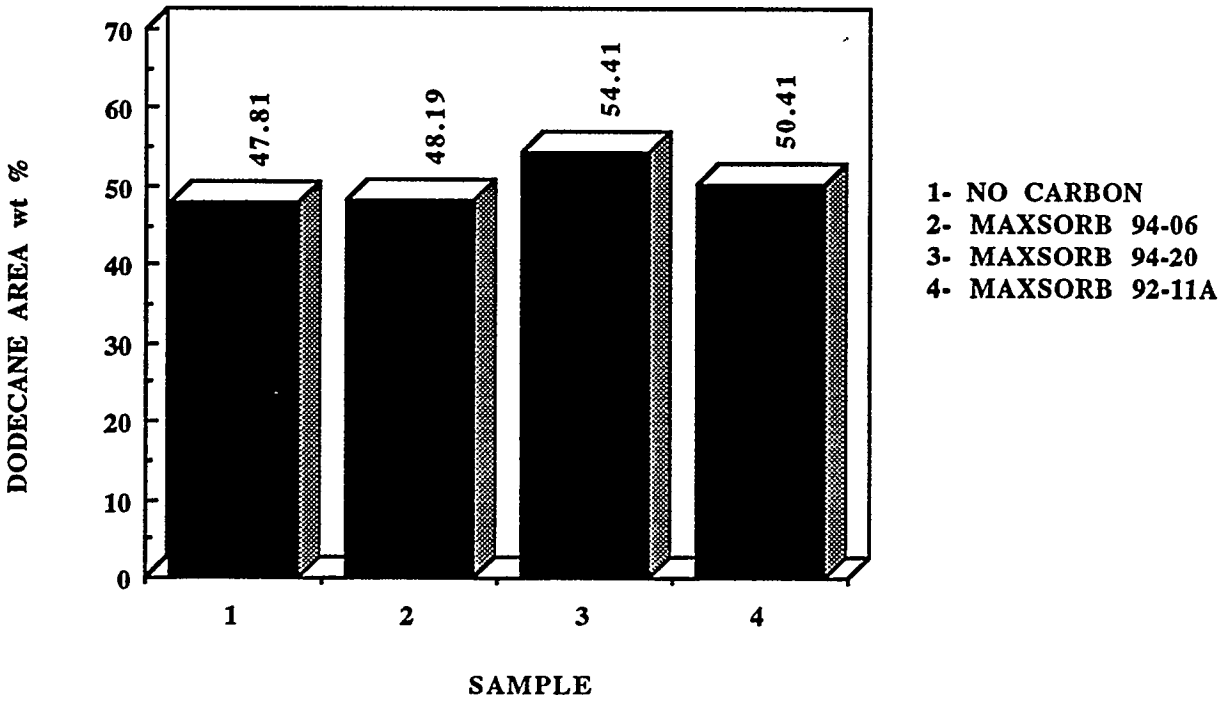

Figure 34. The Area Percent of Dodecane in the Liquids Obtained after Thermal Stressing of Dodecane + 5% Decalin + 50 mg Maxsorb Carbons at 425°C for 5h.

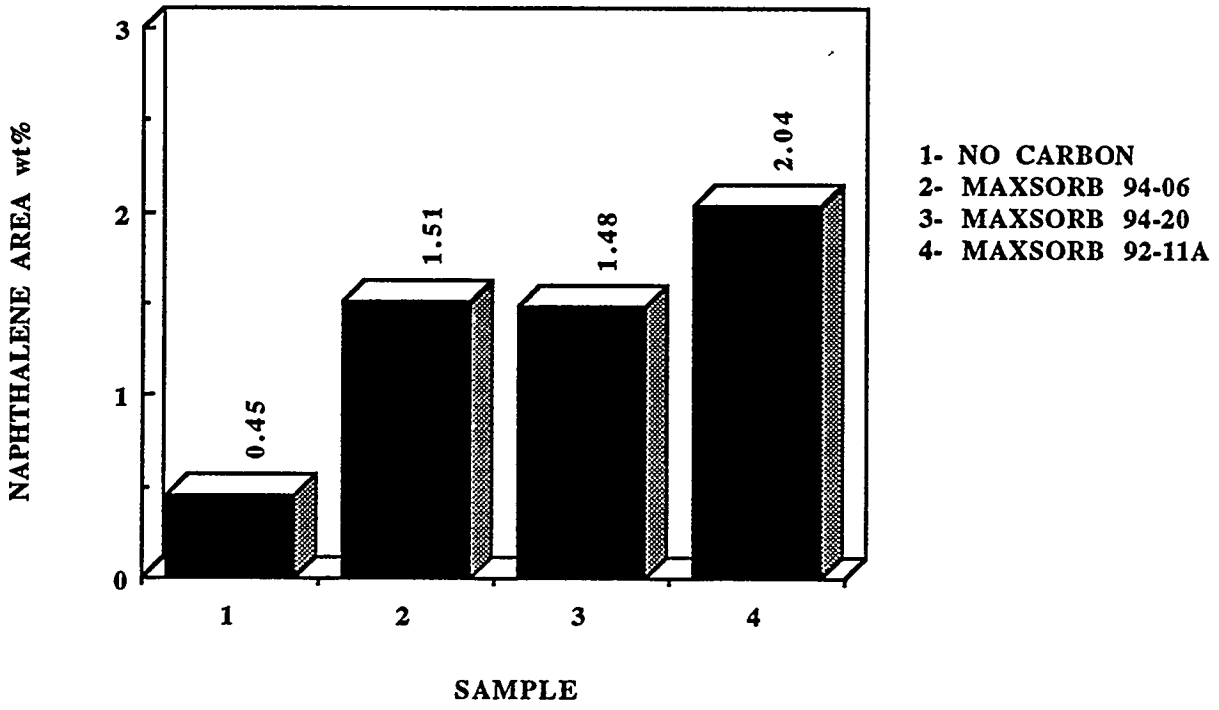

Figure 35. The Area Percent of Naphthalenes in the Liquids Obtained after Thermal Stressing of Dodecane + 5% Decalin + 50 mg Maxsorb Carbons at 425°C for 5h.

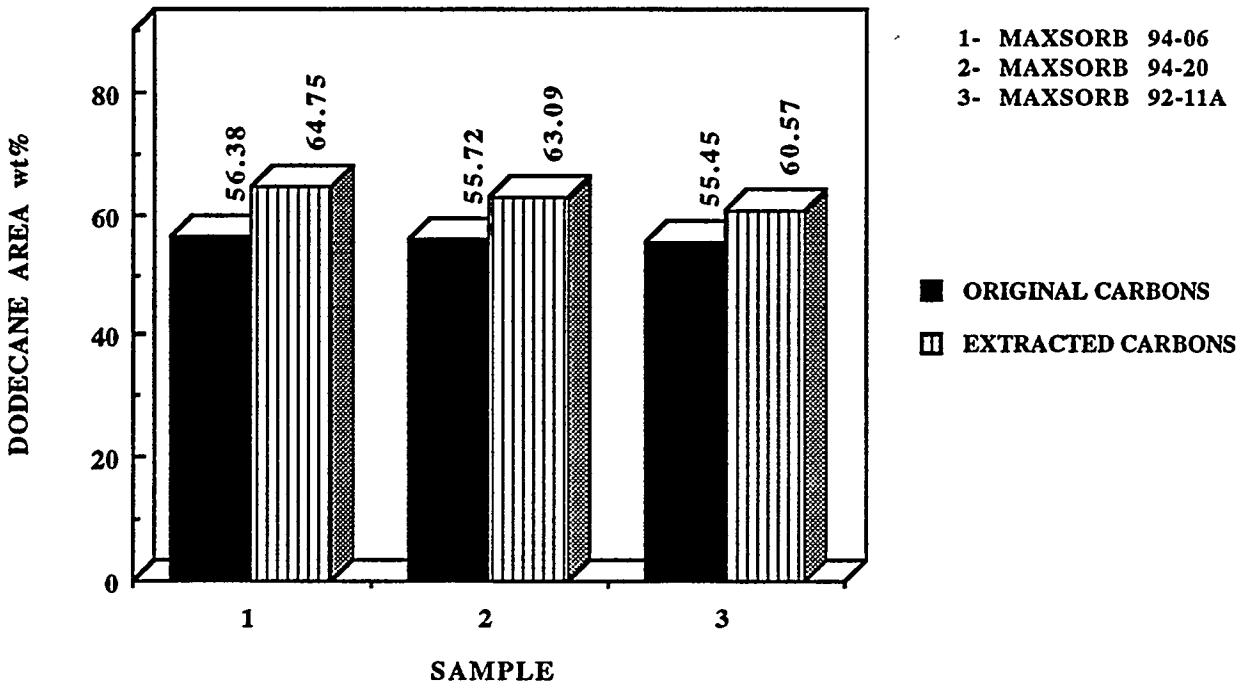

Figure 36. The Area Percent of Dodecanes in the Liquids Obtained after Thermal Stressing of Dodecane + 5% Decalin + 100 mg Original and Extracted Maxsorb Carbons at 450°C for 1h.

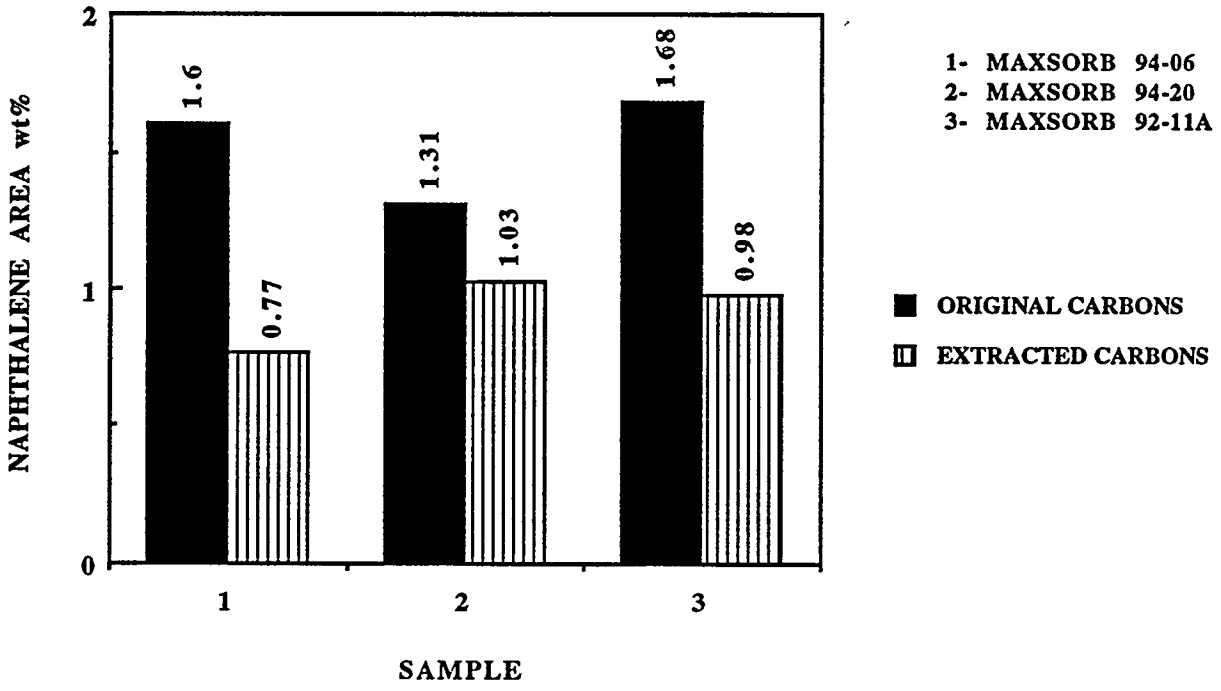

Figure 37. The Area Percent of Naphthalenes in the Liquids Obtained after Thermal Stressing of Dodecane + 5% Decalin + 100 mg Original and Extracted Maxsorb Carbons at 450°C for 1h.

a

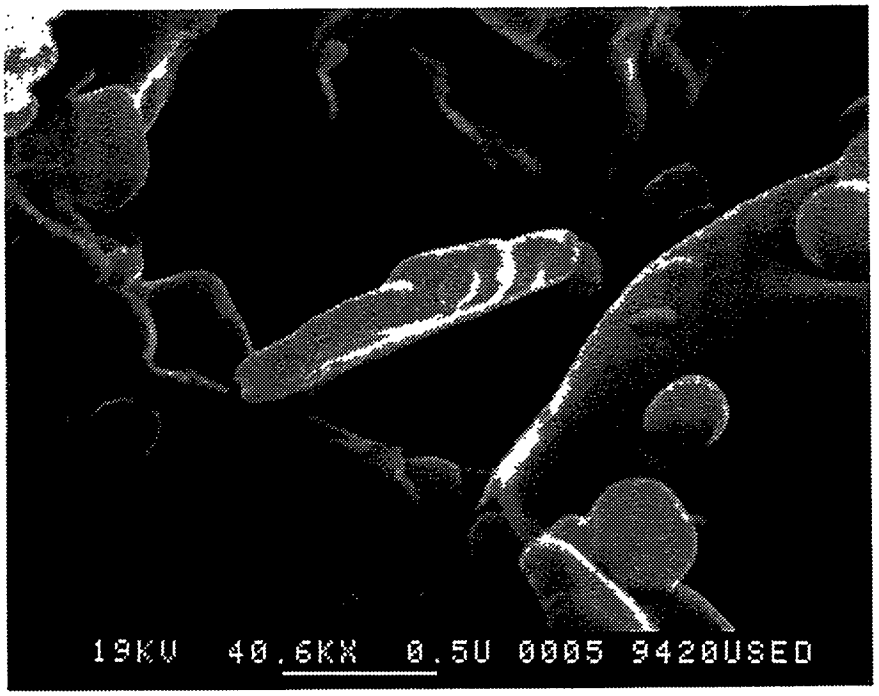

b

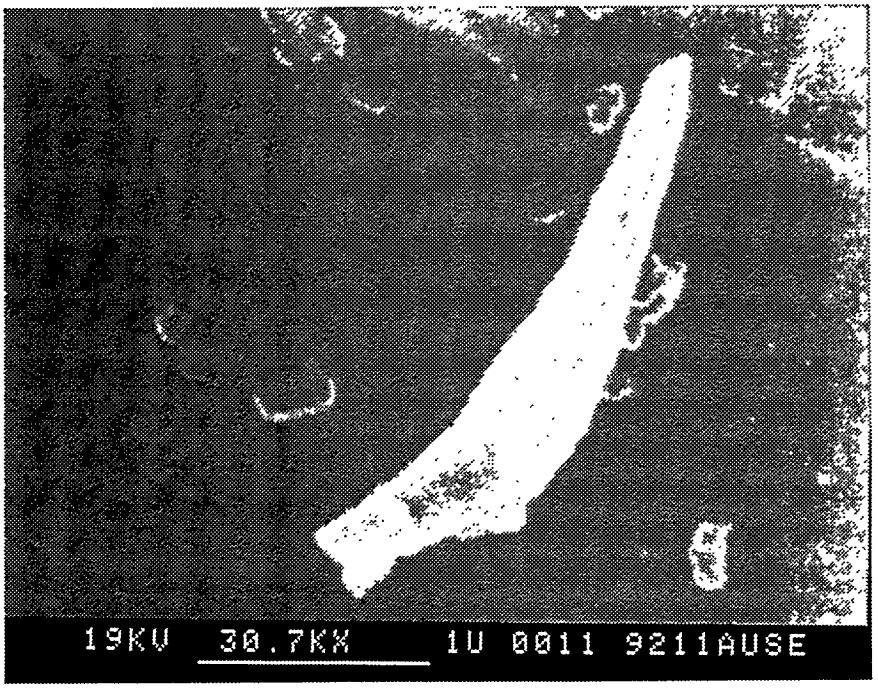

Figure 38. Scanning Electron Micrographs of (a) Used Maxsorb 94-20; (b) Used Maxsorb 92-11A Stressed subsequently with Dodecane + 5% Decalin at 425°C for 5h.

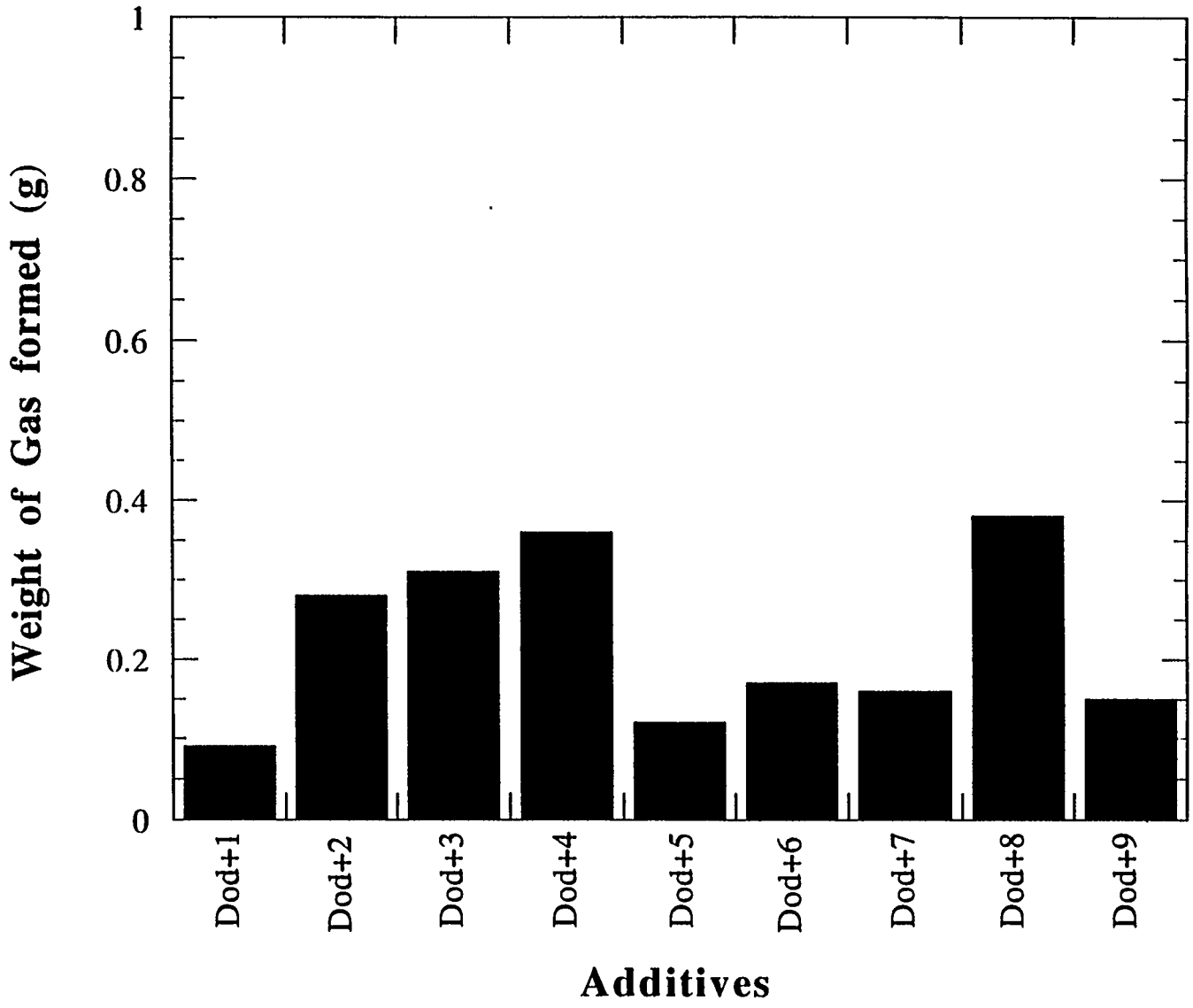

Figure 39. Weight of gas formed after stressing dodecane for 3h at 425°C in the presence of additives

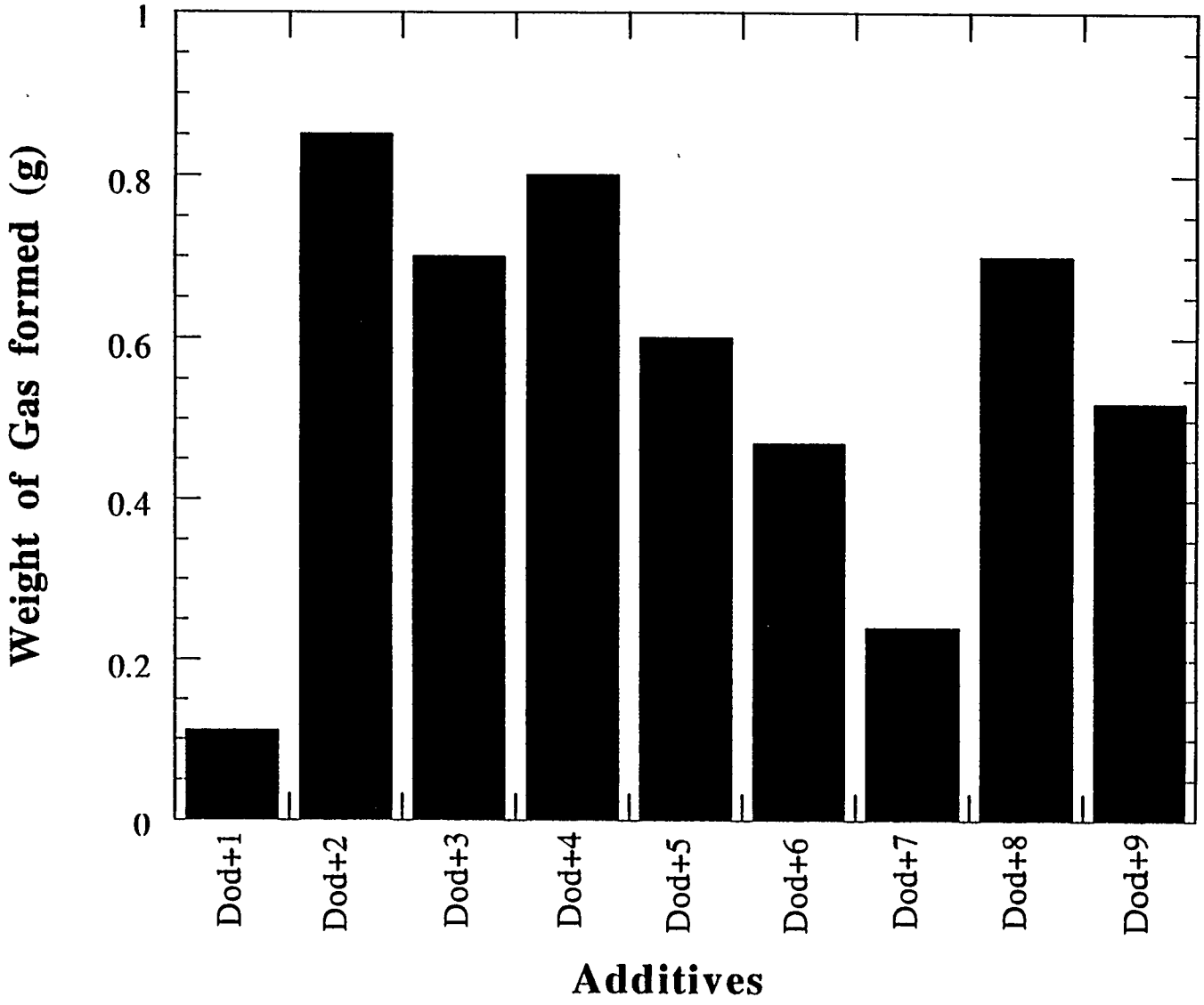

Figure 40. **Weight of gas formed after stressing dodecane for 6h at 425°C in the presence of additives.**

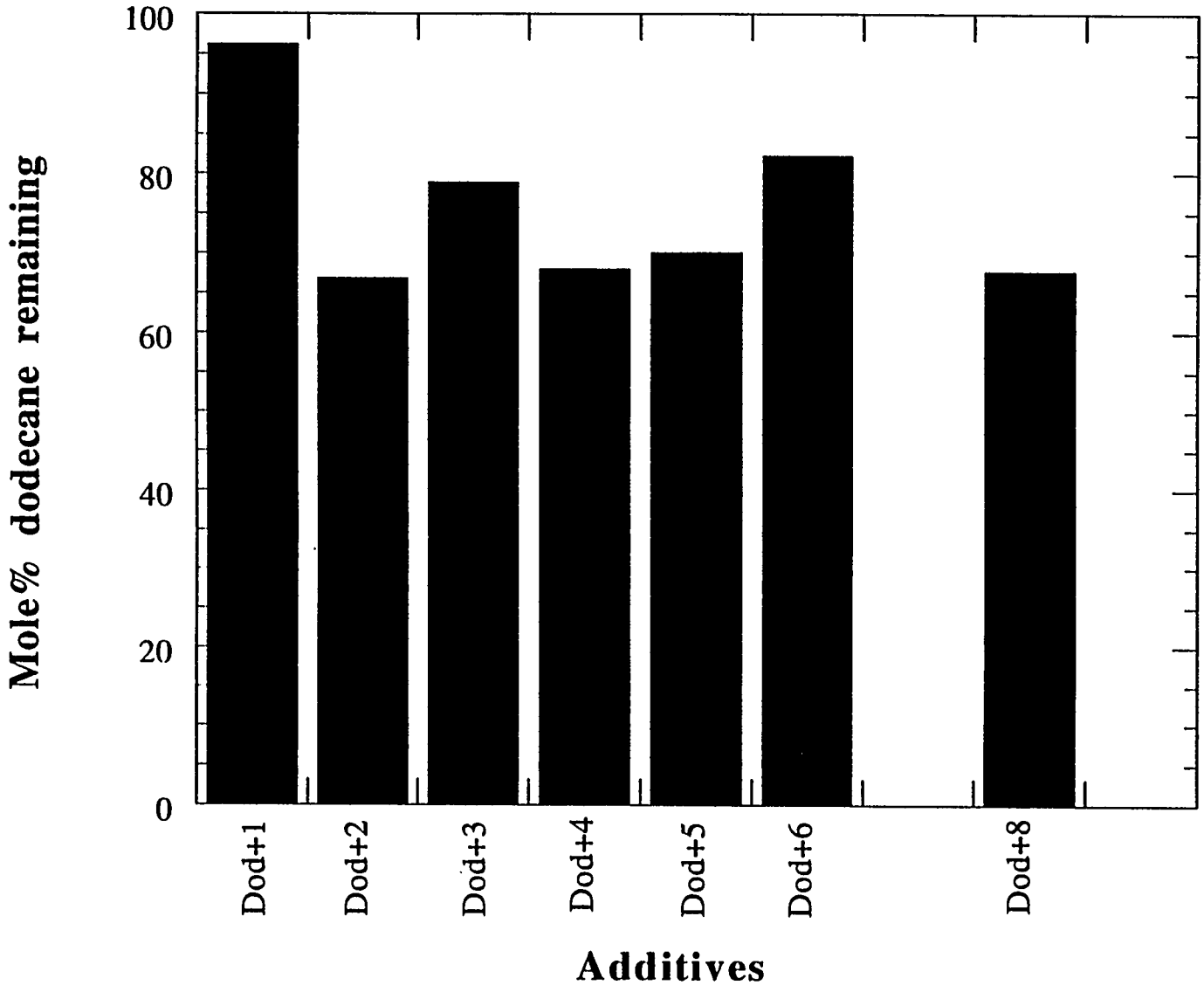

Figure 41. Mole% dodecane remaining after stressing dodecane for 3h at 425°C in the presence of additives.

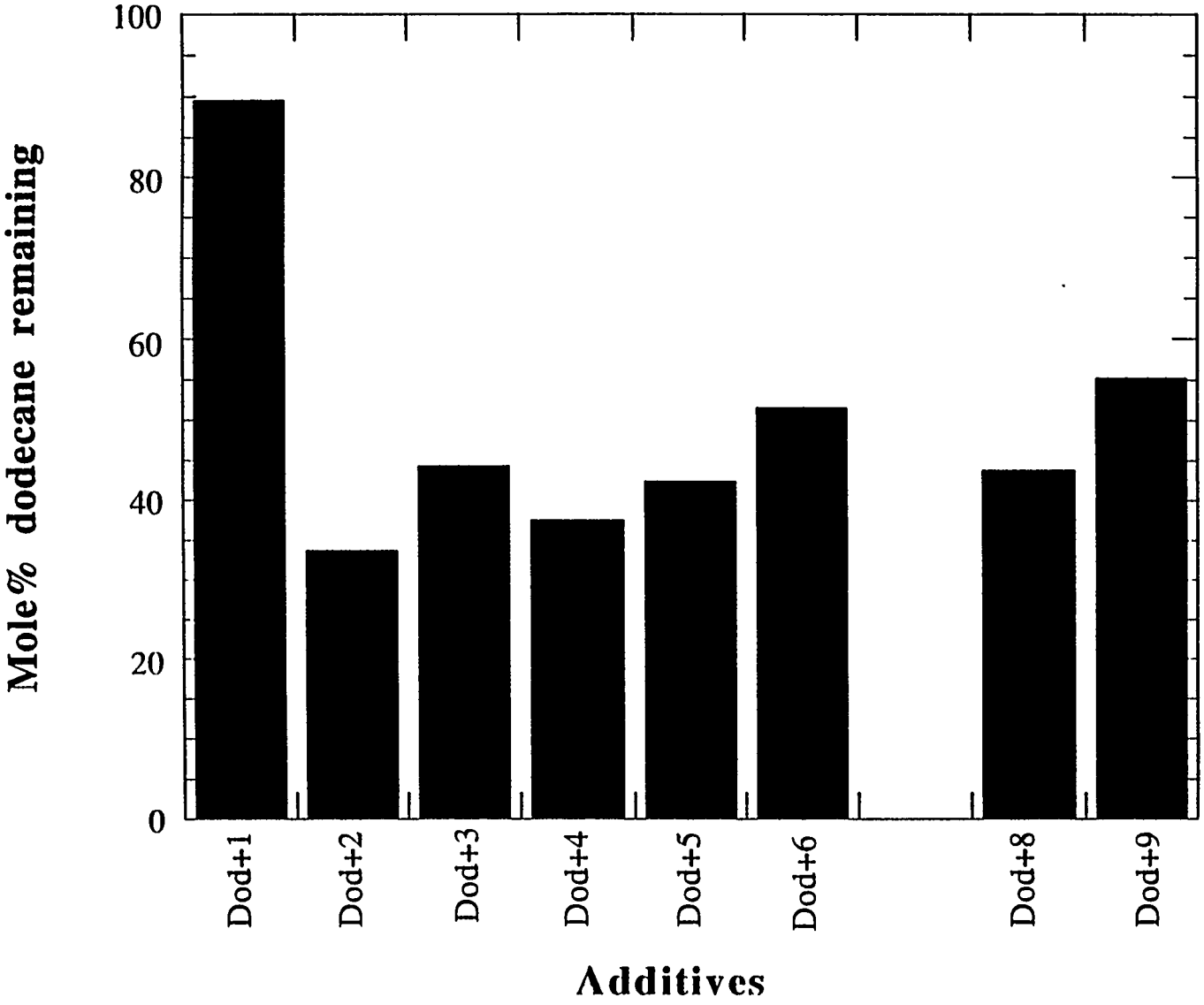

Figure 42. Mole% dodecane remaining after stressing dodecane for 6h at 425°C in the presence of additives.

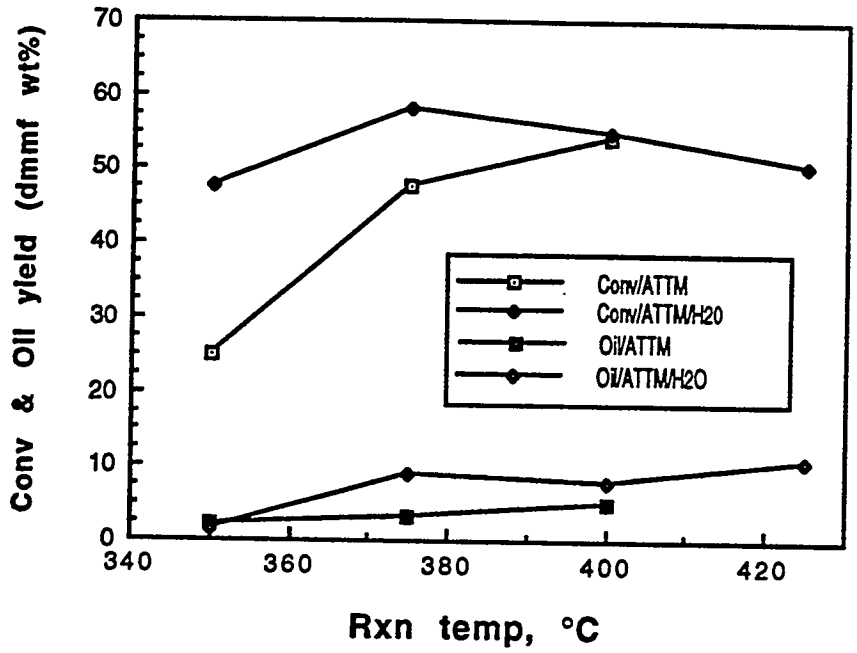

Figure 43. Temperature Versus Conversion Profiles for Catalytic Runs of Pittsburgh #8 Coal with ATTM and ATTM + Water.

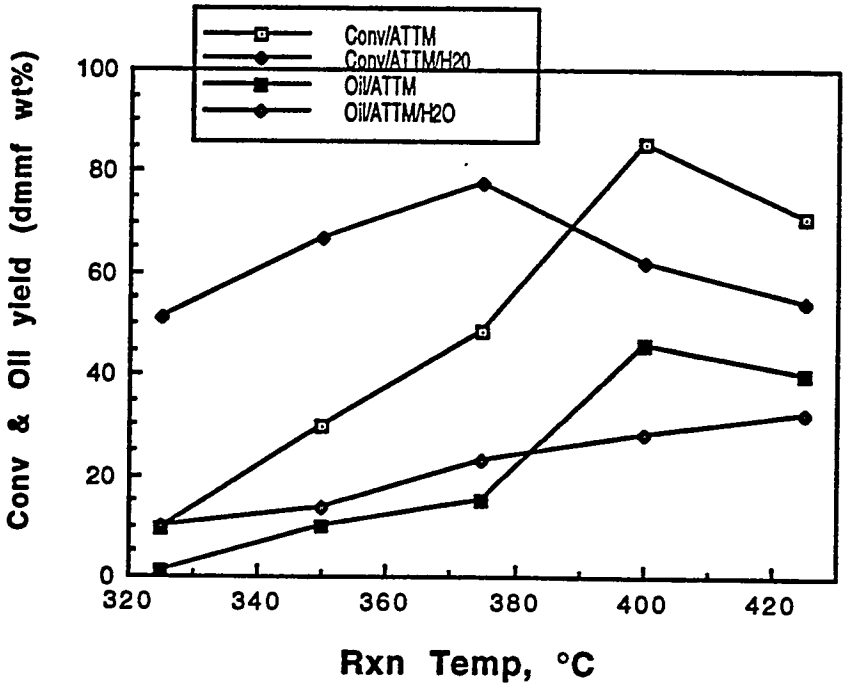

Figure 44. Temperature Versus Conversion Profiles for Catalytic Runs of Wyodak Coal with ATTM and ATTM + Water.

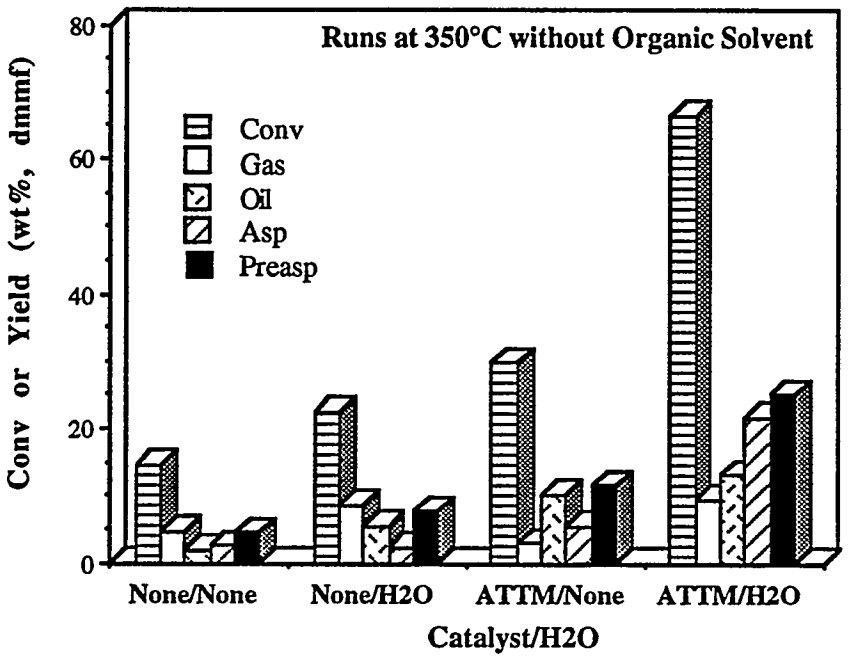

Figure 45 Effect of Water on Catalytic Liquefaction of Wyodak Coal at 350°C for 30 min. (1.0 wt% Mo to dmmf Coal).

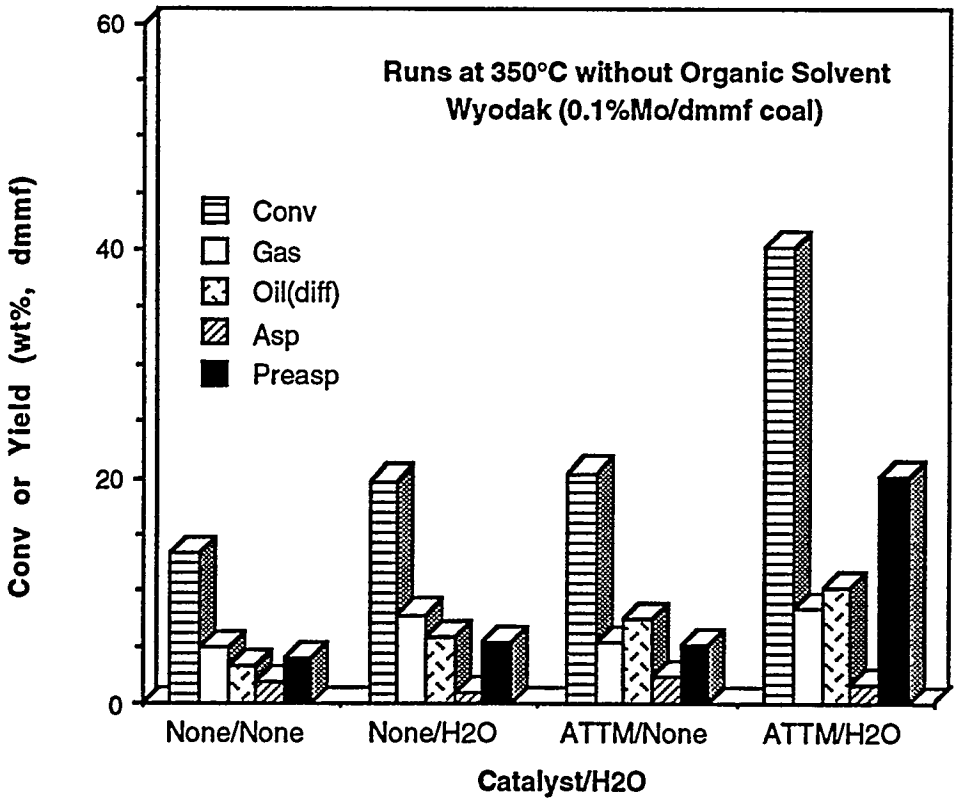

Figure 46. Effect of Water on Catalytic Liquefaction of Wyodak Coal at 350°C for 30 min. (0.1 wt% Mo to dmmf Coal).

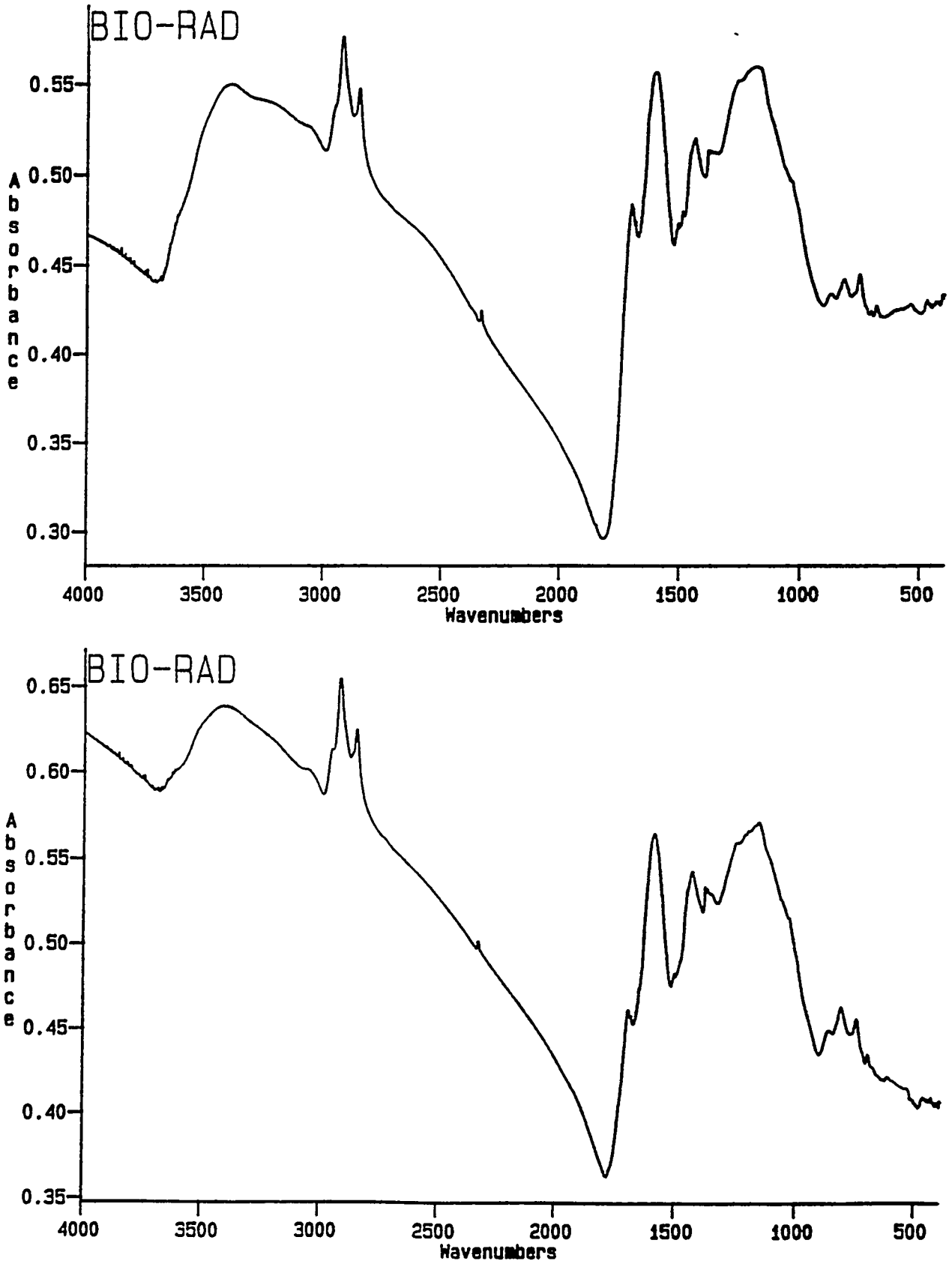

Figure 47. FTIR Spectra of Demineralised Wyodak Coal and Whole Products (350 °C, 6.9 MPa H_2, 30 min).

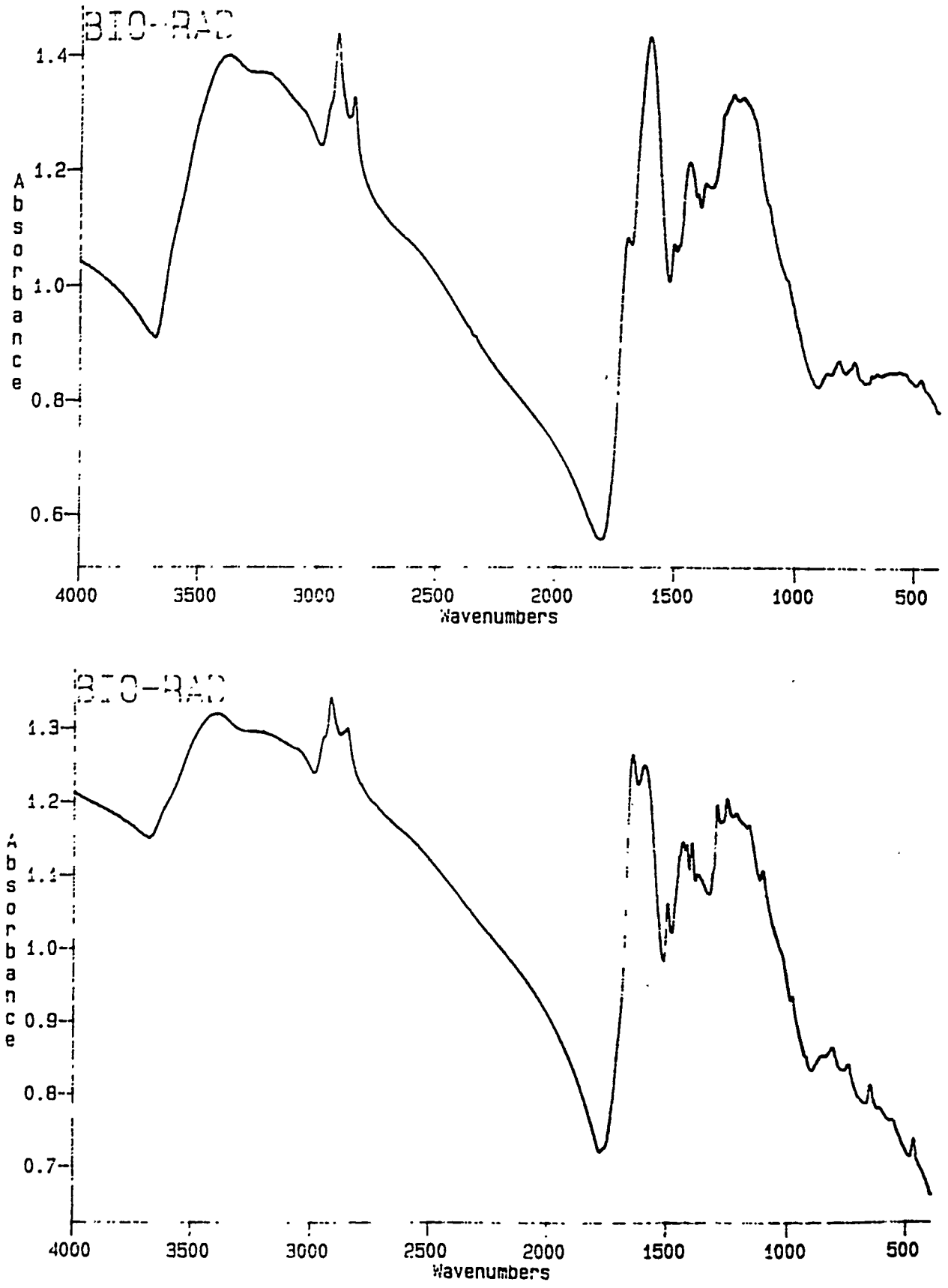

Figure 48. FTIR Spectra of Demineralised Wyodak Coal and THF-Insoluble Residue from Reaction in Absence of Solvent (350 °C, 6.9 MPa H_2, 30 min).

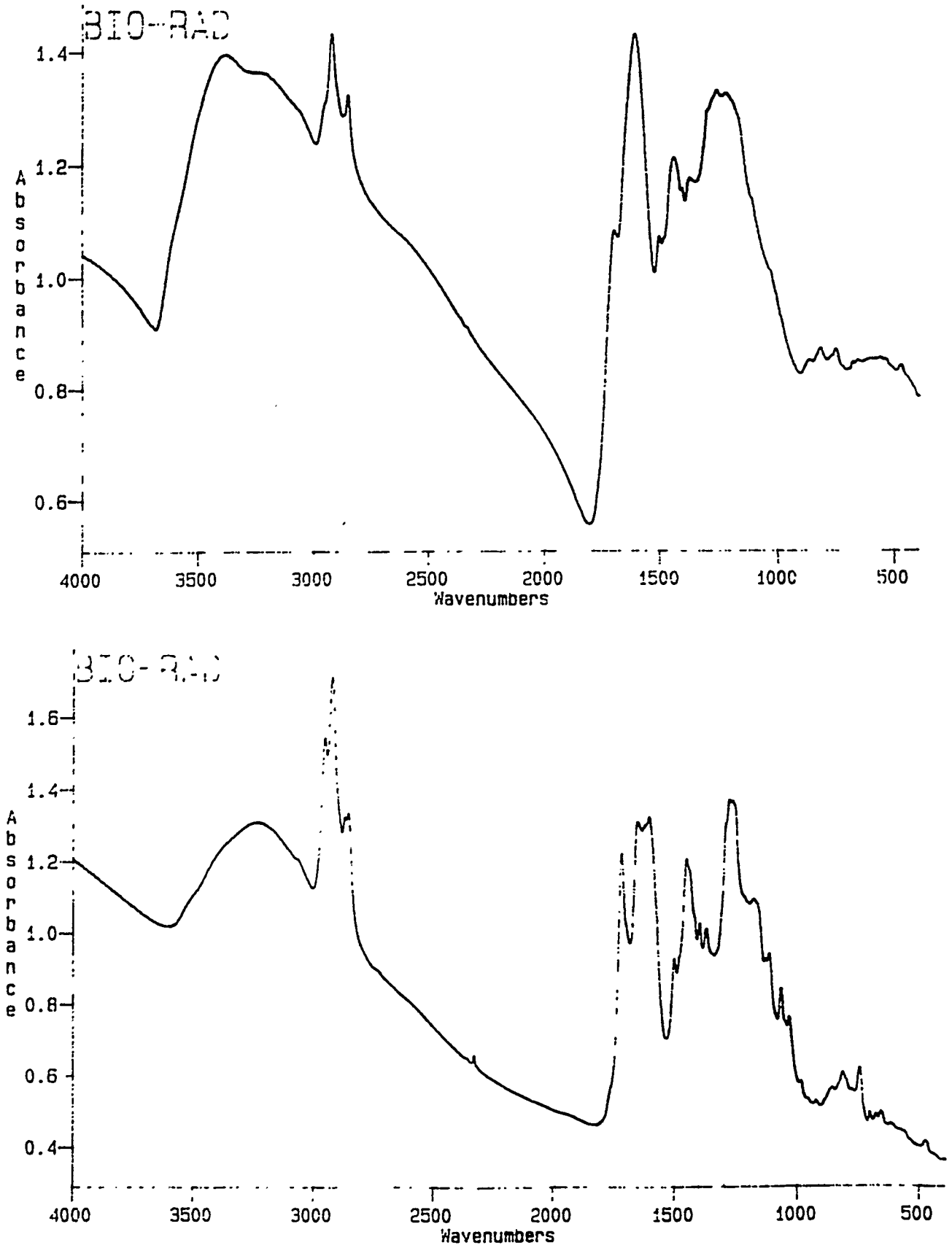

Figure 49. FTIR Spectra of Demineralised Wyodak Coal and THF-Insoluble Residue from Reaction in Presence of Solvent (350 °C, 6.9 MPa H_2, 30 min, Tetralin).

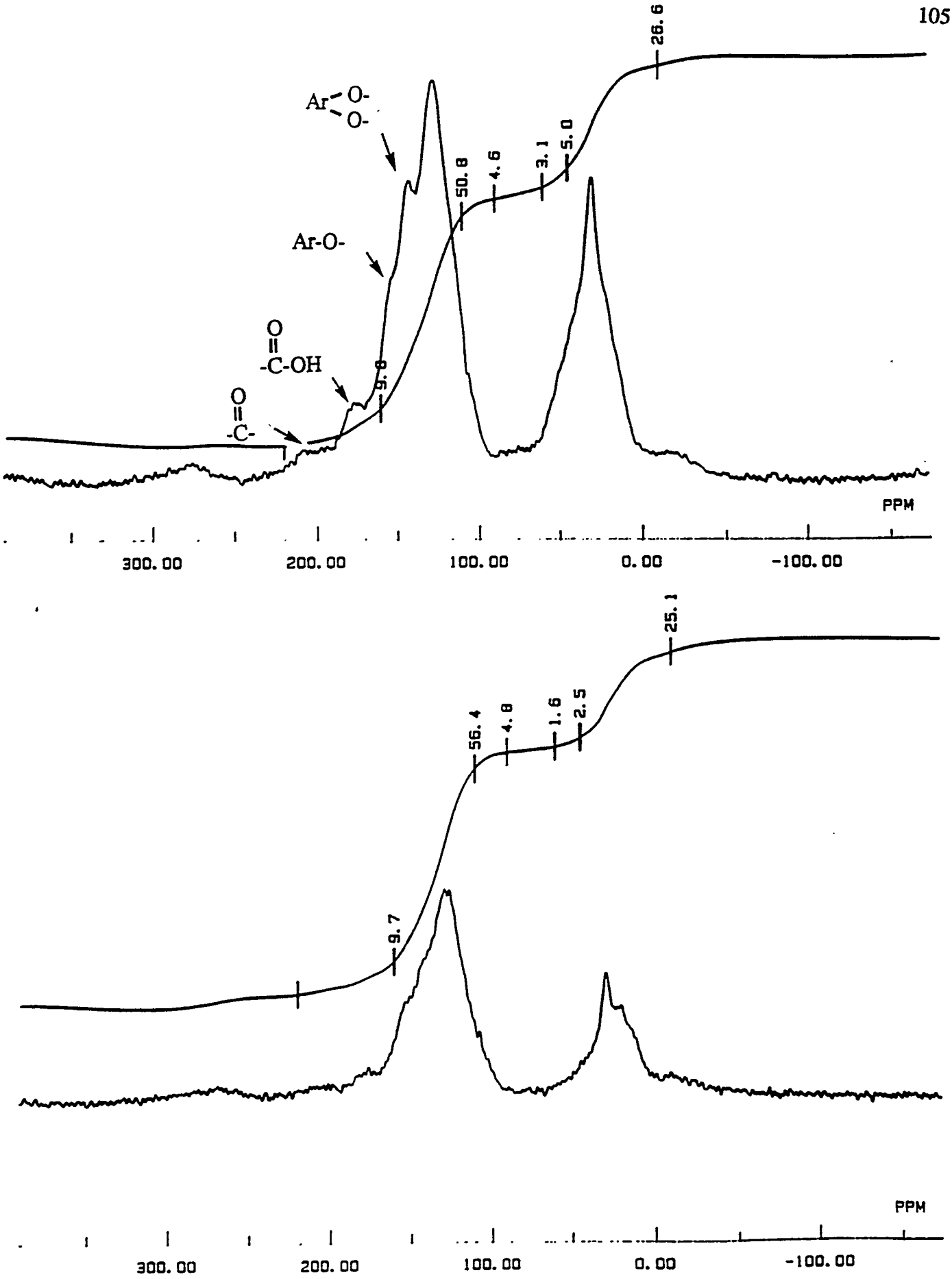

Figure.50. ^{13}C CP-MAS Spectra of Demineralised Wyodak Coal and Whole Products (350°C, 6.9 MPa H_2, 30 min).

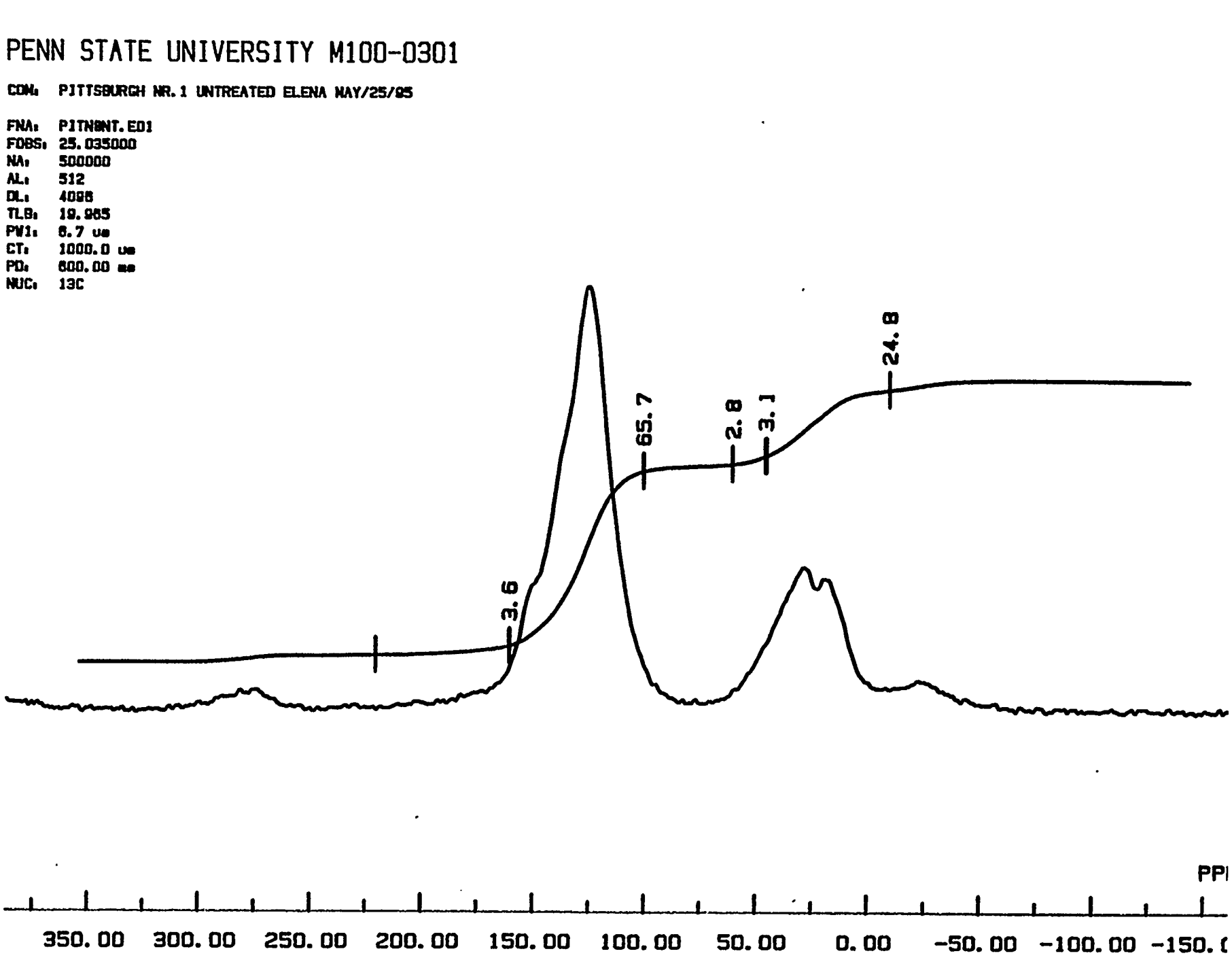

Figure 51. NMR Spectra of Untreated Coal Sample

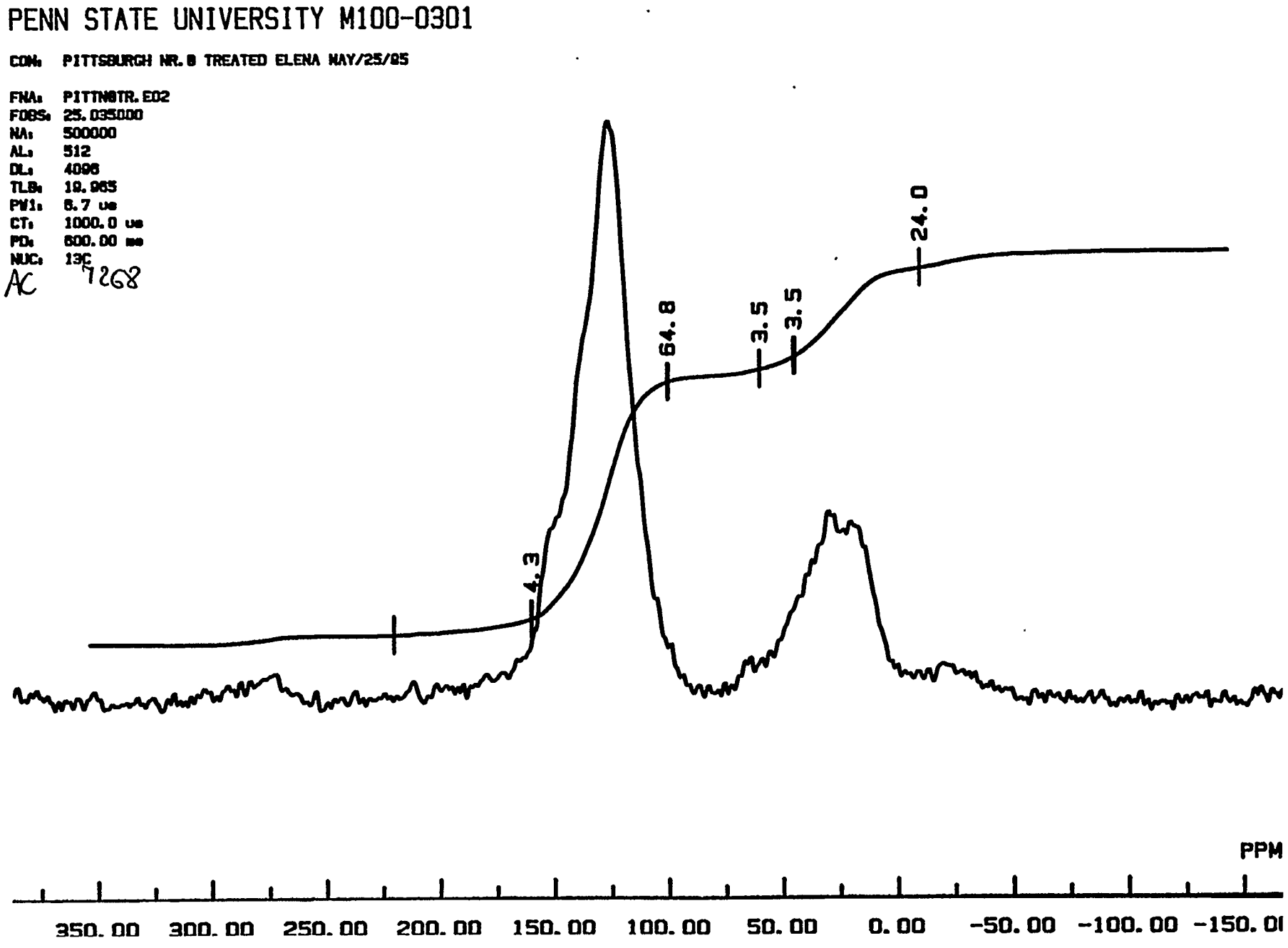

Figure 52. NMR Spectra of Residue of Treated Coal Sample

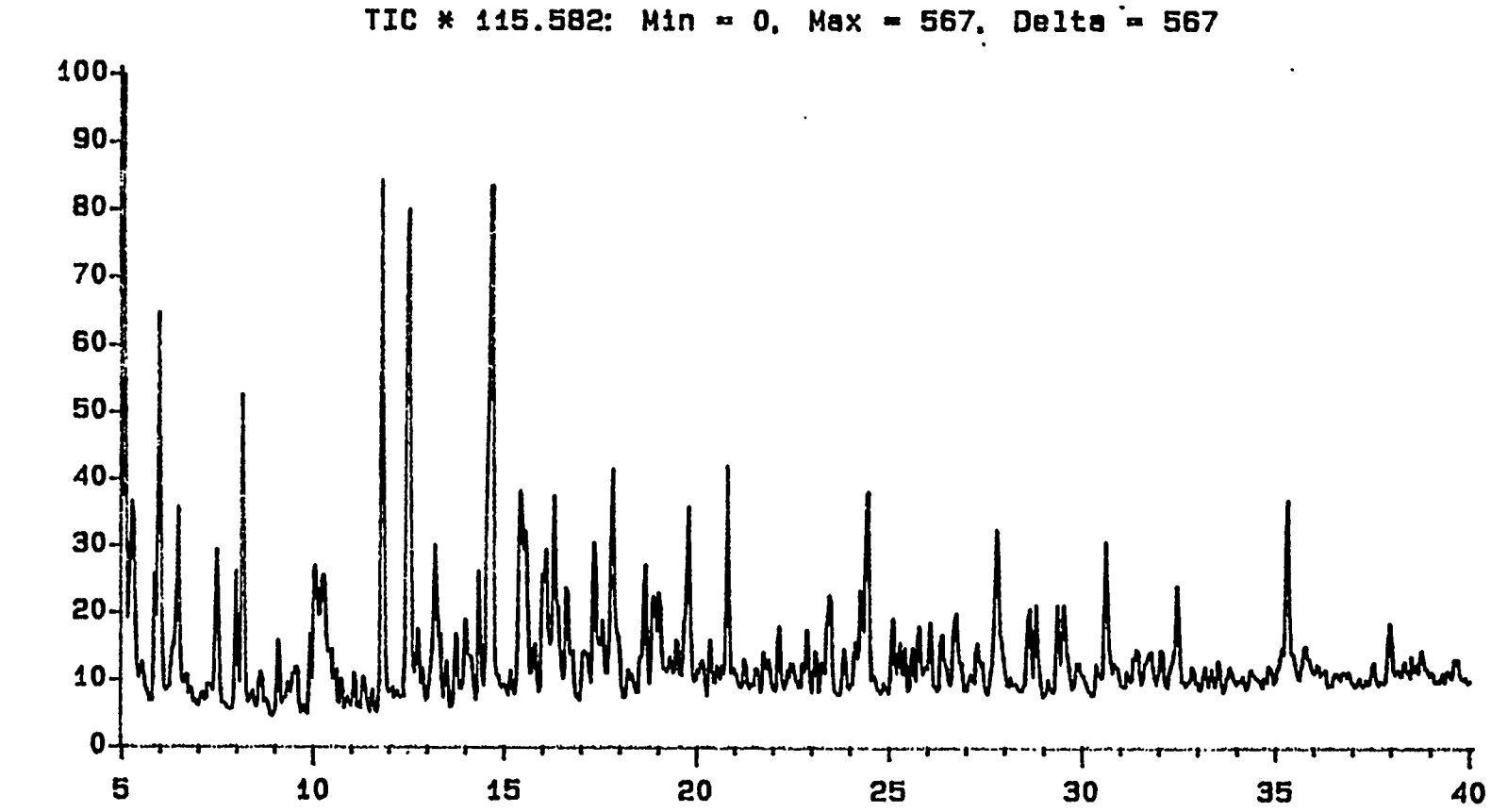

Figure 53. Pyrolysis GCMS Spectra of Residue of Treated Coal Sample.

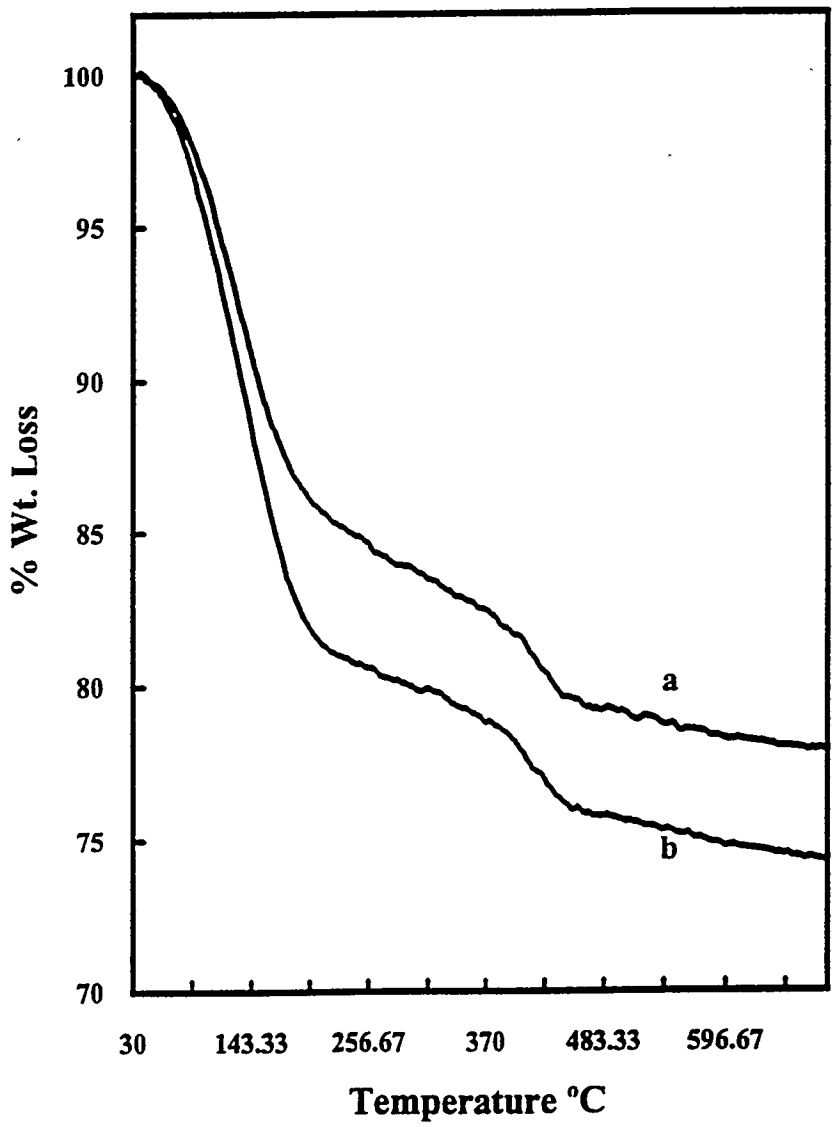

Figure 54. TGA of n-butylamine desorption from Al-MCM-41 molecular sieves prepared using sodium aluminate with SiO_2/Al_2O_3 molar ratios a) 50 and b) 25

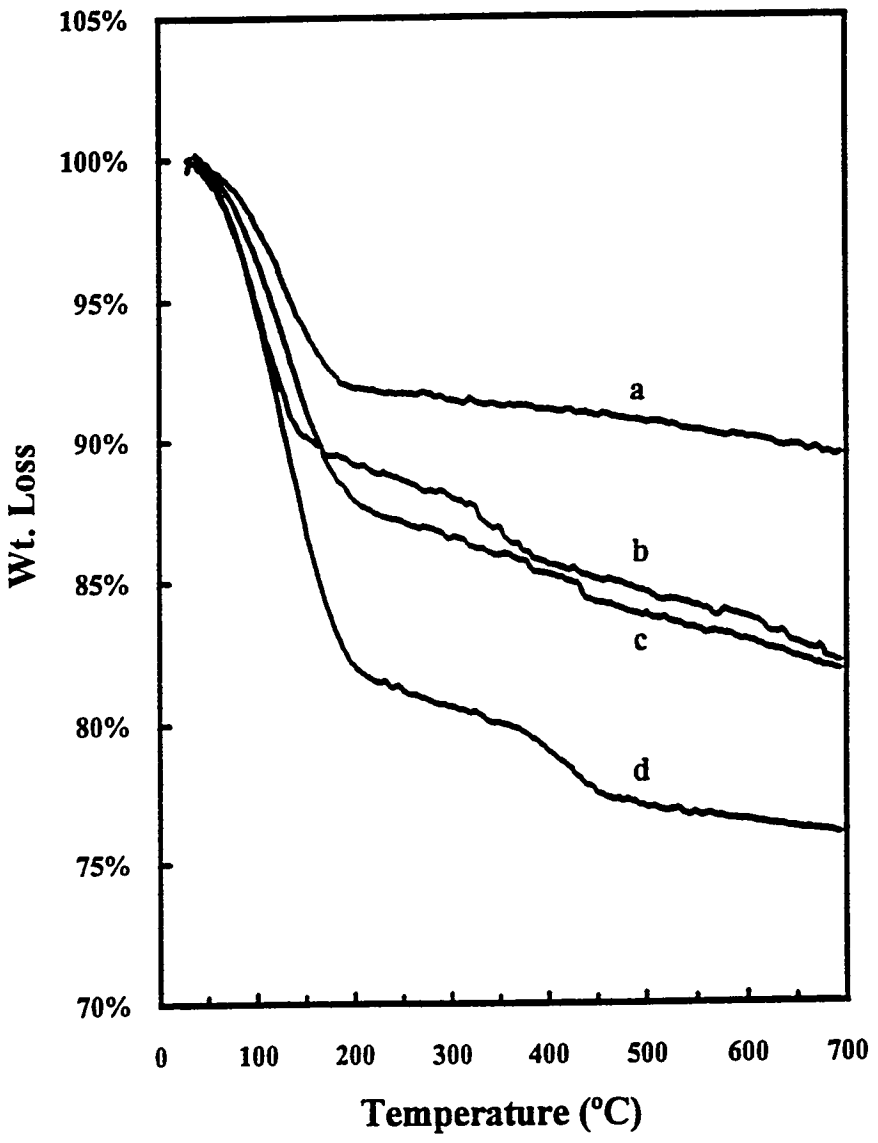

Figure 55. Comparison of TGA of n-butylamine desorption from Al-MCM-41 molecular sieves prepared using a) Catapal B alumina, b) aluminum isopropoxide, c) aluminum sulfate, and d) sodium aluminate

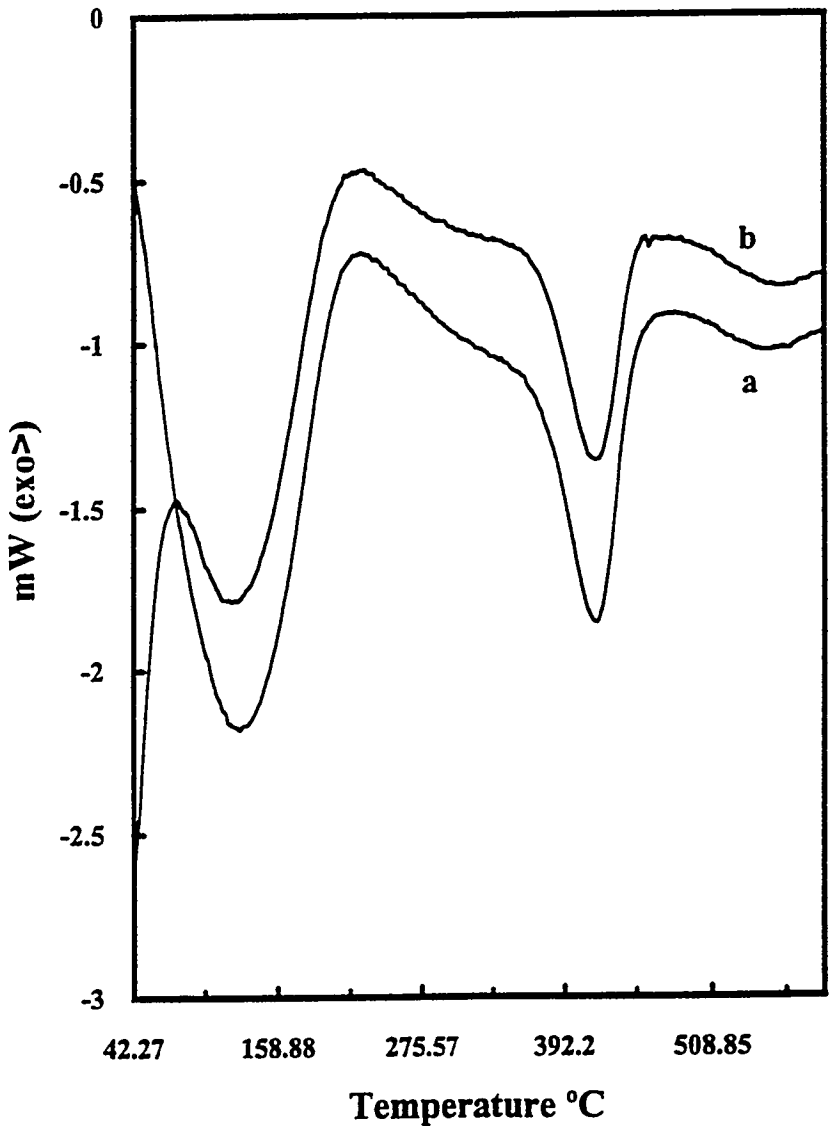

Figure 56. DSC of n-butylamine desorption from Al-MCM-41 molecular sieves prepared using sodium aluminate a) with and b) without initial flushing in nitrogen for 30 min.

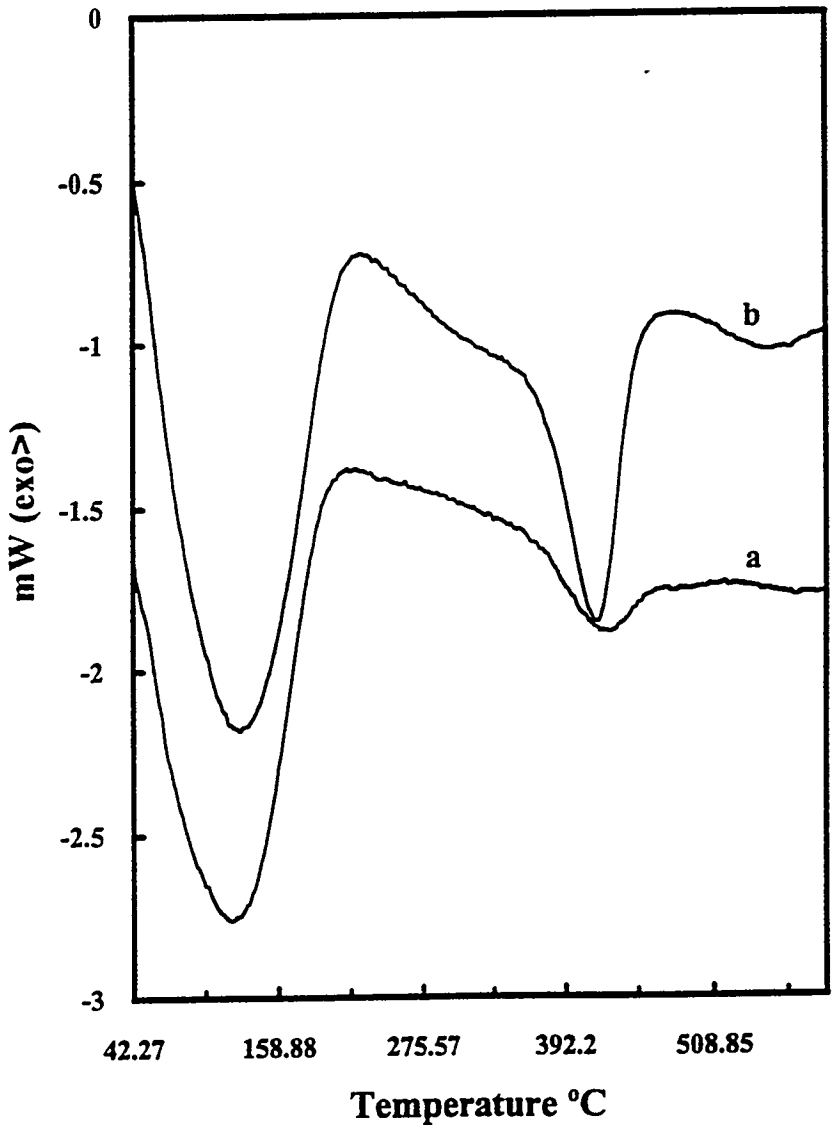

Figure 57. DSC of n-butylamine desorption from Al-MCM-41 molecular sieves prepared using sodium aluminate with SiO_2/Al_2O_3 molar ratios a) 50 and b) 25

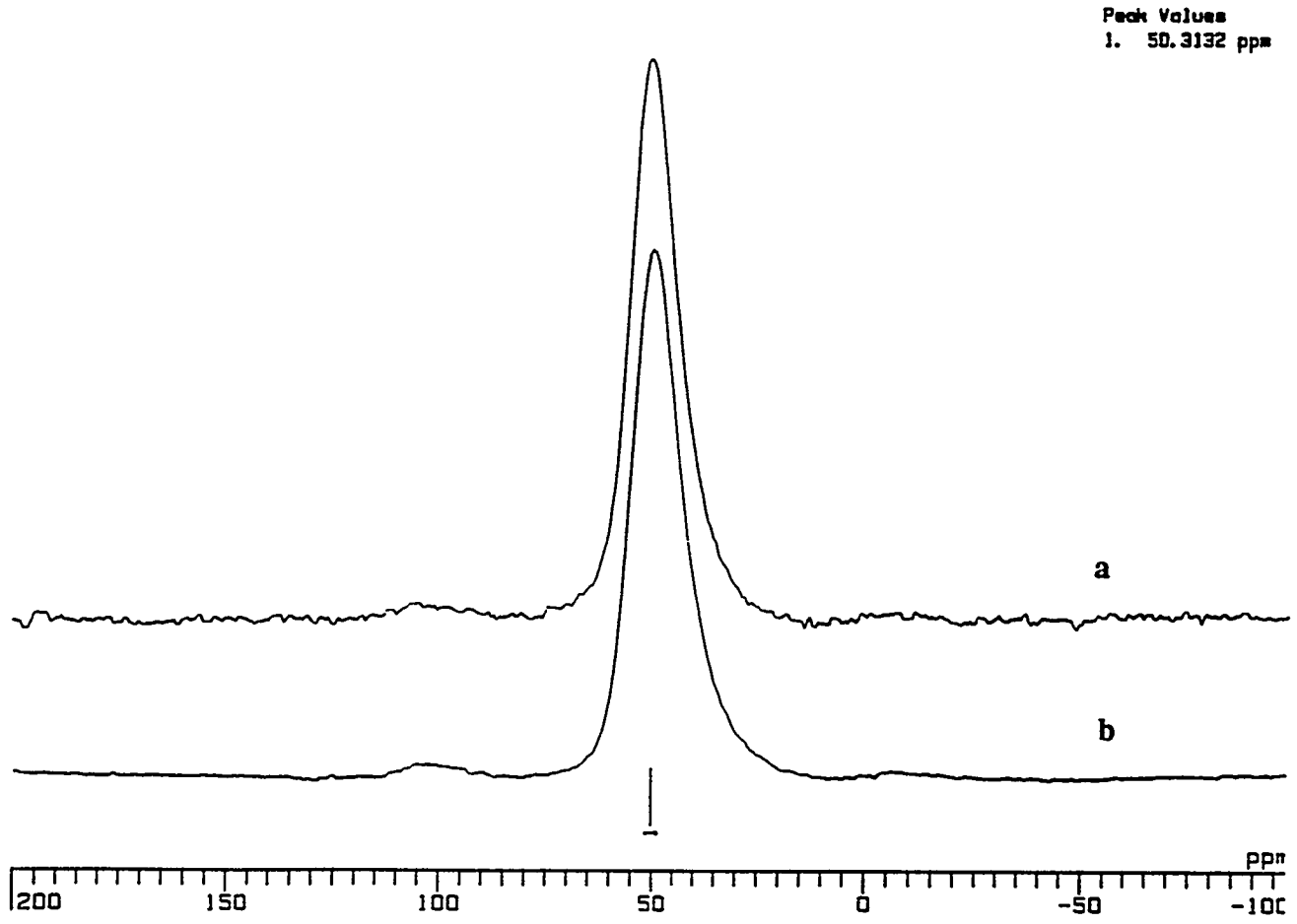

Figure 58. ^{27}Al Solid State NMR of Al-MCM-41 molecular sieves prepared using sodium aluminate with SiO_2/Al_2O_3 molar ratios a) 50 and b) 25

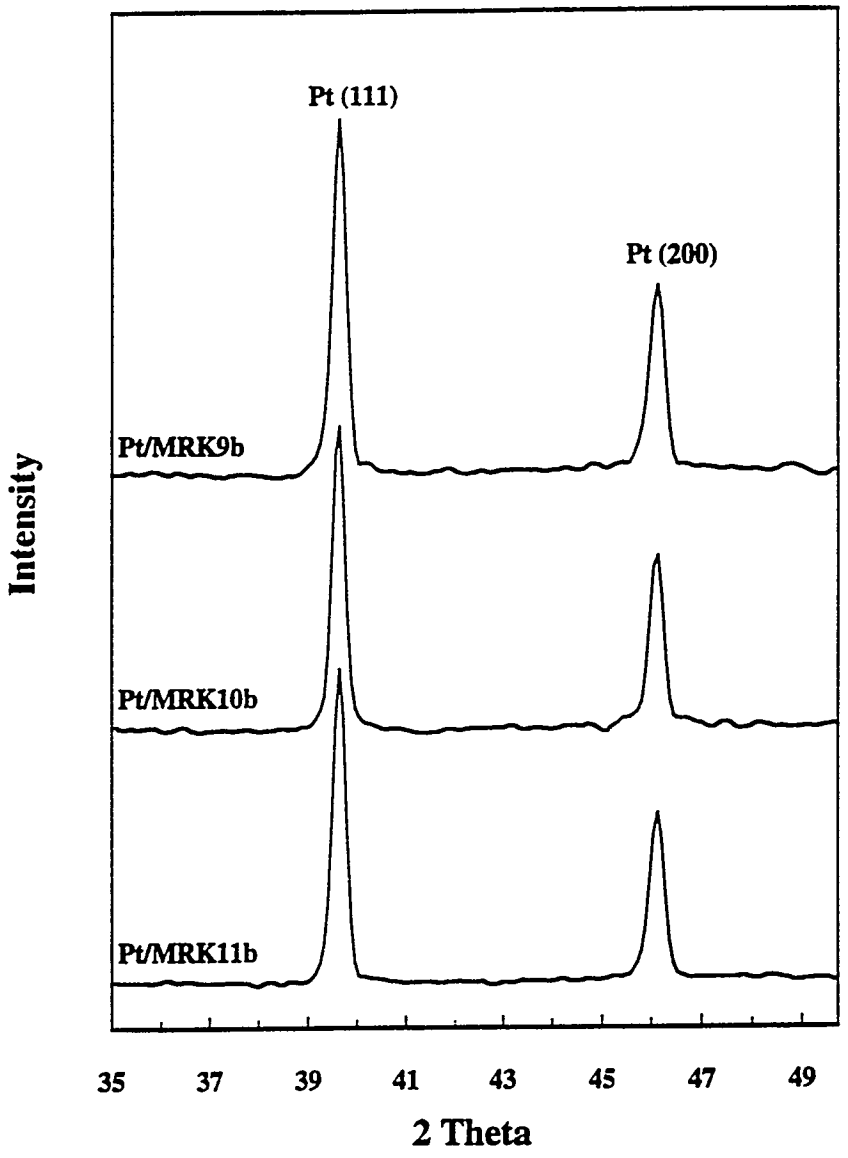

Figure 59 Platinum XRD of Pt loaded Al-MCM-41 molecular sieves prepared using aluminum isopropoxide (MRK9b), Catapal B alumina (MRK10b), and aluminum sulfate (MRK11b)